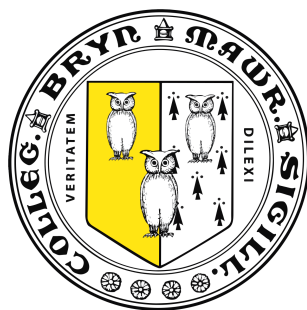# Using Biomathematical Models to Examine Potential Effects of Semaglutide on Polycystic Ovarian Syndrome Treatment

Authored by Jo Amuso

Advised by Professor Erica J. Graham

Thesis presented in partial fulfillment of the requirements for the degree of Master of Arts with Honors in Mathematics

Bryn Mawr College Department of Mathematics

May 2024

Abstract

Semaglutide, better known by its brand name Ozempic, is a drug used to treat Type 2 diabetes. It is a GLP-1 receptor agonist, meaning it activates the GLP-1 receptor, which is vital for the regulation of insulin and glucose levels in the bloodstream. Ozempic has also shown promise as a treatment for polycystic ovarian syndrome (PCOS), a hormone imbalance in people with uteruses often characterized by an abnormal menstrual cycle and insulin resistance. However, the mechanisms behind PCOS are not clearly understood, and the reasons behind the effectiveness of Ozempic as a PCOS treatment remain unclear.

Using systems of ordinary differential equations, it is possible to model the menstrual cycle, GLP-1 receptor activation and the release of insulin separately. Since GLP-1 receptors belong to a class of receptors called G protein-coupled receptors, we can form hypotheses about the relationship between Ozempic and PCOS by adapting general models of G protein-coupled receptors to fit the specifications of GLP-1 receptors. We can also simulate the relationship between GLP-1 and insulin at the macroscopic level using a system of differential equations that accounts for the impact of insulin and glucose on this GLP-1-mediated feedback loop. The last component of this overarching model is a system of differential equations representing the change in hormone levels and ovarian follicle mass during the menstrual cycle, with a term reflecting insulin-mediated testosterone production. By modifying each of these models to incorporate the effects of Ozempic, we create a combined model to simulate the effects of Ozempic on GLP-1 receptors, insulin release, and ovarian testosterone production, connecting Ozempic and PCOS mathematically.

Contents

1 Introduction

Semaglutide, better known by its brand name Ozempic, has gained notoriety as a fast-acting weight-loss drug. Ozempic was created as a second line treatment for Type 2 diabetes and obesity and is part of a class of drugs called glucagon-like peptide-1 (GLP-1) receptor agonists [20]. These drugs were developed to counter insulin resistance present in diseases like Type 2 diabetes by replicating the amino acid structure of the incretin hormone GLP-1 and modifying it in a few key places to extend its half-life [20]. Insulin resistance occurs when normal or elevated insulin levels have a reduced impact on the removal of glucose from the bloodstream [40]. Since the activation of GLP-1 receptors on the exterior of pancreatic $\beta-$cells triggers the rise of insulin, extending the half life of GLP-1 causes a higher concentration of insulin to be released into the bloodstream.

Polycystic ovarian syndrome (PCOS) is caused by a hormonal imbalance in people with uteruses, and is characterized by various symptoms across 3 phenotypes. PCOS is currently poorly understood, and there are no known direct treatments of the syndrome. Instead, doctors target symptoms of PCOS, such as insulin resistance, irregular periods, weight gain and acne, in their treatment regimens, which can include birth control pills and metformin [8, 42]. Metformin is another treatment developed for Type 2 diabetes targeting insulin resistance, and has anecdotally been shown to ameliorate symptoms of PCOS [8]. While the mechanisms of insulin resistance in PCOS are unclear, treating insulin resistance present in certain phenotypes of PCOS can be very effective.

After semaglutide became widely available, physicians, such as Dr. Melanie Cree BMC '99, noticed that prescribing it to patients with treatment resistant PCOS was highly effective in easing some of their worst symptoms [19]. However, the mechanisms behind this have not been studied, and in the absence of scientific evidence backing this phenomenon, the FDA has not approved semaglutide for the treatment of PCOS [19]. Dr. Cree is currently publishing the results of a Phase 3 clinical trial she conducted this past summer, and is currently planning a large-scale study to better understand why semaglutide can be effective in treating PCOS that has otherwise been treatment resistant [19].

In the meantime, it is possible to use mathematical modeling to examine the various mechanisms underlying GLP-1 receptor dynamics, insulin-glucose-incretin hormone dynamics and hormonal regulation of the menstrual cycle. In this paper, we are looking to clarify the connection between insulin resistance and testosterone levels in people with PCOS, and how introducing semaglutide as a longer-lasting form of GLP-1 effects this system. By simulating the effect of an extended GLP-1 half-life on insulin release and the subsequent insulin-mediated testosterone production, we see how this could affect reproductive hormone levels in people with PCOS.

2 Biological Background

The mechanisms underlying polycystic ovarian syndrome are complex, as are those underlying glucose-insulin dynamics. Understanding the scope of the models in this paper requires under-

standing these mechanisms, as well as the biochemical properties of semaglutide and glucagon-like peptide 1. We will first review the biological processes behind insulin synthesis and release and insulin signaling. Then, we will provide an overview of the hormones glucagon and GLP-1, as well as the GLP-1 receptor agonist semaglutide, or Ozempic. Finally, we will cover the dynamics of the menstrual cycle and how PCOS impacts the hormone balance necessary to maintain a healthy menstrual cycle.

2.1 Insulin

Insulin is a hormone secreted by $\beta-$cells in the islets of Langerhans region of the pancreas for the purpose of lowering blood glucose levels [31].

2.1.1 Insulin synthesis and release

Insulin is produced in the $\beta-$cell, shown in Figure 1, and then stored in granules until its secretion into the bloodstream [31]. This release is governed by a large influx of calcium (Ca^{2+}) ions into the cell [31]. This can occur when glucose enters the $\beta-$cell through glucose transporter-2 (GLUT-2) receptors on the exterior of these cells [31].
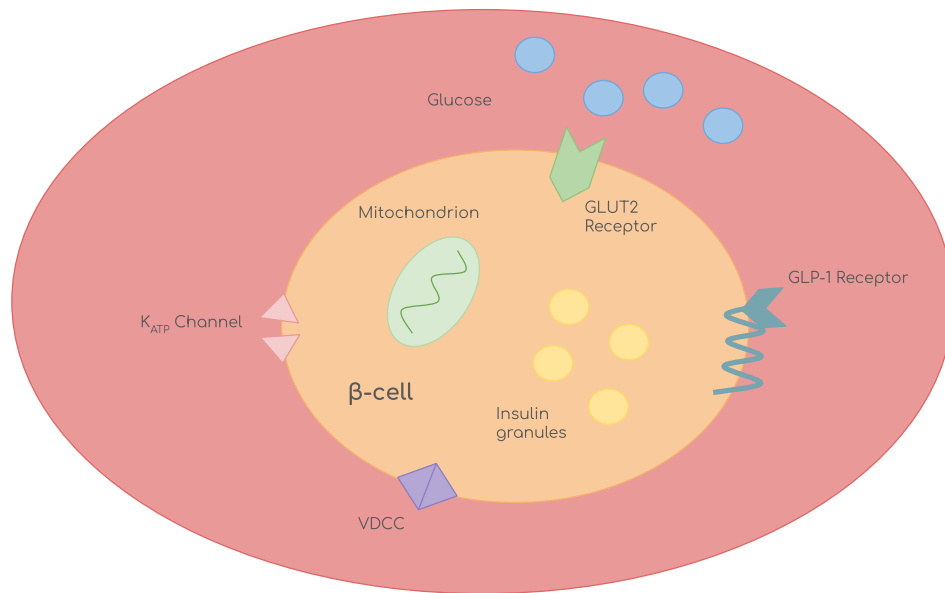
Figure 1: Schematic of a pancreatic β-cell [27].

After glucose enters the $\beta-$cell, as shown in step (1) in Figure 2, it is metabolized into adenosine triphosphate, or ATP, which provides energy to cells and closes the $\beta-$cell's K_{ATP} channels (2) [31]. K_{ATP} channels are ATP-sensitive potassium channel proteins that allow K^+ ions to enter

and exit the $\beta-$cell [31]. At low glucose concentration, K_{ATP} channels allow K^+ ions to enter the $\beta-$cell, generating an "excess of negative charges" inside the cell due to the attraction of positively charged ions to negatively charged particles [31]. This influx of K^+ ions into the $\beta-$cell also creates a negative membrane voltage on the exterior of the cell [31]. However, once the newly metabolized ATP closes the K_{ATP} channels, the membrane voltage becomes positive, leading to the depolarization of the $\beta-$cell membrane and a change in the cell's electrical activity [31]. This new electrical activity and resulting membrane voltage change opens the $\beta-$cell's voltage-dependent calcium channels (3), or VDCCs, which allows for an influx of Ca^{2+} ions into the $\beta-$cell (4) [31]. This further depolarizes the cell membrane, promoting the release of insulin granules into the bloodstream (5) [31]. Insulin secretion then happens in two phases: a rapid initial phase in which a high concentration of insulin is released in a 5 minute period, followed by an extended phase where insulin is gradually released [31]. However, only a small percentage of a $\beta-$cell's insulin granules are released during this process [31].
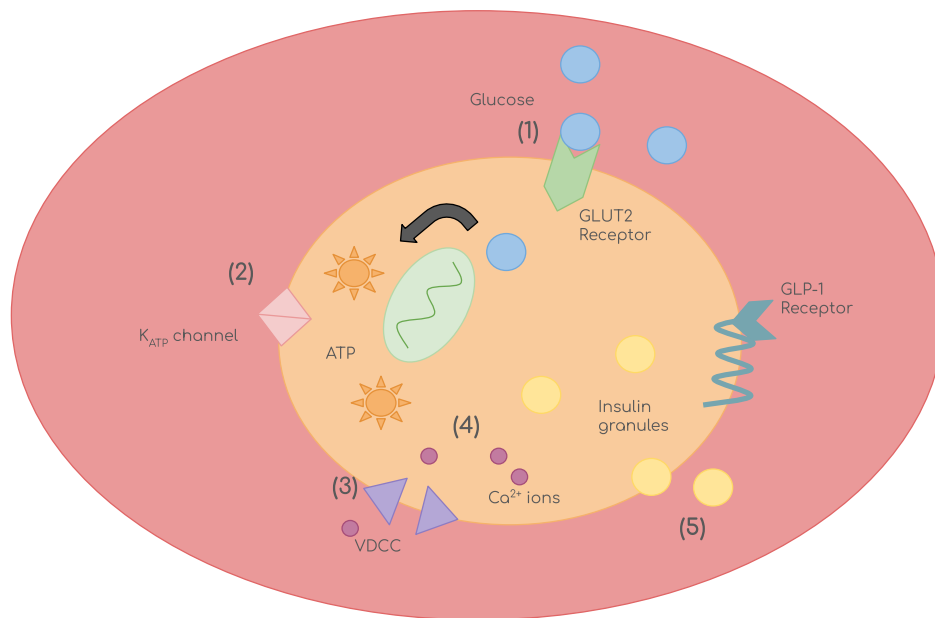
Figure 2: Diagram depicting initial insulin release [31].

2.1.2   Insulin signaling

Once released into the bloodstream, insulin plays a crucial role in many of the body's metabolic processes. Insulin first binds to insulin receptors present on a cell's exterior [40]. This triggers a signaling cascade, resulting in the activation of insulin responsive substrate (IRS) proteins in the cell [40]. After this process is complete, IRS proteins can bind to signaling molecules and mediate insulin's role in a number of intracellular processes [40]. Insulin lowers blood glucose levels

in part by aiding in the "facilitated diffusion of glucose into fat and muscle tissue" [40]. In this process, phosphorylated IRS proteins move GLUT-4 receptors to the cell membrane, allowing for an increased glucose uptake as well as glycogen synthesis [40]. Insulin increases protein synthesis and mRNA transcription in various types of cells and tissues and fatty acid synthesis in fat tissue, liver cells, and mammary glands [40]. Insulin also suppresses gluconeogenesis, or glucose synthesis, from amino acids in muscle tissue [40]. Overall, insulin is the central hormone in the body's regulation of "cellular energy supply and macronutrient balance" [40].

2.1.3   Insulin resistance

Due to the importance of insulin in the body's most critical metabolic processes, insulin resistance can have widespread and damaging effects. Insulin resistance is thought to originate in insulin signaling defects after binding to the insulin receptor [40]. For example, in muscle and adipose tissue, insulin resistance results in decreased movement of GLUT-4 receptors, which impairs glycogen synthesis [40]. In patients with type 2 diabetes, there is an significant reduction in pancreatic $\beta-$cell mass in addition to insulin resistance, which leads to insufficient insulin production [4]. Treatment for diabetes has historically focused on supplementing a diminished insulin output with insulin injections and medication to increase insulin sensitivity, such as metformin or drugs that replicate the insulin-stimulatory effects of glucagon-like peptide 1 (GLP-1), an incretin hormone that is synthesized in the intestine [4, 27]. This new class of drugs is known as GLP-1 receptor analogs, or GLP-1 RAs, and they have been shown to increase both insulin production and $\beta-$cell mass [4, 20]. In order to enhance the general understanding of the biological properties of GLP-1, it is important to first discuss the biological properties of glucagon.

2.2   Glucagon and glucagon-like peptide 1 (GLP-1)

Glucagon, which stands for glucose agonist, was discovered during development of a more efficient insulin purification process [27]. Glucagon, which was initially extracted from the pancreas, acts alongside insulin to balance blood glucose levels [27]. While insulin lowers blood glucose, glucagon both raises glucose levels and stimulates insulin secretion to maintain balanced blood glucose levels [27].

The initial discovery of glucagon showed that the hormone originates from the islets of Langerhans in the pancreas, which contain both $\alpha-$ and $\beta-$cells [27]. More specifically, the pancreas could no longer produce glucagon when its islet α-cells became damaged or compromised in some way [27]. Islet α-cells in the pancreas can be further categorized as α_1-cells or α_2-cells, and glucagon originates from α_2-cells [27]. Glucagon-like material was also discovered in the intestine through the usage of radioimmunoassays [27]. However, this intestinal glucagon-like material is distinctive from pancreatic glucagon; it is "heterogeneous, comprising several fractions of different molecular size. . . with apparently distinct biological actions relative to pancreatic derived glucagon" [27]. While pancreatic glucagon originates from pancreatic α_2-cells, this glucagon-like material originates

from intestinal L-cells, which differ from α-cells in form and structure [27]. Despite their biological distinctions, though, it was discovered that the glucagon-like material still stimulates insulin secretion like pancreatic glucagon, which implied that this intestinal material was either a different substance unrelated to glucagon or different forms of pancreatic-derived glucagon [27]. This new material was significantly larger than glucagon, lending credibility to the theory that glucagon is derived from a large "precursor" molecule which is split into several distinct fractions with differing sizes and functions [27]. This precursor was identified and classified as intestinal proglucagon [27]. Intestinal proglucagon is split into 4 distinct peptide hormones and 2 smaller peptides [27]. One of these distinct peptide hormones is a glucagon-related peptide aptly named glucagon-like peptide 1, a 30-amino acid often abbreviated as GLP-1 [20, 27].

GLP-1 is secreted by intestinal cells in response to food intake [4, 27]. GLP-1 also lowers food intake and glucagon secretion [20]. It is categorized as an incretin hormone because of its insulinotropic properties [4, 27]. GLP-1 stimulates insulin secretion in pancreatic β-cells through the activation of the GLP-1 receptor, causing a cascading effect similar to the one present in glucose-dependent insulin release [4, 27]. GLP-1 receptors are G protein-coupled receptors, and they specifically couple to G_s proteins [39, 41]. G proteins form the basis of numerous "transmembrane signaling systems" in a variety of cells [39]. G_s proteins in particular mediate glucose dependent insulin release in the $\beta-$cells through the stimulation of the adenylyl cyclase (AC) system, which increases production of cyclic adenosine monophosphate, or cAMP [4, 27, 39]. It is also theorized that G proteins play a role in the stimulation of K^+ ion channels and Ca^{2+} ion channels [22].

Prior to the activation of the GLP-1 receptor (GLP-1R), the inactive G_s protein is a heterotrimeric complex composed of α, β, and γ subunits, with a molecule of guanosine diphosphate, or GDP, bound to the α subunit, as shown in Figure 3 [22]. When GLP-1 binds to the GLP-1R, as shown step (1) of Figure 3, it first activates this G_s protein complex, which allows it to couple to the GLP-1R from the cell's interior (2) [22]. Then, the GDP molecule is converted into guanosine triphosphate (3), or GTP, and the G_s protein complex dissociates into an α subunit bound to a GTP molecule and the bound β and γ subunits (4) [22, 23]. The α-GTP complex activates the AC system, which allows ATP to be converted into cAMP [4, 23, 27]. The $\beta\gamma$-complex can also activate certain forms of adenylyl cyclase [39]. The GTP molecule then undergoes hydrolysis to become a GDP molecule (5), and the α-GDP complex combines with the $\beta\gamma$ complex to form a new heterotrimer (6) [22, 23].
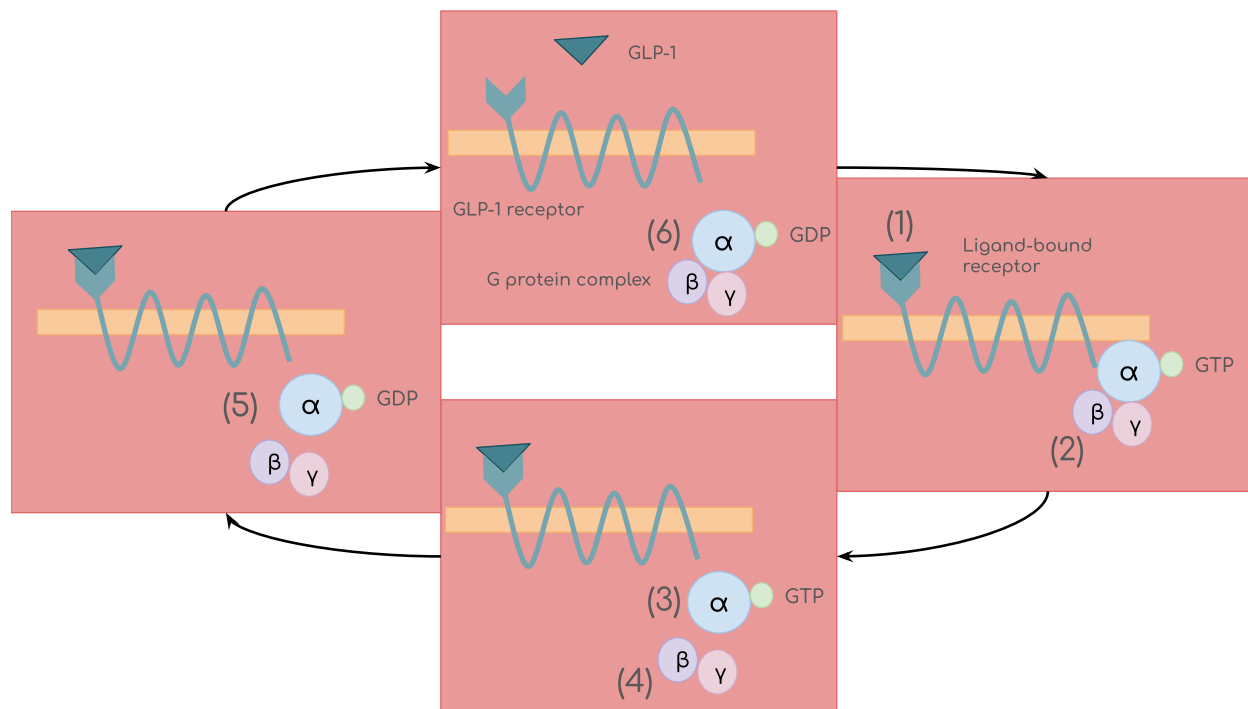
Figure 3: Diagram showing the activation of the GLP-1 receptor and the G protein complex [22].

As shown in Figure 4, the increase in cAMP due to GLP-1R binding (1) stimulates protein kinase A (PKA) (2), which controls the activity of K_{ATP} channels and VDCCs [27]. PKA inhibits K_{ATP} channels so potassium ions can not exit the β-cell (3) [27]. At the same time, PKA opens the VDCCs, allowing an influx of Ca^{2+} ions into the β-cell (4) [25, 27]. The inflow of Ca^{2+} depolarizes the cell membrane and promotes the release of insulin granules (5) [25, 27, 35]. At a certain point, the GLP-1R bound to the GLP-1 ligand is desensitized [27]. However, the mechanisms of this receptor desensitization are not yet completely understood [27].

In addition to promoting insulin secretion from $\beta-$cells, GLP-1 promotes $\beta-$cell proliferation and survival [4]. Since diabetes results when there is an "inadequate functional mass of $\beta-$cells," using GLP-1 to treat type 2 diabetes, which results from the "progressive deterioration of $\beta-$cell mass and function," is the next logical step in the development of effective diabetes treatment [4]. However, GLP-1 has a half life of less than two minutes, as it is quickly metabolized by dipeptidyl peptidase-4 (DPP4) [4, 27]. Therefore, in order to fully harness the insulinotropic properties of GLP-1, it is necessary to explore GLP-1 RAs, a class of medications that replicate the properties of GLP-1 and extend its half life.
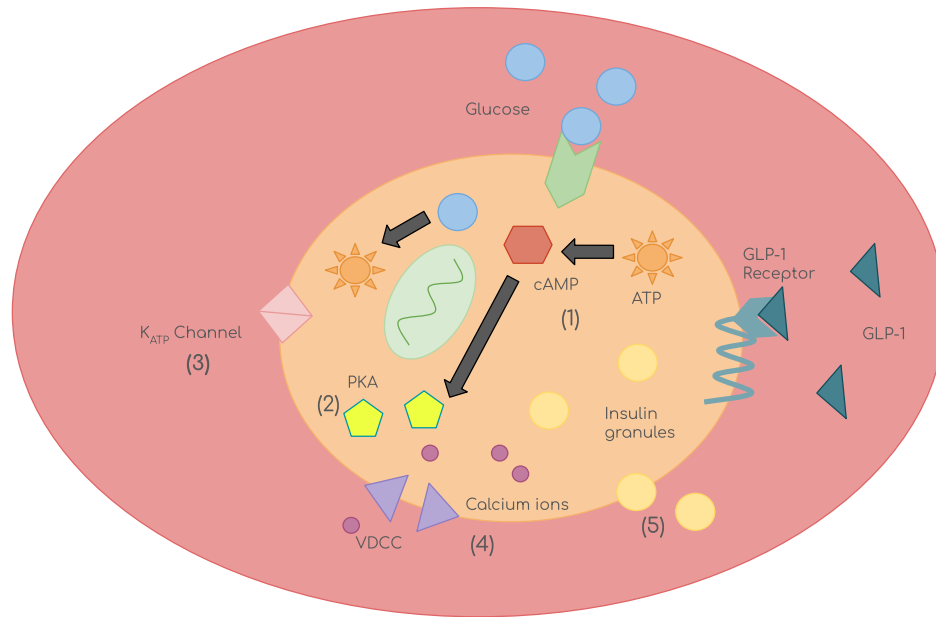
Figure 4: Diagram depicting GLP-1 receptor signaling in $\beta-$cells and the subsequent insulin secretion [27].

2.3 Semaglutide

Several GLP-1 RAs were developed prior to the invention of semaglutide, namely liraglutide [20]. These medications were created to replicate the properties of GLP-1 in a molecule with an extended half life [20]. This was accomplished by modifying the GLP-1 amino acid chain so it could effectively bind to human serum albumin [20]. Albumin is a plasma protein produced in the liver [20]. Its longevity, abundance and stability make it the ideal candidate for binding GLP-1 amino acids to extend the half-life of GLP-1 analogs [20].

By modifying certain amino acids on the GLP-1 peptide chain, as shown in Figure 5, researchers were able to create a molecule that reversibly binds to albumin; that is, it is able to uncouple itself from the albumin binding, activate the GLP-1 receptor and then rebind to the albumin [20]. It is also partially protected from rapid metabolism by DPP-4 enzymes [20]. The mechanism for this process is currently unclear, although the current theory is that the part of the molecule not bound to the albumin is able to bind to the GLP-1R [20]. This new molecule was called liraglutide, and was made available as a GLP-1 RA [20].

A fatty acid is added here to facilitate albumin binding.

H₂N–HAEGTFTSDVSSYLEGQAA**K**EFIAWLVRGRG–COOH

Liraglutide

X is an amino acid designed to prevent degradation.

The fatty acid added here is optimized to strengthen albumin binding.

H₂N–H**X**EGTFTSDVSSYLEGQAA**K**EFIAWLVRGRG–COOH
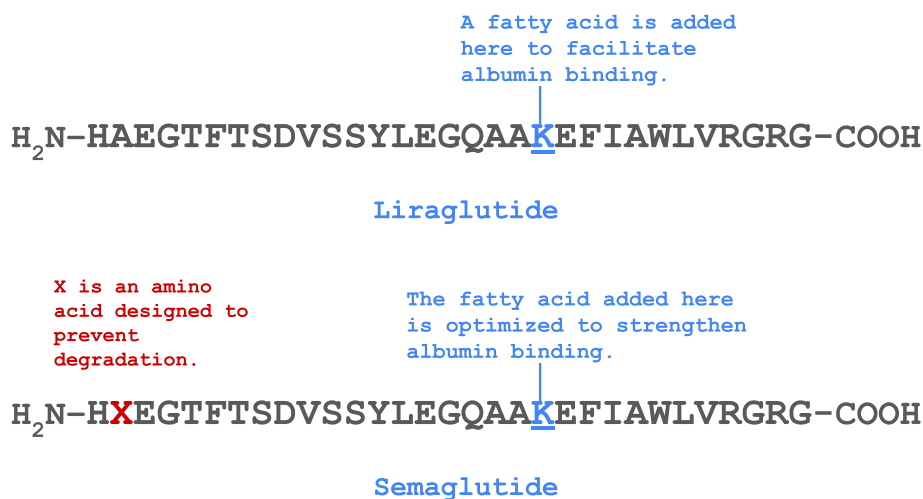
Semaglutide

Figure 5: Diagram comparing the amino acid chains of liraglutide and semaglutide. Image taken and modified from [20].

However, liraglutide requires a once-daily subcutaneous injection, which made the drug inaccessible to some patients [20]. Therefore, researchers sought to modify liraglutide to make it a once-weekly injection [20]. By ensuring that the resulting medication had the "highest albumin affinity combined with GLP-1R potency," they created a once weekly injectible medication known as semaglutide, or Ozempic [20]. Semaglutide has been found to cause a greater reduction in insulin resistance compared to other GLP-1 RAs [20]. The overall structure of semaglutide is very similar to human GLP-1, and the less-frequent injection cycle makes it more accessible to patients who greatly benefit from GLP-1 RAs [20]. A more recent development is the advent of oral semaglutide, which requires a once-daily dose [37]. While the connection between PCOS treatment and semaglutide is still unclear, there exists promising signs of the medication's effectiveness, due to existing evidence of GLP-1 RAs being an effective treatment for PCOS [37].

2.4 Polycystic ovarian syndrome (PCOS)

GLP-1 RAs are emerging as a new class of drugs able to treat PCOS, and by developing a better understanding of PCOS, we can hypothesize the link between semaglutide and PCOS. Polycystic ovarian syndrome is a hormonal imbalance in people with uteruses that can result in various, seemingly unrelated symptoms. There are three phenotypes of PCOS, and a person meets the diagnostic criteria for PCOS if they experience 2 of the 3 following phenomena: absence of ovulation or irregular ovulation (oligo-anovulation), high levels of androgens (hyperandrogenism) and ovarian growths [7, 10]. Additionally, acne, excess hair growth, weight gain and oily skin are symptoms

of PCOS, but these symptoms on their own are not typically indicative of a health condition, making obtaining a PCOS diagnosis difficult. Irregular periods in general, including no menstrual periods, frequently missed periods and very heavy periods, are also symptoms of PCOS [10]. PCOS is commonly associated with infertility and changes in physical appearance, and while these are symptoms of PCOS, people with PCOS are also at a higher risk for Type 2 diabetes, heart disease, and endometrial cancer [10]. The mechanism of hyperandrogenism in PCOS is currently unknown, and PCOS in general is very poorly understood [7].

2.4.1 Menstrual cycle dynamics

In order to understand PCOS, it is important to understand the dynamics of the menstrual cycle. As shown in Figure 6, the menstrual cycle is divided into 3 main phases centered around the development of ovarian follicles, or sacs containing eggs not yet ready for sperm fertilization: the follicular phase, ovulation and the luteal phase [15]. The average length of a normal menstrual cycle in an adult female is 28 days, with the follicular phase and luteal phase each lasting about 14 days [17]. The follicular phase begins when blood levels of follicle stimulating hormone, or FSH, rise and promote the growth of 6-12 primordial, or premature, follicles by adding layers of granulosa cells, which are the main synthesizers of estrogen, to the follicles [16, 17]. Testosterone, an androgen hormone and precursor of the ovarian hormone estradiol, or E_2, also plays a key role in the E_2 synthesis process by entering the granulosa cells to be converted into E_2 [14]. During the late stages of the follicular phase, the production of E_2, increases, and testosterone levels also rise [14, 17]. Ultimately only one follicle continues development, growing rapidly and synthesizing large amounts of E_2 [17]. At the midpoint of the menstrual cycle, one day after the maximum amount of E_2 is reached, the concentration of the luteinizing hormone (LH), which promotes ovulation, also reaches its peak, and continues to rise and fall rapidly over the next 5 days. This period of LH surge is essential for ovulation, which occurs within 24 hours of the surge's conclusion [17].
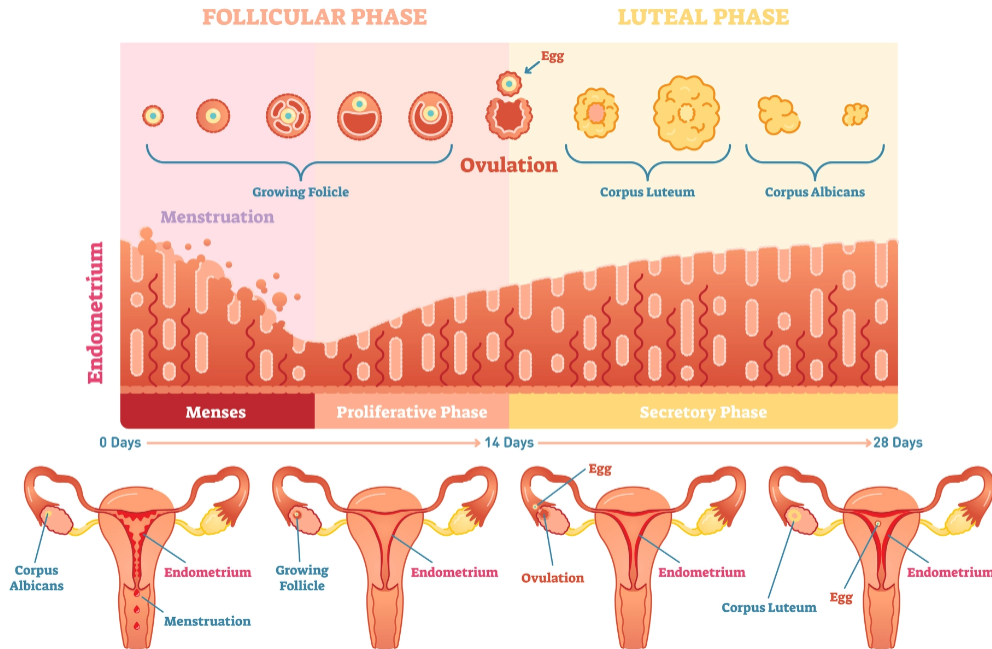
Figure 6: Illustration showing the stages of the menstrual cycle [26].

The luteal phase follows the completion of the ovulatory phase. This occurs once the follicle is empty and has transformed into the corpus luteum, which synthesizes hormones such as progesterone, or P_4, and inhibin A [18]. As a result, P_4 and inhibin levels increase greatly after ovulation, and both hormones reach their maximum concentration halfway through the luteal phase [17]. The rise in P_4 and inhibin causes a decrease in LH and FSH levels to prevent the development of follicles prior to the start of the next follicular cycle [17]. Additionally, E_2 and testosterone levels both decline as P_4 levels increase, with the decrease in testosterone being more pronounced, as shown in Figure 16 [14]. If there is no pregnancy at the end of the menstrual cycle, the corpus luteum slowly becomes inactive, causing a decline in P_4 and Inh levels and a subsequent rise in FSH and LH levels, signaling the beginning of the next menstrual cycle [17]. Figure 7 depicts normal hormone dynamics over one menstrual cycle, providing a visualization for the phases where the levels of a given hormone may be increasing or decreasing.
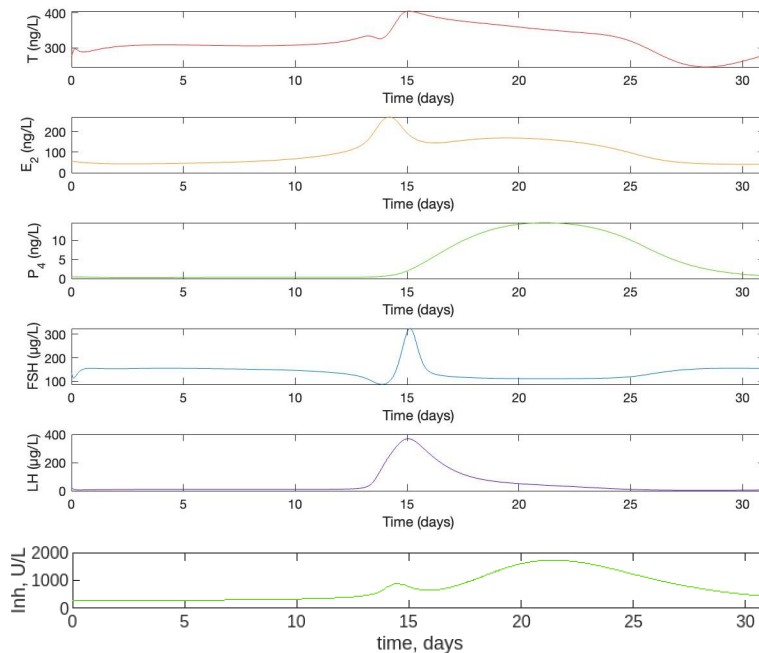
Figure 7: A normal hormone profile over 31 days, or approximately 1 menstrual cycle. *Inh* is inhibin concentration, and T is testosterone concentration [14, 17].

2.4.2 Hormonal imbalances

People with PCOS typically have heightened LH levels, due to low P_4 levels, and a greater LH/FSH ratio even during the luteal phase, which can cause premature follicular development [7]. The excess of developing follicles can also result in abnormal growths in the ovaries. Additionally, the larger LH/FSH ratio, as well as an increase in "serum androgen", can inhibit ovulation [7]. Hyperandrogenic PCOS also typically results in hyperinsulinemia, or abnormally high blood insulin levels [7]. It is for these reasons that doctors focus on balancing hormone levels and combatting hyperinsulinemia in PCOS patients through hormone treatments such as birth control and insulin sensitizing treatments such as metformin [8, 42].

The relationship between insulin sensitivity and PCOS remains unclear, but it is clear that insulin resistance is often a major symptom of PCOS. Since GLP-1 RAs treat insulin resistance, this provides a plausible connection between Ozempic and PCOS, as shown with the schematic in Figure 8. Additionally, there is already scientific evidence that GLP-1 RAs such as liraglutide are effective PCOS treatments, providing another tentative connection [37]. Analyzing the connection between insulin and the ovarian system can provide key insights into the usage of semaglutide to treat PCOS. Ovarian insulin receptors remain sensitive to insulin even in people struggling with insulin resistance, but it is theorized that theca cells, which produce testosterone and other androgens, synthesize excess androgens in response to hyperinsulinemia, leading to symptoms of

hyperandrogenic and insulin resistant PCOS [14]. Additionally, people with PCOS are believed to have a defect in their insulin-mediated glucose uptake, or IMGU [6]. In order to fully understand potential effects of semaglutide on PCOS symptoms, it is necessary to understand current mathematical models of GLP-1 mediated insulin release and insulin mediated testosterone production [2, 14, 38].
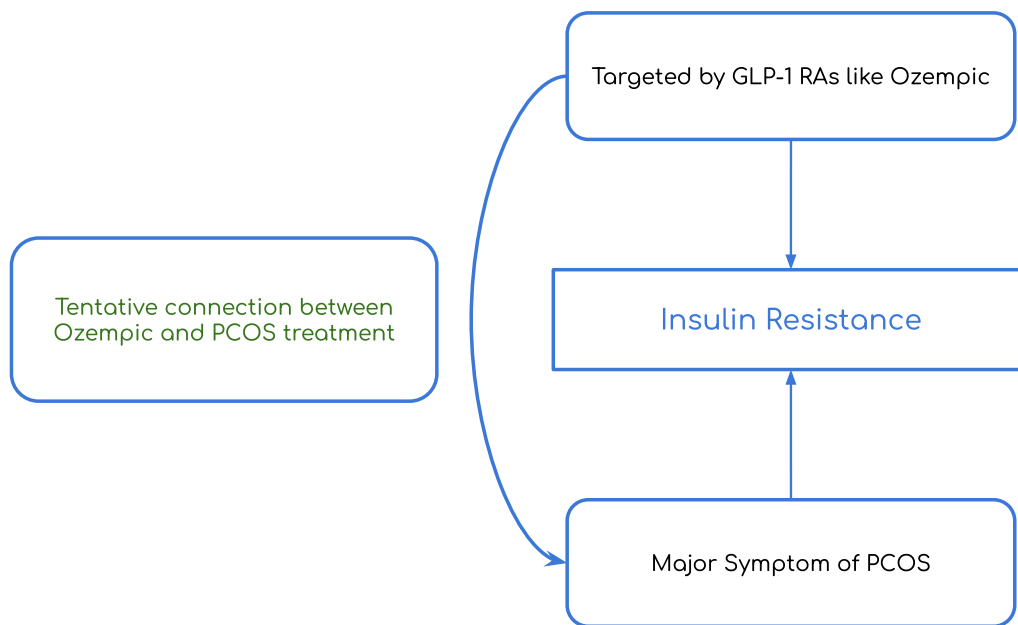
Figure 8: Schematic showing the possible connection between PCOS treatment and Ozempic.

3 Mathematical Background

Because of the prevalence of certain biochemical phenomena, such as enzyme reactions and cellular receptor dynamics, researchers have developed mathematical models that are widely utilized across many fields of scientific research. Using systems of ordinary differential equations, researchers can study biological processes through a mathematical lens and generate simulations to gain a better understanding of these processes. Before developing specific models, it is important to under the guiding principles behind generalized models of cellular receptor activation.

3.1 Enzyme Kinetics

3.1.1 Chemical complexes

Because differential equations measure rates of change, they are used in the mathematical modeling of biochemical reactions. A simple example of such a reaction is two compounds X and Y combining to create a product Z at a rate given by the rate constant k_1. Z is also able to decompose back into X and Y at a rate k_{-1}. The following reaction diagram represents this reaction and is extremely

useful in creating the corresponding mathematical model:

$$X + Y \underset{k_{-1}}{\overset{k_1}{\rightleftharpoons}} Z.$$
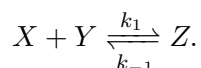
The rate of change of the concentrations of each product with respect to time would be the difference between the rate of change in concentration through the forward reaction and the rate of change in concentration through the backwards reaction [9]. Additionally, this reaction is governed by the law of mass action, which holds that the rate of a chemical reaction is proportional to the product of the concentrations of the reactants [9]. Therefore, the system of ordinary differential equations representing this system is given by

$$\frac{dx}{dt} = k_{-1}z - k_1xy,$$

$$\frac{dy}{dt} = k_{-1}z - k_1xy,$$

$$\frac{dz}{dt} = k_1xy - k_{-1}z,$$

where x, y and z are the concentrations of X, Y and Z respectively.

The ratio of the backwards reaction rate to the forwards reaction rate given by $\frac{k_{-1}}{k_1}$ is the dissociation constant, often represented as K_D [41]. The dissociation constant measures the propensity of a product to separate into its reactants under equilibrium conditions [41]. If the rate of a given reaction between two reactants is sufficiently fast, we can assume the reaction reaches instantaneous equilibrium; that is, $k_1xy = k_{-1}z$, which implies $xy = K_D z$.

3.1.2   Receptor signaling

The principles illustrated by this example also apply to mathematical models of more complicated chemical reactions. One chemical dynamic that is often studied through the lens of mathematical modeling is cell receptor signaling and receptor binding. Let C be an external molecule binding to an empty receptor, denoted by X_0, at a rate of k_1 and let X_1 be the molecule-receptor complex that is created once the molecule binds to the receptor [9]. It is possible for C to unbind from X_0 at a rate of k_{-1} [9]. However, some of C enters the cell and becomes a new product P at a rate k_2, so we are left with P and the empty receptor X_0 [9]. This reaction is not reversible, so we only have the forward reaction in this case [9]. This process can be illustrated with the following chemical reaction diagrams [9]:

$$C + X_0 \underset{k_{-1}}{\overset{k_1}{\rightleftharpoons}} X_1,$$

$$X_1 \overset{k_2}{\rightarrow} P + X_0.$$
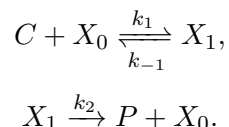
If c, x_0, x_1, and p are the concentrations of each molecule or compound in this process, the system of differential equations obtained from this reaction is

$$\frac{dc}{dt} = -k_1cx_0 + k_{-1}x_1,$$

$$\frac{dx_0}{dt} = -k_1 c x_0 + k_{-1} x_1 + k_2 x_1,$$

$$\frac{dx_1}{dt} = k_1 c x_0 - k_{-1} x_1 - k_2 x_1.$$

$$\frac{dp}{dt} = k_2 x_1,$$

By adding $\frac{dx_0}{dt}$ and $\frac{dx_1}{dt}$, we find that $\frac{dx_1}{dt} + \frac{dx_0}{dt} = 0$, implying that the total number of receptors remains constant, a mathematical result that also makes sense physiologically since receptors are neither created nor destroyed in this type of reaction process [9]. This is a common result of enzymatic reactions, including receptor binding, and will be extremely useful in the development of a model of GLP-1 receptor activation [9]. If r represents the initial receptor concentration, then $x_0 + x_1 = r$, and we can rewrite either x_0 or x_1 in terms of r [9]. In this case, we set $x_0 = r - x_1$ and substitute this back into the system of differential equations [9]:

$$\frac{dc}{dt} = -k_1 c(r - x_1) + k_{-1} x_1 = -k_1 cr + (k_1 c + k_{-1}) x_1, \tag{1}$$

$$\frac{dx_1}{dt} = k_1 c(r - x_1) - k_{-1} x_1 - k_2 x_1 = k_1 cr - (k_1 c + k_{-1} + k_2) x_1. \tag{2}$$

Since these equations are not dependent on p, we can set aside $\frac{dp}{dt}$, which can be solved after the solutions to $\frac{dc}{dt}$ and $\frac{dx_1}{dt}$ are found [9].

Although there are variations in this model across more specific types of receptor binding, the general principles remain the same, and there are common assumptions made across many types of models of receptor dynamics. In particular, the instantaneous equilibrium assumption and the assumption that total receptor concentration remains the same are crucial in our derivation of a GLP-1 receptor model. Another concept central to modeling biological processes is Michaelis-Menten kinetics.

3.2   Michaelis-Menten Kinetics

Equations modeling Michaelis-Menten kinetics develop general models of enzyme kinetics further by making additional simplifying assumptions. Michaelis-Menten equations model reaction rates under the assumption that there is an upper limit to the speed at which the reaction can occur [9]. A key assumption central to developing the general Michaelis Menten rate equation is the *quasi-steady state assumption*, or the assumption that changes in a certain concentration are so minimal that the overall concentration is essentially constant [9, 29]. In the case of a Michaelis-Menten rate equation for a receptor model, we assume that the receptors are always at maximal capacity, so the concentration of bound receptors remains constant [9]. Under this quasi-steady state assumption, Equation (2) is 0, which means

$$0 = k_1 c(r - x_1) - k_{-1} x_1 - k_2 x_1 = k_1 cr - (k_1 c + k_{-1} + k_2) x_1. \tag{3}$$

We then solve Equation (3) for x_1 to get

$$x_1 = \frac{k_1 cr}{k_1 c + k_{-1} + k_2}. \tag{4}$$

Substituting Equation (4) into Equation (1) gives us

$$\frac{dc}{dt} = -k_1 cr + (k_1 c + k_{-1}) \cdot \frac{k_1 cr}{k_1 c + k_{-1} + k_2},$$

which can rewritten as

$$\frac{dc}{dt} = rc \left[-k_1 + \frac{k_1(k_1 c + k_{-1})}{k_1 c + k_{-1} + k_2} \right].$$

Multiplying $\frac{k_1(k_1 c + k_{-1})}{k_1 c + k_{-1} + k_2}$ by $\frac{1/k_1}{1/k_1}$ transforms $\frac{dc}{dt}$ further:

$$\frac{dc}{dt} = rc \left[-k_1 + \frac{k_1 c + k_{-1}}{c + \frac{k_{-1} + k_2}{k_1}} \right].$$

Finally, combining the terms in the brackets gives us

$$\frac{dc}{dt} = rc \left[\frac{-k_1 c - k_{-1} - k_2 + k_1 c + k_{-1}}{c + \frac{k_{-1} + k_2}{k_1}} \right] = \frac{-k_2 rc}{c + \frac{k_{-1} + k_2}{k_1}}.$$

Let $K_{max} = k_2 r$ be the maximum velocity of the reaction, and let $K_m = \frac{k_{-1} + k_2}{k_1}$ be the concentration of C where the reaction velocity is half of K_{max} [9]. K_m is also called the Michaelis constant or the half-maximal concentration [9]. Then, we have

$$\frac{dc}{dt} = -\frac{K_{max} c}{c + K_m}.$$

Additionally, substituting Equation (4) into the expression for $\frac{dp}{dt}$ yields

$$\frac{dp}{dt} = k_2 \frac{k_1 cr}{k_1 c + k_{-1} + k_2},$$

and dividing both the numerator and the denominator by k_1 gives us

$$\frac{dp}{dt} = \frac{k_2 cr}{c + \frac{k_{-1} + k_2}{k_1}}.$$

Substituting K_{max} and K_m into this equations gives us the Michaelis-Menten equation

$$\frac{dp}{dt} = \frac{K_{max} c}{c + K_m} = v, \tag{5}$$

where v is the velocity, or rate, of the reaction [9]. This makes sense physiologically, since if the concentration of reactant C is decreasing at a rate of $\frac{K_{max} c}{c + K_m}$, then the concentration of the product of the chemical reaction P should increase at the same rate. Figure 9 provides a qualitative plot of v as a function of c to better visualize the behavior of Michaelis-Menten kinetics.
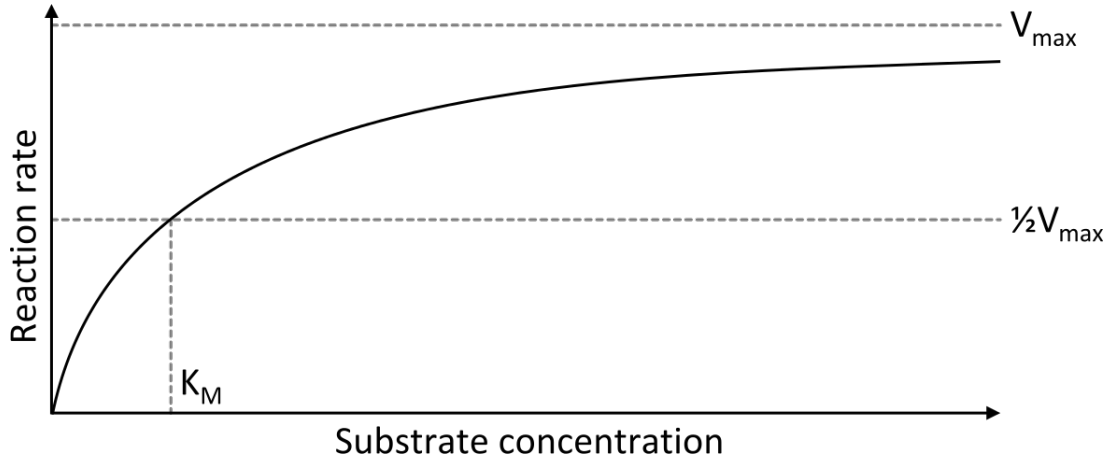
Figure 9: A general Michaelis-Menten curve. It is clear from this diagram that the higher K_m is, the greater the concentration of substrate c required to increase the reaction rate v [34].

The assumptions made in the process of deriving the general Michaelis-Menten equation can not be made in all circumstances. The assumption of the quasi-steady state means that at least one receptor population remains essentially constant, which is not always the case. However, this rate equation is highly useful in modeling many of the simplest cases of enzymatic reactions, and is used in both our GLP-1 receptor model and the addition of an Ozempic dosage to our models. Some biological processes that fall in the purview of enzyme and Michaelis-Menten kinetics are so widely studied that general models of these processes have been made that are then modified and adapted in more specific scenarios. The activation of G coupled protein receptors is one such process [3, 22].

3.3   Models of G Protein Coupled Receptors

Once receptors are activated, they need a way to transmit signals. As previously described, G protein-coupled receptors use G proteins to conduct their signaling once activated. To model this process more generally, we can describe it as a series of enzymatic reactions [22]. We can then provide a model for GLP-1 receptors specifically [38].

3.3.1   General model of G protein-coupled receptors

First, a ligand L binds to an empty receptor R to create a ligand-bound receptor complex LR:

$$L + R \underset{k_{-1}}{\overset{k_1}{\rightleftharpoons}} LR.$$
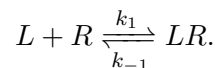
Then, the side of the G protein complex containing the $G_\alpha GDP$ subunit binds to the LR complex from inside the cell, so we initially assume that only $G_\alpha GDP$ binds to LR to create the complex

$LRG_\alpha GDP$ [22]:

$$LR + G_\alpha GDP \underset{k_{-2}}{\overset{k_2}{\rightleftharpoons}} LRG_\alpha GDP.$$
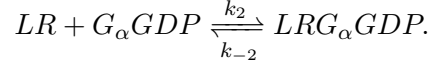
After the formation of $LRG_\alpha GDP$, the GDP molecule becomes GTP, a reaction that is not included in the original model. In the interim, the LR complex is bound to the G protein complex G without GDP or GTP, so we have the complex LRG:

$$LRG_\alpha GDP \underset{k_{-3}}{\overset{k_3}{\rightleftharpoons}} LRG + GDP.$$
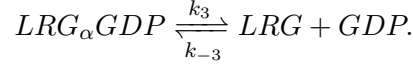
Once GDP becomes GTP and binds to the G protein complex again, we get the complex $LRG_\alpha GTP$:

$$LRG + GTP \underset{k_{-4}}{\overset{k_4}{\rightleftharpoons}} LRG_\alpha GTP.$$
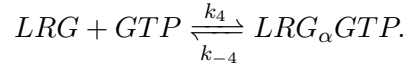
Once fully activated, the $G_\alpha GTP$ compound detaches from the LR and activates other processes within the cell, creating a product P:

$$LRG_\alpha GTP \overset{k_5}{\longrightarrow} LR + G_\alpha GTP,$$

$$G_\alpha GTP \overset{k_6}{\longrightarrow} P.$$
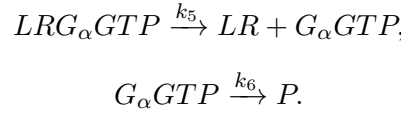
Based on these reactions and the principles of modeling enzyme kinetics, we obtain to following system of differential equations, where brackets indicate concentration of a molecule or compound [9]:

$$\frac{d[LR]}{dt} = k_1[L][R] + k_{-2}[LRG_\alpha GDP] - k_{-1}[LR] - k_2[G_\alpha GDP][LR] + k_5[LRG_\alpha GTP],$$

$$\frac{d[LRG_\alpha GDP]}{dt} = k_2[G_\alpha GDP][LR] + k_{-3}[GDP][LRG] - k_{-2}[LRG_\alpha GDP] - k_3[LRG_\alpha GDP],$$

$$\frac{d[LRG]}{dt} = k_3[LRG_\alpha GDP] + k_{-4}[LRG_\alpha GTP] - k_{-3}[GDP][LRG] - k_4[LRG][GTP],$$

$$\frac{d[LRG_\alpha GTP]}{dt} = k_4[LRG][GTP] - k_{-4}[LRG_\alpha GTP] - k_5[LRG_\alpha GTP],$$

$$\frac{d[G_\alpha GTP]}{dt} = k_5[LRG_\alpha GTP] - k_6[G_\alpha GTP].$$

Additionally, this model assumes that total extracellular ligand concentration $[L]$ is constant, so $\frac{d[L]}{dt} = 0$. This model also assumes the total receptor concentration is a constant value $[R_T]$, where

$$[R_T] = [R] + [LR] + [LRG] + [LRG_\alpha GTP] + [LRG_\alpha GDP].$$

While this is a good general model of G coupled protein receptors, it does not account for important steps in the activation process, such as the separation of $G_\alpha GTP$ from the G protein β and γ subunits and the desensitization of the activated receptors [22]. The GLP-1 receptor model developed in this paper, based on results from Takeda et al., will fit a general model of G protein-coupled receptors to the specific properties of GLP-1 receptors while accounting for these missing pieces [38].

3.3.2 Model of GLP-1 receptors

It is important to understand the existing mathematical models of GLP-1 receptor signaling in pancreatic $\beta-$cells in order to fully understand how Ozempic affects insulin release. Takeda et al. created a system of ordinary differential equations to describe the mechanisms of GLP-1 receptor activation and the subsequent increase in cAMP concentration [38]. Figure 10 shows the process of GLP-1 receptor activation depicted in Figure 3 as a series of chemical reactions, which forms the basis for the Takeda et al. model [22, 38].
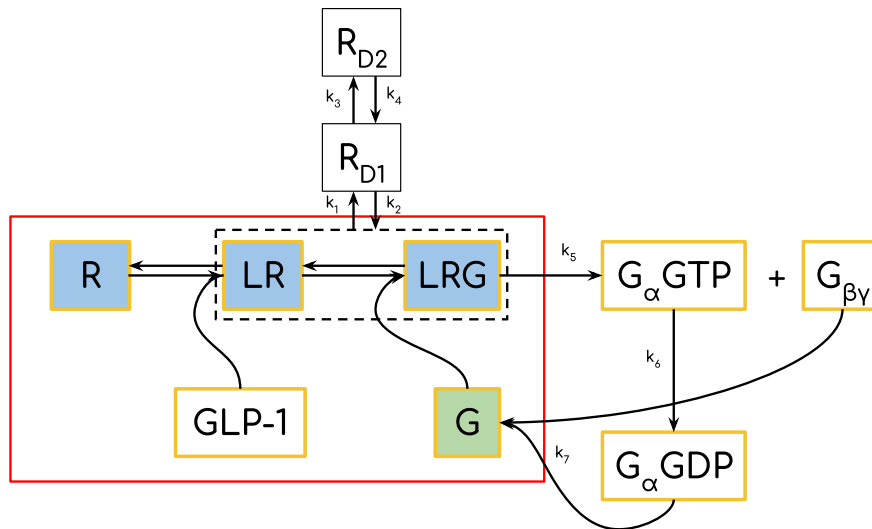
Figure 10: Reaction diagram showing GLP-1 receptor activation with rate constants. The variables in the yellow boxes can be modeled by the general G protein-coupled receptor model, with GLP-1 as the ligand [22]. Densensitized receptors only move from the populations of bound receptors, LR and LRG. Due to the rate at which GLP-1 and G combine with the receptor to create LRG, a receptor bound with both the GLP-1 ligand and the G_s complex, which is extremely rapid compared to the other reactions in the system, the reactions in the red rectangle are assumed to be at instantaneous equilibrium. Image taken and modified from [38].

$[R]$ is the concentration of free, inactivated receptors, $[LR]$ is the concentration of GLP-1 bound receptors, and $[LRG]$ is the concentration of receptors bound to GLP-1 on the cell exterior and a complete G protein complex on the cell's interior [38]. The mechanisms behind GLP-1 receptor desensitization are unclear; however, biochemical evidence indicates that the desensitization process occurs in two phases [38]. Takeda et al. include the desensitization phase in their model in order to better understand the kinetics of the "reaction cascade during GLP-1 stimulation", which had not been determined in $\beta-$cells at the time their paper was published [38]. $[R_{D1}]$ is the concentration of receptors in the first phase of deactivation, and $[R_{D2}]$ is the concentration of receptors in the

second, more gradual phase of deactivation [38]. $[G_{\beta\gamma}]$ is the total concentration of combined G protein β and γ subunits and $[G]$ is the mass of heterometric, or combined, G_s protein subunits [38]. $[G_\alpha GTP]$ and $[G_\alpha GDP]$ represent the concentrations of G protein α subunits bound to GTP and GDP respectively [38].

Takeda et al. provide 5 ordinary differential equations modeling the fluctuations in concentrations of desensitized receptors, $G_\alpha GTP$, $G_\alpha GDP$, and $G_{\beta\gamma}$:

$$\frac{d[R_{D1}]}{dt} = k_1([LR] + [LRG]) - k_2[R_{D1}] - k_3[R_{D1}] + k_4[R_{D2}], \tag{6}$$

$$\frac{d[R_{D2}]}{dt} = k_3[R_{D1}] - [k_4 R_{D2}], \tag{7}$$

$$\frac{d[G_\alpha GTP]}{dt} = k_5[LRG] - k_6[G_\alpha GTP], \tag{8}$$

$$\frac{d[G_\alpha GDP]}{dt} = k_6[G_\alpha GTP] - k_7[G_\alpha GDP][G_{\beta\gamma}], \tag{9}$$

$$\frac{d[G_{\beta\gamma}]}{dt} = k_5[LRG] - k_7[G_\alpha GDP][G_{\beta\gamma}]. \tag{10}$$

Additionally, the total receptor mass, given by $[R_t]$, and the total G_s protein mass, given by $[G_t]$, are represented by auxiliary Equations (11)-(14) [38]:

$$[R_t] = [R_a] + [R_{D1}] + [R_{D2}], \tag{11}$$

$$[R_a] = [R] + [LR] + [LRG], \tag{12}$$

$$[G_t] = [G_{\alpha\beta\gamma}] + [G_{\beta\gamma}], \tag{13}$$

$$[G_{\alpha\beta\gamma}] = [G] + [LRG]. \tag{14}$$

$[R_a]$ is the mass of activated GLP-1 receptors, and $[G_{\alpha\beta\gamma}]$ represents the complexes that contain the fully combined G_s trimer [38].

From a mathematical standpoint, this model as presented is only partially complete. There are no differential equations describing the change in concentrations of the free receptors, GLP-1 bound receptors, and complete G_s complexes, which are crucial components of the GLP-1 receptor activation process. To fully understand the GLP-1 receptor dynamics presented by Takeda et al., a complete model is essential. Therefore, we will derive the missing differential equations given by $\frac{d[R]}{dt}$, $\frac{d[LR]}{dt}$, and $\frac{d[G]}{dt}$ to develop this completed model of GLP-1 receptor signaling.

4 Model Development

The beauty of mathematical models is their ability to convey crucial information about biological processes without the need to run multiple trials on human subjects. By running multiple simulations, the range of possibilities is narrowed down, and conducting efficient clinical trials becomes

easier. In order to better understand the biological processes underlying the incretin effect, the complex relationship between insulin and testosterone, and GLP-1 receptor signaling in pancreatic $\beta-$cells, we can examine systems of differential equations.

The model developed in this paper consists of 2 major submodels, as outlined in Figure 11. We will first provide separate overviews of the GLP-1 receptor activation model, the incretin model, and the model of insulin-mediated testosterone production. Then, we will create our combined model in Figure 11 by incorporating the influence of Ozempic.
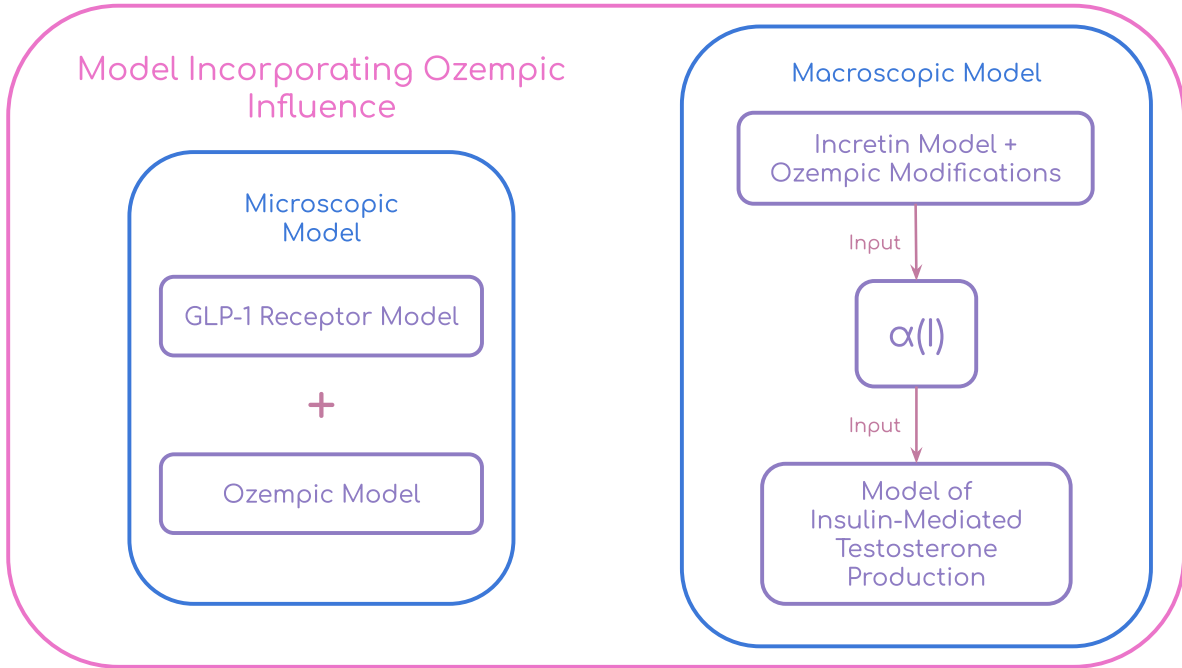
Figure 11: Overview of the combined model presented in this paper.

4.1 Completed Model of GLP-1 Receptor Signaling

The original Takeda et al. model is missing important differential equations $\frac{d[R]}{dt}$, $\frac{d[LR]}{dt}$, and $\frac{d[G]}{dt}$, but it is possible to derive them using the equations given and the model assumptions. This model assumes total masses $[R_t]$ and $[G_t]$ remain constant, so $\frac{d[R_t]}{dt}$ and $\frac{d[G_t]}{dt}$ both equal zero [38]. Therefore, taking the first derivative of Equations (11) and (13) with respect to time yields

$$0 = \frac{d[R]}{dt} + \frac{d[LR]}{dt} + \frac{d[LRG]}{dt} + \frac{d[R_{D1}]}{dt} + \frac{d[R_{D2}]}{dt}, \tag{15}$$

$$0 = \frac{d[G]}{dt} + \frac{d[LRG]}{dt} + \frac{d[G_{\beta\gamma}]}{dt}. \tag{16}$$

Due to the assumption that the reactions between GLP-1 and R and LR and G reach instantaneous equilibrium, we also have that $K_{d_1}[LR] = [GLP1][R]$ and $K_{d_2}[LRG] = [LR][G]$, where $[GLP1]$ is

the concentration of GLP-1, K_{d_1} is the dissociation constant for GLP-1 and R, and K_{d_2} is the dissociation constant for LR and G. This implies

$$[LR] = \frac{[GLP1][R]}{K_{d_1}}, \tag{17}$$

$$[GLP1] = \frac{K_{d_1}[LR]}{[R]}, \tag{18}$$

$$[LRG] = \frac{[LR][G]}{K_{d_2}}. \tag{19}$$

We can also write $[LRG]$ in terms of the concentrations of receptors and the concentrations of G_s proteins using Equations (11) and (13), which imply that $[LRG] = [R_t] - [R] - [LR] - [R_{D1}] - [R_{D2}]$ and $[LRG] = [G_t] - [G] - [G_{\beta\gamma}]$.

We first take the derivatives of Equations (17) and (19) with respect to time, giving us

$$\frac{d[LR]}{dt} = \frac{1}{K_{d_1}}\left[[GLP1]\frac{d[R]}{dt} + [R]\frac{d[GLP1]}{dt}\right], \tag{20}$$

$$\frac{d[LRG]}{dt} = \frac{1}{K_{d_2}}\left[[LR]\frac{d[G]}{dt} + [G]\frac{d[LR]}{dt}\right]. \tag{21}$$

In this initial construction of the expanded Takeda et al. model, we can assume that at the cellular level the concentration of the ligand outside of the cell is constant due to the high volume of hormones released during certain body functions compared to the volume of the cell [22]. Therefore, $\frac{d[GLP1]}{dt}$ is 0, so Equation (20) becomes

$$\frac{d[LR]}{dt} = \frac{[GLP1]}{K_{d_1}} \cdot \frac{d[R]}{dt}. \tag{22}$$

Then, combining Equations (10), (16), and (21) gives us

$$0 = \frac{d[G]}{dt} + \frac{[LR]}{K_{d_2}} \cdot \frac{d[G]}{dt} + \frac{[G]}{K_{d_2}} \cdot \frac{d[LR]}{dt} + k_5[LRG] - k_7[G_\alpha GDP][G_{\beta\gamma}]$$

We then solve this equation for $\frac{d[G]}{dt}$ by first rearranging it to get

$$k_7[G_\alpha GDP][G_{\beta\gamma}] - k_5[LRG] - \frac{[G]}{K_{d_2}} \cdot \frac{d[LR]}{dt} = \frac{d[G]}{dt}\left(1 + \frac{[LR]}{K_{d_2}}\right).$$

By dividing both sides of this equation by $1 + \frac{[LR]}{K_{d_2}}$ and substituting $[G_t] - [G] - [G_{\beta\gamma}]$ in for $[LRG]$, we derive the differential equation $\frac{d[G]}{dt}$:

$$\frac{d[G]}{dt} = \frac{k_7[G_\alpha GDP][G_{\beta\gamma}] - k_5\left([G_t] - [G] - [G_{\beta\gamma}]\right) - \frac{[G]}{K_{d_2}} \cdot \frac{d[LR]}{dt}}{1 + \frac{[LR]}{K_{d_2}}}. \tag{23}$$

The term $1 + \frac{[LR]}{K_{d_2}}$ in the denominator reflects the inhibitory nature of GLP-1 receptor binding on G_s trimer accumulation, as the activation of the receptor causes the trimer to split. Finally, to find $\frac{d[R]}{dt}$, we first combine Equations (6), (7), (15) to get

$$0 = \frac{d[R]}{dt} + \frac{d[LR]}{dt} + \frac{d[LRG]}{dt} + k_1([LR] + [LRG]) - k_2[R_{D1}].$$

Since $[LRG] = [G_t] - [G] - [G_{\beta\gamma}]$, it follows that $\frac{d[LRG]}{dt} = -\frac{d[G]}{dt} - \frac{d[G_{\beta\gamma}]}{dt}$, so we substitute this into the above equation along with Equation (10):

$$0 = \frac{d[R]}{dt} + \frac{d[LR]}{dt} - \frac{d[G]}{dt} - (k_5[LRG] - k_7[G_\alpha GDP][G_{\beta\gamma}]) + k_1([LR] + [LRG]) - k_2[R_{D1}].$$

Then, by rearranging this equation and combining it with Equations (22) and (23), we get

$$k_2[R_{D1}] - k_1([LR] + [LRG]) - (k_7[G_\alpha GDP][G_{\beta\gamma}] - k_5[LRG])$$

$$= \frac{d[R]}{dt} + \frac{[GLP1]}{K_{d_1}} \cdot \frac{d[R]}{dt} + \frac{\frac{[G]}{K_{d_2}} \cdot \frac{[GLP1]}{K_{d_1}}}{1 + \frac{[LR]}{K_{d_2}}} \cdot \frac{d[R]}{dt}$$

$$- \frac{k_7[G_\alpha GDP][G_{\beta\gamma}] - k_5[LRG]}{1 + \frac{[LR]}{K_{d_2}}},$$

By adding the term $\frac{k_7[G_\alpha GDP][G_{\beta\gamma}] - k_5[LRG]}{1 + \frac{[LR]}{K_{d_2}}}$ to the left side of the equation, we can factor out $(k_7[G_\alpha GDP][G_{\beta\gamma}] - k_5[LRG])$ from two terms on the left side, and we can factor out $\frac{d[R]}{dt}$ from every term on the right side of the equation to get

$$k_2[R_{D1}] - k_1([LR] + [LRG]) + (k_7[G_\alpha GDP][G_{\beta\gamma}] - k_5[LRG])\left[\frac{1}{1 + \frac{[LR]}{K_{d_2}}} - 1\right]$$

$$= \frac{d[R]}{dt}\left(1 + \frac{[GLP1]}{K_{d_1}} + \frac{\frac{[G]}{K_{d_2}} \cdot \frac{[GLP1]}{K_{d_1}}}{1 + \frac{[LR]}{K_{d_2}}}\right).$$

We can also simplify $\frac{1}{1 + \frac{[LR]}{K_{d_2}}} - 1$ and $\frac{\frac{[G][GLP1]}{K_{d_1}K_{d_2}}}{1 + \frac{LR}{K_{d_2}}}$:

$$\frac{1}{1 + \frac{[LR]}{K_{d_2}}} - 1 = \frac{1 - \left(1 + \frac{[LR]}{K_{d_2}}\right)}{1 + \frac{[LR]}{K_{d_2}}} = \frac{-\frac{[LR]}{K_{d_2}}}{1 + \frac{[LR]}{K_{d_2}}} = -\frac{[LR]}{K_{d_2} + [LR]},$$

$$\frac{\frac{[G][GLP1]}{K_{d_1}K_{d_2}}}{1 + \frac{LR}{K_{d_2}}} = \frac{[G][GLP1]}{K_{d_1}K_{d_2}} \cdot \frac{1}{1 + \frac{[LR]}{K_{d_2}}} = \frac{[G][GLP1]}{K_{d_1}(K_{d_2} + [LR])}.$$

Then, after substituting $[R_t] - [R] - [LR] - [R_{D1}] - [R_{D2}]$ and $[G_t] - [G] - [G_{\beta\gamma}]$ for $[LRG]$, the equation for $\frac{d[R]}{dt}$ is

$$\frac{d[R]}{dt} = \frac{k_2[R_{D1}] - k_1([R_t] - [R] - [R_{D1}] - [R_{D2}])}{1 + \frac{[GLP1]}{K_{d_1}} + \frac{[G][GLP1]}{K_{d_1}(K_{d_2}+[LR])}}$$

$$- \frac{(k_5([G_t] - [G] - [G_{\beta\gamma}]) - k_7[G_\alpha GDP][G_{\beta\gamma}])\left[\frac{[LR]}{K_{d_2}+[LR]}\right]}{1 + \frac{[GLP1]}{K_{d_1}} + \frac{[G][GLP1]}{K_{d_1}(K_{d_2}+[LR])}}, \quad (24)$$

where $\frac{[LR]}{K_{d_2}+[LR]}$ is a Michaelis-Menten equation describing the reaction rate of $[LR]$. The inclusion of the terms $\frac{[GLP1]}{K_{d_1}}$ and $\frac{[G][GLP1]}{K_{d_1}(K_{d_2}+[LR])}$ in the denominator reflects how GLP-1 receptor binding and GLP-1 and G_s protein complex interactions inhibit the accumulation of free receptors. It is important to note that in the derivation of $\frac{d[R]}{dt}$, the second term initially contains $(k_7[G_\alpha GDP][G_{\beta\gamma}] - k_5[LRG])$ in the numerator; however, we switch $(k_7[G_\alpha GDP][G_{\beta\gamma}] - k_5([G_t] - [G] - [G_{\beta\gamma}]))$ to be $(k_5([G_t] - [G] - [G_{\beta\gamma}]) - k_7[G_\alpha GDP][G_{\beta\gamma}])$ to better fit the model results from Takeda et al. [38].

4.1.1 Adenylyl cyclase system submodel

Since cyclic AMP, or cAMP, is rapidly accumulated after the activation of a GLP-1 receptor and is a primary contributor to the release of insulin from the $\beta-$cell, the Takeda et al. model also contains a differential equation describing the change in concentration of cAMP after the activation of the GLP-1 receptor, adapted from an earlier model of Ca^{2+}-mediated regulation of cAMP and G coupled protein receptors by Fridlyand et al. [11, 38]:

$$\frac{d[cAMP]}{dt} = V_{AC_t} - V_{PDE}. \tag{25}$$

V_{AC_t} gives the total activity of the adenylyl cyclase (AC) system activated by $G_\alpha GTP$, and V_{PDE} is the activity of phosphodiesterase (PDE), the enzyme that inactivates cAMP [1, 38]. V_{AC_t} is given in turn by the auxiliary equation

$$V_{AC_t} = V_{AC} + V_{AC_G}, \tag{26}$$

where V_{AC} is the activity of the part of AC system that maintains basal cAMP levels without activitation by G proteins and V_{AC_G} is the activity of the part of AC system activated by G proteins [38]. V_{AC} is defined as

$$V_{AC} = V_{max_{AC}} \cdot \frac{0.4}{0.4 + [G_\alpha GTP]} \cdot \frac{[ATP]}{[ATP] + 1030}, \tag{27}$$

where $V_{max_{AC}}$ is the maximum basal AC activity [38]. The term $\frac{0.4}{0.4+[G_\alpha GTP]}$ reflects the baseline activity of the $G_\alpha GTP$ subunit in regulating the AC system without activation of the GLP-1 receptor and $\frac{[ATP]}{[ATP]+1030}$ is the ATP dependent basal AC activity [38]. V_{AC_G} is given by

$$V_{AC_G} = V_{max_{AC_G}} \cdot \frac{[G_\alpha]GTP}{0.4 + [G_\alpha GTP]} \cdot \frac{[ATP]}{[ATP] + 315}$$
$$\cdot \left((1 - f_{Cd_{AC}}) + f_{Cd_{AC}} \cdot \frac{[Ca_3CaM] + [Ca_4CaM]}{[Ca_3CaM] + [Ca_4CaM] + 0.348} \cdot \frac{75}{75 + [Ca^{2+}]} \right). \tag{28}$$

V_{AC_G} is the product of Michaelis-Menten equations describing reaction rates of $G_\alpha GTP$, ATP and calmodulin compounds ($Ca_x CaM$), which consist of multiple Ca^{2+} atoms and regulate both the AC system and the PDE system [11, 38]. The inclusion of these equations in equation 28 reflects the stimulatory effects of $G_\alpha GTP$, ATP, Ca_3CaM, and Ca_4CaM on the AC system when it is activated by G_s proteins [11, 38]. The term $\frac{75}{75+[Ca^{2+}]}$ represents the inhibitory nature of free Ca^{2+}

atoms on the AC system [11, 38]. $f_{Cd_{AC}}$ is the fraction of the AC system regulated by G_s proteins that is dependent on Ca^{2+} [38]. The last term of Equation (25), V_{PDE}, is defined as

$$V_{PDE} = V_{max_{PDE}} \left(\frac{f[cAMP]}{[cAMP] + K_{mL}} + \frac{(1-f)[cAMP]}{[cAMP] + K_{mH}} \right)$$
$$\cdot \left((1 - f_{Cd_{PDE}}) + f_{Cd_{PDE}} \cdot \frac{[Ca_3CaM] + [Ca_4CaM]}{[Ca_3CaM] + [Ca_4CaM] + 0.348} \right). \quad (29)$$

$V_{max_{PDE}}$ is the maximal activity of the PDE system [11, 38]. Since evidence indicates there are two different fractions of PDE that act on cAMP, $\frac{f[cAMP]}{[cAMP]+K_{mL}} + \frac{(1-f)[cAMP]}{[cAMP]+K_{mH}}$ is the sum of two Michaelis-Menten equations, where $\frac{f[cAMP]}{[cAMP]+K_{mL}}$ represents the activity of one fraction f of PDE on cAMP regulation and $\frac{(1-f)[cAMP]}{[cAMP]+K_{mH}}$ is the activity of the remaining fraction of PDE [38]. Additionally, there is a form of PDE known as PDE1C that is sensitive to calmodulin compounds and plays an extremely important role in cAMP degradation in $\beta-$cells [38]. The role of PDE1C is represented in Equation (29) through the term $(1 - f_{Cd_{PDE}}) + f_{Cd_{PDE}} \cdot \frac{[Ca_3CaM]+[Ca_4CaM]}{[Ca_3CaM]+[Ca_4CaM]+0.348}$ [38].

For the purposes of model simplification and focusing on the role of GLP-1 receptor activation on $\beta-$cell regulation as opposed to other complicated intracellular complexes, $[Ca^{2+}]$ and $[ATP]$ are assumed to be constant [38]. $[Ca_3CaM]$ and $[Ca_4CaM]$, in addition to $[Ca_2CaM]$ and $[CaCaM]$ from the calcium-calmodulin reactions prior to the creation of Ca_3CaM and Ca_4CaM, are given by the following equations from Fridlyand et al. [11]:

$$\frac{d[CaCaM]}{dt} = k_{1f}[Ca^{2+}][CaM] - k_{1b}[CaCaM], \quad (30)$$

$$[Ca_2CaM] = \frac{k_{2f}}{k_{2b}}[Ca^{2+}][CaCaM], \quad (31)$$

$$[Ca_3CaM] = \frac{k_{3f}}{k_{3b}}[Ca^{2+}][Ca_2CaM], \quad (32)$$

$$[Ca_4CaM] = \frac{k_{4f}}{k_{4b}}[Ca^{2+}][Ca_3CaM]. \quad (33)$$

While the rate of the initial reaction of CaM and Ca^{2+} is not assumed to be at instantaneous equilibrium, the subsequent reactions are, due to the rapid nature of these reactions compared to other reactions within the $\beta-$cell, such as steady state and slow $[Ca^{2+}]$ and $[cAMP]$ oscillations [11]. The rate constants in Equations (30)-(33) were taken from an earlier study by Yu et al. on Ca^{2+} and cAMP regulation of neurons and adapted to fit $\beta-$cells [11, 43].

Although it is valid, based on previous models of G coupled protein receptors, to assume initially that external GLP-1 concentration is constant, that does not provide a realistic picture of changes in GLP-1 concentration as it interacts with GLP-1 receptors [22]. Now that we have a complete version of the Takeda et al. model, we can include a differential equation representing the change in non-constant GLP-1 concentration. Siewe and Friedman developed a mathematical model that simulates the effect of Ozempic on GLP-1 concentration and contains a differential equation describing the

rate of change of GLP-1 concentration, which we can modify to fit our current model [36]:

$$\frac{d[GLP1]}{dt} = \gamma_L - \mu_{LR}[GLP1][R]. \tag{34}$$

γ_L is the "baseline secretion rate of GLP-1", and μ_{LR} is the rate at which free GLP-1 concentration diminishes as GLP-1 binds to free GLP-1 receptors [36]. Since we now have a non-zero $\frac{d[GLP1]}{dt}$, $\frac{d[LR]}{dt}$ becomes

$$\frac{d[LR]}{dt} = \frac{1}{K_{d_1}}\left[[GLP1]\frac{d[R]}{dt} + [R]\frac{d[GLP1]}{dt}\right],$$

as initially described in Equation (20). Applying the same methods we used to initially derive $\frac{d[R]}{dt}$, the new equation for $\frac{d[R]}{dt}$ under a non-constant GLP-1 concentration is

$$\frac{d[R]}{dt} = \frac{k_2[R_{D1}] - k_1([R_t] - [R] - [R_{D1}] - [R_{D2}])}{1 + \frac{[GLP1]}{K_{d_1}} + \frac{[G][GLP1]}{K_{d_1}(K_{d_2}+[LR])}}$$
$$- \frac{(k_5([G_t] - [G] - [G_{\beta\gamma}]) - k_7[G_\alpha GDP][G_{\beta\gamma}])\left[\frac{[LR]}{K_{d_2}+[LR]}\right] + \frac{[G][R]}{K_{d_1}(K_{d_2}+[LR])} \cdot \frac{d[GLP1]}{dt}}{1 + \frac{[GLP1]}{K_{d_1}} + \frac{[G][GLP1]}{K_{d_1}(K_{d_2}+[LR])}}. \tag{35}$$

The term $\frac{[G][R]}{K_{d_1}(K_{d_2}+[LR])} \cdot \frac{d[GLP1]}{dt}$ represents the interactions of G_s protein trimer and GLP-1 with the free receptor during the binding process. The equation $\frac{d[G]}{dt}$ remains unchanged, as all of the changes are contained in the $\frac{d[LR]}{dt}$ term.

The Siewe and Friedman model can also be used to add Ozempic to our model to simulate the effect of Ozempic on GLP-1 receptors and cAMP accumulation in the $\beta-$cell [36]. However, before proceeding with this additional modification, it is important to have an understanding of the interactions between GLP-1 and insulin at the macroscopic level as well as the cellular level. To that end, we will next examine a mathematical model of the incretin effect developed by Brubaker et al. [2].

4.2   Model of the Incretin Effect

The incretin effect describes the release of hormones to stimulate insulin secretion in response to glucose ingestion [2]. In addition to GLP-1, glucose-dependent insulinotropic peptide, or GIP, has been identified as another major incretin hormone [2]. These hormones are released in response to elevated glucose levels in the intestines to regulate blood sugar levels by stimulating insulin release [2]. In order to analyze the dynamics of incretins and insulin and the effects of elevated incretin levels on the release of insulin, Brubaker, et al. created a system of three ordinary differential equations to model incretin levels, insulin levels and glucose levels of time after the introduction of glucose into the duodenum, the first part of the small intestines [2, 30]. This rate of delivery of 100 grams of glucose, denoted $Duod_G(100g)$, to the duodenum can be modeled using the following

piecewise function [2]:

$$Duod_G(100g) = \begin{cases} 0 & \text{if } 0 \leq t < 5 \\ 6.349 - 0.0353t & \text{if } 5 \leq t \leq 179.9 \\ 0 & \text{if } 179.9 < t \end{cases}, \tag{36}$$

where time t is measured in minutes. The spike in the glucose delivery rate occurs approximately 5 minutes after liquid glucose ingestion, as this glucose is transferred very rapidly from the stomach to the duodenum [2]. After glucose enters the duodenum, it is absorbed into the bloodstream and distributed to the gastrointestinal tract via mesenteric circulation [2]. The rate of change in blood glucose kinetics, denoted by $Ra_{GutG}(100g)$, is given by Equation 37 [2]:

$$Ra_{GutG}(100g) = \begin{cases} 0 & \text{if } 0 \leq t < 5 \\ 0.36(t-5)^{1.05}e^{-0.029(t-5)} & \text{if } 5 \leq t \end{cases}. \tag{37}$$

Hepatic glucose balance, given by $Hepbal_G$, is the net absorption and production of glucose by the liver [2]. After glucose is distributed to the GI tract, $Hepbal_G$ is no longer at equilibrium and becomes a time dependent parameter given by

$$Hepbal_G = Hepbal_{GB} + M(G_B - Gluc)I. \tag{38}$$

$Gluc$ and I are state variables representing glucose and insulin levels respectively. G_B is the basal glucose level, given by $Gluc(0)$, $Hepbal_{GB}$ is the basal hepatic glucose balance, and M measures "effects of counter-regulatory factors on the liver" and changes to reflect hypoglycemic conditions [2]. The parameter values are given in Table 1 in Appendix 1.

Because GIP and GLP-1 are both believed to contribute to the incretin effect equally, Brubaker, et al. created one differential equation to account for both hormones in the system:

$$\frac{dInc}{dt} = \frac{Ra_{Inc}}{V} + k_5 Duod_G - k_6 Inc, \tag{39}$$

where Ra_{Inc} represents the rate of introduction of incretin hormones over volume V, $k_5 Duod_G$ measures the glucose levels in the upper GI tract and and $k_6 Inc$ is the clearance rate of incretin hormones from the GI tract [2]. In addition to modeling incretin kinetics, Brubaker et al. also modeled insulin kinetics and glucose kinetics in this system. The differential equation representing change in insulin levels in the system is given by

$$\frac{dI}{dt} = k_7 Gluc^{1.3} + k_8 Inc - k_9 I + \beta, \tag{40}$$

where $k_7 Gluc^{1.3}$ reflects the influence of plasma glucose on accelerating the release of insulin, $k_8 Inc$ reflects the incretin effect on the $\beta-$cell, $k_9 I$ is the clearance rate of insulin, and β is a constant representing the influence of known regulators of the $\beta-$cell [2]. The differential equation representing glucose kinetics in this system is given by

$$\frac{dGluc}{dt} = \frac{Ra_{GutG}}{V} + \frac{Hepbal_G}{V} - k_1 Gluc^{1.3} - k_2 I + \gamma \frac{dI}{dt}. \tag{41}$$

As mentioned previously, Ra_{GutG} and $Hepbal_G$ represent mesenteric circulation and balance of glucose in the liver over a volume V [2]. Non-insulin mediated glucose uptake is represented by $k_1Gluc^{1.3}$, while insulin-mediated glucose uptake is represented by k_2I [2]. $\gamma\frac{dI}{dt}$ reflects the impact of changing insulin levels on glucose production and absorption [2]. By using MATLAB to solve this system, we can visualize the fluctuations in insulin levels due to the incretin effect, as well as changes in incretin and glucose levels over a period of 300 minutes. Figure 12 depicts the solutions to Equations (39)-(41).
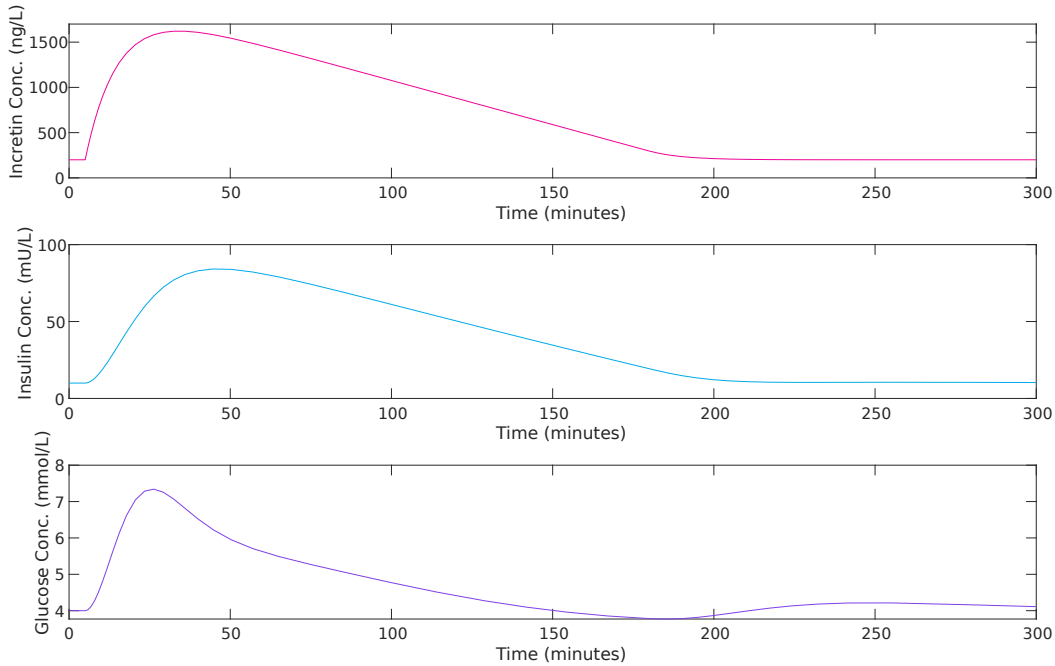
Figure 12: Plasma insulin, incretin and glucose levels from time 0 to 300 minutes.

For the first 5 minutes after measurements begin, insulin, incretin and glucose remain at basal levels. After glucose is ingested into the duodenum, incretin and insulin levels increase sharply. Glucose levels peak around 25 minutes after initial glucose consumption, while insulin and incretin levels peak around 50 minutes after initial consumption. The plasma levels of all three substances then gradually decline until they reach basal levels again around the 180 minute mark. Glucose level dip below basal levels of 4 mmol/L before returning to initial levels.

We can see from Figure 12 that an initial spike in glucose concentration in the GI tract leads to a dramatic increase in plasma incretin concentration. This in turn causes an increase in insulin concentration. The incretin effect becomes more apparent by setting $Duod_G$ equal to zero, which forces incretins to remain at basal levels for the entire 300 minute period. Figure 13 depicts the changes in insulin and glucose concentration when incretin concentration remains at the basal level of 200 ng/L.
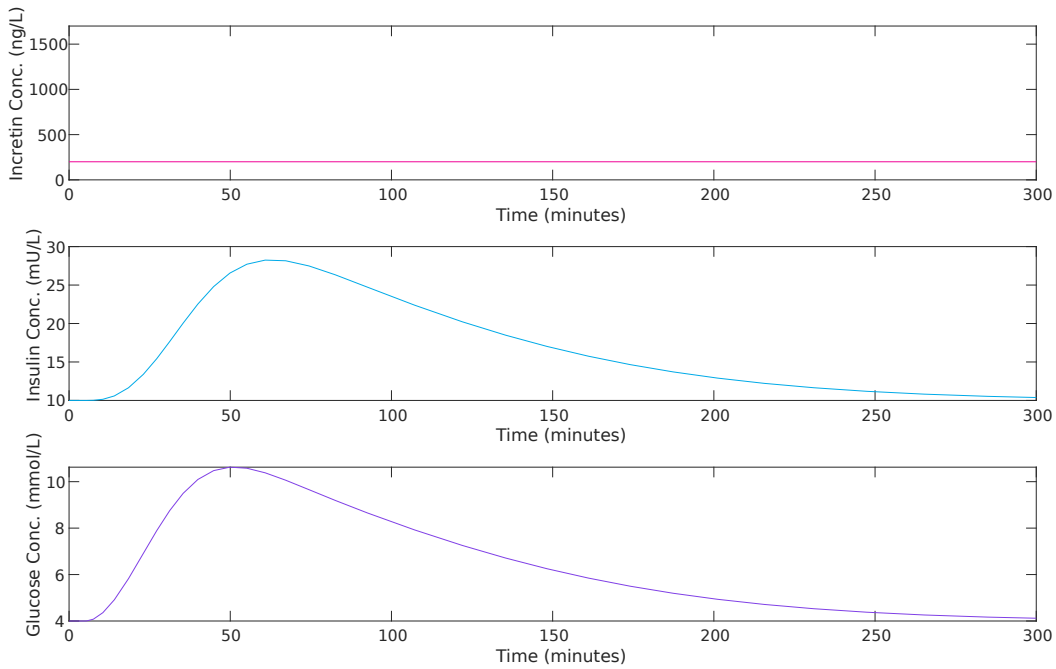
Figure 13: Plasma insulin and glucose levels when plasma incretin concentration remains at basal levels.

Under these conditions, glucose concentration reaches a peak level of approximately 9.5 mmol/L and insulin reaches a peak concentration of 25 mU/L. The glucose levels are much higher than they would be under normal incretin conditions, while insulin concentration is significantly lower without the incretin effect. While insulin still increases in repsonse to increased glucose levels, the link between insulin and incretin hormones is clear. GLP-1 plays a critical role in maintaining the balance between insulin and glucose and is crucial in preventing insulin abnormalities.

The previously mentioned Siewe-Friedman model of Ozempic-mediated GLP-1 regulation also contains a regulatory term for glucose levels, as GLP-1 and GLP-1 receptor agonists lower blood glucose levels [20, 36]. We can use the Siewe-Friedman model to modify this model in addition to the expanded Takeda et al. model to simulate the effects on Ozempic on insulin release. Before taking that final step, however, we need to understand the relationship between insulin and testosterone in the ovulatory cycle in order to form a connection between semaglutide and PCOS treatment. The Graham-Selgrade model provides a mathematical basis for this relationship [14].

4.3   Model of Ovulatory Regulation

The Graham-Selgrade model is a system of 12 ordinary differential equations modeling the fluctuations in reproductive hormones and ovarian follicle growth during the menstrual cycle [14]. More specifically, the Graham-Selgrade model examines the effects of "insulin-mediated testos-

terone production on ovulatory function," providing insight into the crucial link between insulin and testosterone [14].

As hyperinsulinemia is a symptom of many PCOS cases, it is critical to incorporate insulin into a mathematical model of the ovulatory cycle. Research has found that reducing plasma insulin levels by taking insulin sensitizing drugs, such as metformin and thiazolidiones, reduces testosterone levels [14]. However, testosterone is important in the ovulatory cycle as a regulator of LH synthesis, so it is important to maintain normal levels of the androgen [14]. The production and release of pituitary hormones LH and FSH is modeled in a subsystem of 4 ordinary differential equations [14]. These equations include both serum LH and FSH circulating in the bloodstream, indicated by state variables LH and FSH respectively, and LH and FSH on reserve in the pituitary gland that is released into the bloodstream, indicated by LH_ρ and FSH_ρ respectively.

$$\frac{dFSH_\rho}{dt} = \frac{v_F}{1 + c_{F,I}\frac{S\Lambda}{K_{F,I}+\Lambda}} - k_F\frac{1 + c_{F,P}P_4}{1 + c_{F,E}E_2^2}FSH_\rho, \tag{42}$$

$$\frac{dFSH}{dt} = \frac{1}{V} \cdot k_F\frac{1 + c_{F,P}P_4}{1 + c_{F,E}E_2^2}FSH_\rho - \delta_F FSH, \tag{43}$$

$$\frac{dLH_\rho}{dt} = \left[v_{0L} \cdot \frac{T}{K_{L,T}+T} + v_{1L} \cdot \frac{E_2^n}{K_{mL}^n + E_2^n}\right] \cdot \frac{1}{1 + \frac{P_4}{K_{iL,P}(1+c_{L,T}T)}} - k_L\frac{1 + c_{L,P}P_4}{1 + c_{L,E}E_2}LH_\rho, \tag{44}$$

$$\frac{dLH}{dt} = \frac{1}{V} \cdot k_L\frac{1 + c_{L,P}P_4}{1 + c_{L,E}E_2}LH_\rho - \delta_L LH. \tag{45}$$

In Equation (42), v_F is the velocity of the reaction which produces FSH, and the term $\frac{S\Lambda}{K_{F,I}+\Lambda}$ in the denominator reflects the suppression of FSH synthesis during the luteal phase of the ovulatory cycle [14, 17]. $K_{F,I}$ is the concentration of inhibin required to inhibit FSH synthesis, and the term E_2^2 in the denominator of $\frac{1+c_{F,P}P_4}{1+c_{F,E}E_2^2}$ reflects the inhibitory effects of E_2 on FSH release [14, 17]. Similarly, the term E_2 in the denominator of $\frac{1+c_{L,P}P_4}{1+c_{L,E}E_2}$ in Equations (44) and (45) reflects the less pronounced inhibitory effect of E_2 on LH release, which the presence of P_4 in the numerators of these terms reflects the positive effect of P_4 on FSH and LH release [14, 33]. $\frac{1}{V}$ accounts for blood FSH and LH concentration. k_F and k_L are the release rates of FSH and LH respectively, and δ_F and δ_L are the clearance rates of FSH and LH [14].

In Equation (44), v_{0L} is the maximal saturation rate of testosterone dependent LH synthesis given by the term $\frac{T}{K_{L,T}+T}$, where $K_{L,T}$ is the concentration of testosterone needed to promote LH synthesis [14, 16]. v_{1L} is the velocity of the reaction between E_2 and LH and K_{mL} is the half-maximal concentration of LH [14, 16]. Heightened E_2 levels over an extended period promote LH synthesis, which is reflected in the Hill function $\frac{v_{1L}E_2^n}{K_{mL}^n+E_2^n}$ with a Hill coefficient of $n = 8$ [14, 33]. The Hill function increases rapidly as E_2 levels rise to account for the rapid synthesis of LH during this period [14, 17].

The appearance of P_4 in the denominator of the term $\frac{1}{1+\frac{P_4}{K_{iL,P}(1+c_{L,T}T)}}$ reflects the inhibitory effects of P_4 on LH synthesis [14]. However, it is currently theorized that testosterone inhibits P_4's

suppressive effects, which would explain why people with hyperandrogenic PCOS have higher blood LH concentration than normal [14]. This reduction in P_4 mediated LH suppression is given by the term $K_{iL,P}(1 + c_{L,T}T)$ [14]. $c_{F,I}$, $c_{F,E}$, $c_{F,P}$, $c_{L,T}$, $c_{L,E}$, and $c_{L,P}$ are all dimensionless parameters of E_2, P_4 and T, respectively [14]. The values of all parameters used in this first submodel can be found in Table 3 in the appendix [14]. By using MATLAB to solve this system of differential equations, we can better visualize the pituitary hormone dynamics during ovulation. Figure 14 depicts the solutions to Equations (42)-(45) over a 400 day period.
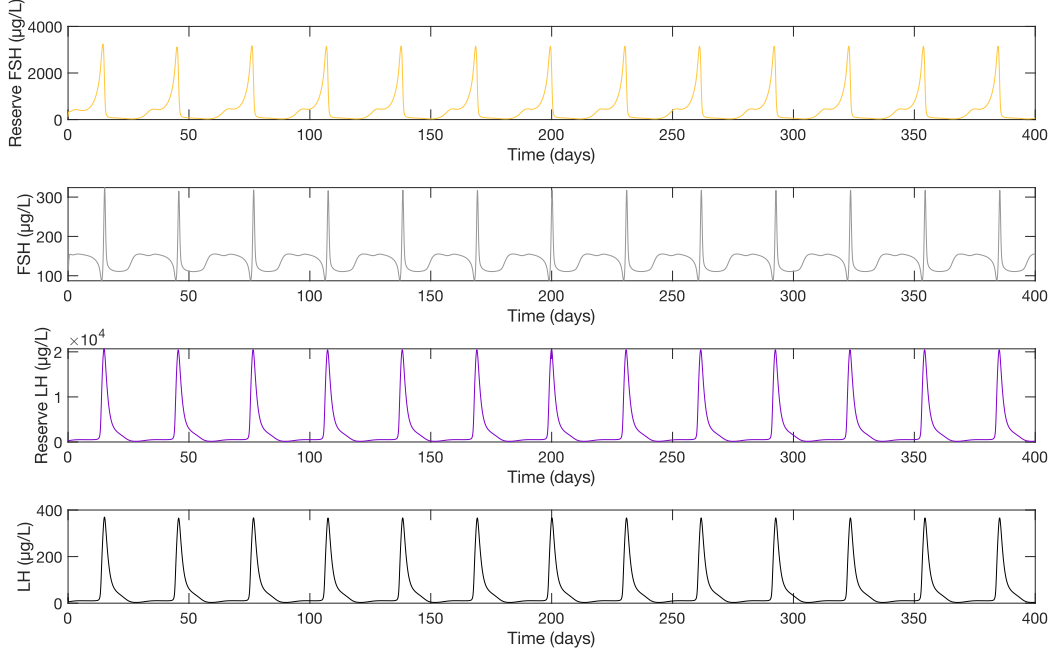
Figure 14: Pituitary hormone dynamics over 400 days.

The second subsystem of this model reflects follicular dynamics during the ovulatory cycle [14]. The ovulatory cycle consists of the follicular phase Φ, the ovulatory phase Ω and the luteal phase Λ [14]. LH support, which can be seen as a "permissive state during which normal luteal activity, specifically luteal growth and hormone production can occur", is given by Equation (49) [14]. Modeling follicle dynamics plays a crucial role in enhancing understanding of ovulation and of testosterone's role in ovulation, as it is assumed that testosterone is responsible for increasing FSH sensitivity [14].

$$\frac{d\Phi}{dt} = f_0 \cdot \frac{T}{T_0} + \left[\frac{f_1 FSH^2}{\left(\frac{h_1}{1+\frac{T}{T_0}}\right)^2 + FSH^2} - \frac{f_2 LH^2}{\left(\frac{h_2}{1+c_{\Phi,F}FSH}\right)^2 + LH^2} \right] \cdot \Phi, \tag{46}$$

$$\frac{d\Omega}{dt} = \frac{f_2 LH^2}{\left(\frac{h_2}{1+c_{\Phi,F}FSH}\right)^2 + LH^2} \cdot \Phi - wS\Omega, \tag{47}$$

$$\frac{d\Lambda}{dt} = wS\Omega - l(1-S)\Lambda, \tag{48}$$

$$\frac{dS}{dt} = \frac{\hat{s}LH^m}{h_s^m + LH^m} \cdot (1-S) - \delta_s S. \tag{49}$$

In Equation (46), T_0 is initial testosterone levels, and f_0 reflects the initial rate of follicular growth in terms of follicular mass [14]. f_1 represents the rate of follicular mass increase in response to FSH, and the term $\frac{h_1}{1+\frac{T}{T_0}}$ represents testosterone-mediated follicle sensitivity to LH [14]. f_2 represents the rate at which a mature follicle ruptures into luteal cells and forms the corpus luteum [14]. The term $\frac{f_2 LH^2}{\left(\frac{h_2}{1+c_{\Phi,F}FSH}\right)^2 + LH^2}$ represents the transition from the follicular phase to the ovulatory phase as mediated by FSH and LH [14]. In Equation (47), $wS\Omega$ represents the transition from the ovulatory phase to the luteal phase as mediated by LH support [14].

In Equation (48), the term $l(1-S)\Lambda$ is the rate of luteal regression, assuming that LH support maintains a healthy corpus luteum and prevents premature formation of luteal cells [14]. The term $\frac{\hat{s}LH^m}{h_s^m + LH^m}$ in Equation (49) reflects the extreme sensitivity of support to LH [14]. It is important to note that $0 \leq S(t) \leq 1$, and luteal stage terms are multiplied by S to reflect a "lack of activity in the absence of sufficient functional support by LH" [14]. δ_S reflects the decay of support in the absence of LH [14]. Values for these parameters can be found in Table 4 of the appendix. Figure 15 depicts the solutions to Equations (46)-(49), allowing us to see the transition between phases. Φ sharply decreases as Ω increases, and a rise in LH support prompts the start of Λ.
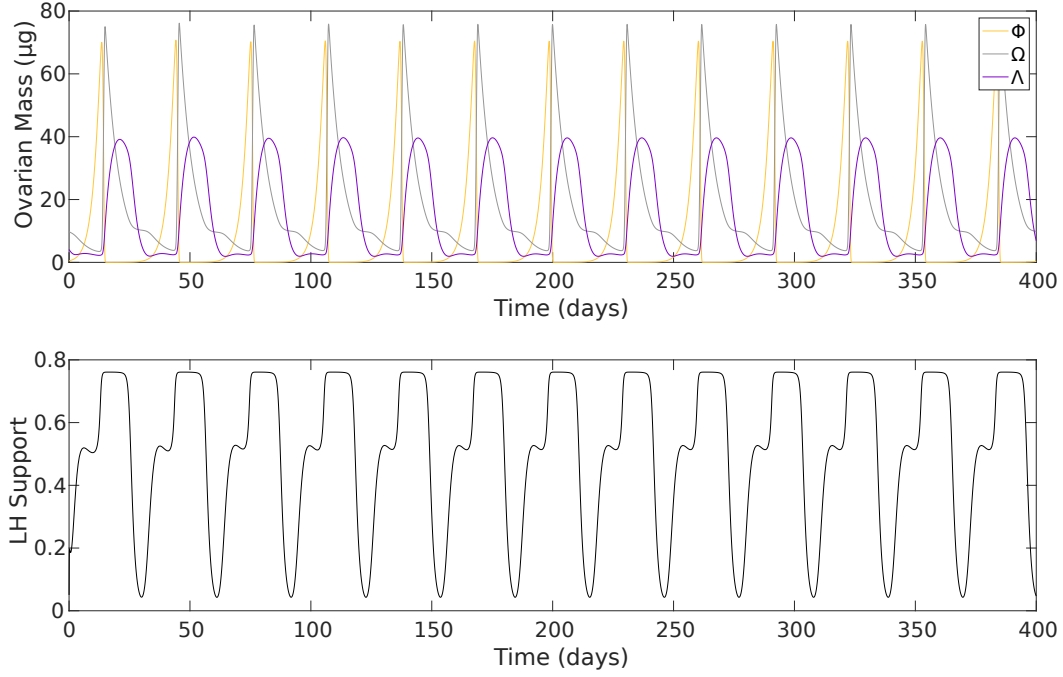
Figure 15: Ovarian follicle mass and LH support over 400 days.

A third subsystem represents the synthesis of ovarian hormones and reflects the influence of hyperinsulinemia on testosterone levels [14]. T reprsents serum testosterone in the bloodstream, T_γ represents testosterone concentration in granulosa cells, E_2 represents serum estradiol and P_4 represents serum progesterone [14].

$$\frac{dT}{dt} = t_0 - \delta_T T + [t_1 G_1 (F_1 + c_{T,F_2} F_2) + t_2 G_1 G_2 F_1]$$

$$\cdot \left[\Phi + \tau_1 \Omega + \tau_2 S \Lambda + \tau_3 \left(1 - \frac{\Phi + \Omega + \Lambda}{\Psi} \right) \right], \quad (50)$$

$$\frac{dT_\gamma}{dt} = t_{g_1} G_1 G_2 F_1 - \frac{t_{g_2} FSH}{h_3 + FSH} T_\gamma, \quad (51)$$

$$\frac{dE_2}{dt} = e_0 - \delta_E E_2 + \frac{t_{g_2} FSH}{h_3 + FSH} T_\gamma \cdot [\Phi + \eta \Lambda S], \quad (52)$$

$$\frac{dP_4}{dt} = -\delta_P P_4 + \frac{pLH}{LH + h_p} \cdot \Lambda S. \quad (53)$$

G_1 and G_2 reflect the influence of insulin in enzyme production for the creation of T. They are functions $G_1(I)$ and $G_2(I)$, but at basal insulin levels, $G_1 = G_2 = 1$ [14]. F_1 and F_2 are dose response curves reflecting testosterone production via LH, given by $F_1 = \frac{LH^2}{\kappa_1 LH^2 + \kappa_2 LH + \kappa_3}$ and $F_2 = \frac{LH}{\kappa_1 LH^2 + \kappa_2 LH + \kappa_3}$ [13, 14]. e_0 and t_0 reflect the initial E_2 and T concentration in reserve respectively, and δ_T, δ_E and δ_P are the clearance rates of T, E_2 and P_4 [14].

The terms $\frac{t_{g_2}FSH}{h_3+FSH}T_\gamma$ in Equations (51) and (52) and $[\Phi + \eta\Lambda S]$ in Equation (52) represents the influence of T on FSH dependent production of E_2 in granulosa cells [14]. In Equation (50), $\Phi + \tau_1\Omega + \tau_2 S\Lambda + \tau_3\left(1 - \frac{\Phi+\Omega+\Lambda}{\Psi}\right)$ reflects the ability of ovarian follicles to produce T [14]. Lastly, $\frac{pLH}{LH+h_p} \cdot \Lambda S$ represents the LH dependent synthesis of P_4 during the luteal phase. Figure 16 gives a plot of the solutions to this system.
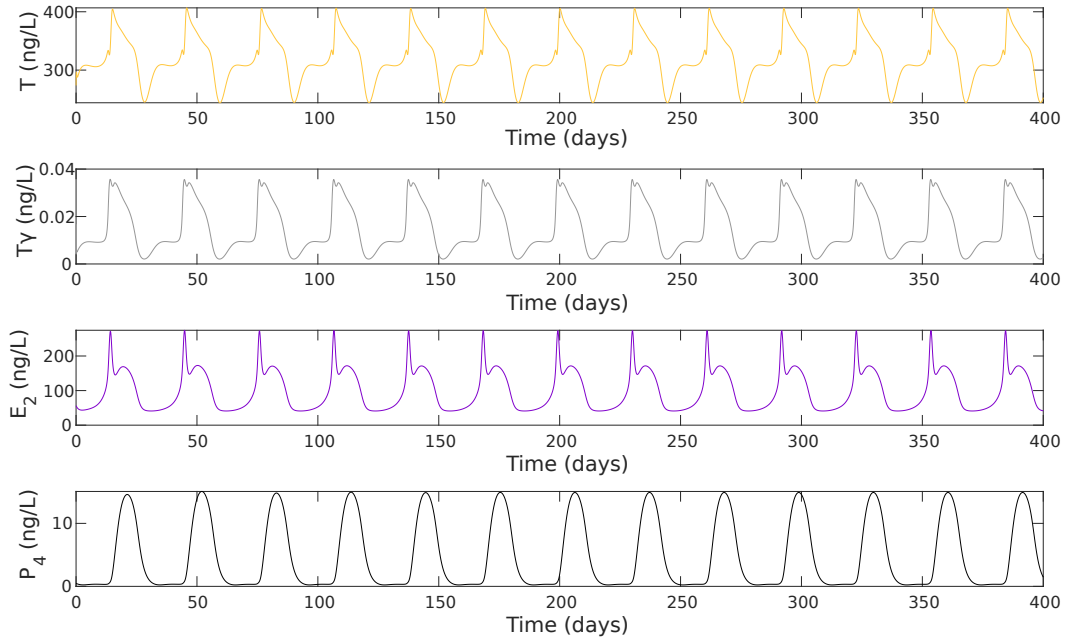
Figure 16: Ovarian hormone dynamics over 400 days.

Recall that Equation (50) contains the term $G_1 = G_1(I)$, which is a function of the body's equilibrium insulin level and provides a way to model the effects of insulin-mediated testosterone levels [14]. $G_1(I)$ is equal to $1+\alpha$, where α is a parameter measuring the degree of insulin influence on the ovulatory cycle [14]. α measures the degree of insulin influence in 6 discrete levels from 0 to 5 [14]. At normal basal insulin levels, which Brubaker et al. gives as 10 mU/L, $\alpha = 0$, so G_1 is 1 [2, 14]. However, as basal insulin levels increase, so does α and, by extension, G_1 [14]. Figure 17 shows the effects of increasing α on the concentrations of T, LH, FSH, E_2, and P_4.
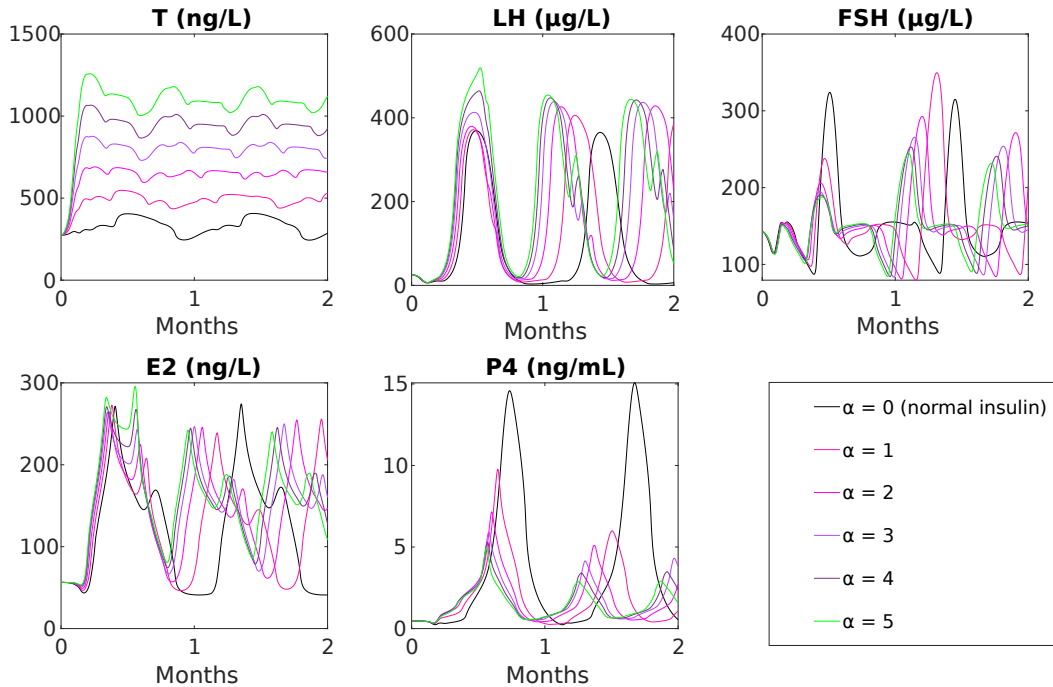
Figure 17: Concentration of key reproductive hormones as the degree of influence of insulin on the system, given by the parameter α, is increased from 0 to 5. As α increases, so does the concentration of testosterone, and the hormone profile overall resembles the profile of an abnormal, anovulatory menstrual cycle.

It is clear from Figure 17 that higher resting insulin levels increase ovulatory dysfunction. The green curve in Figure 17 shows the hormone profile when $\alpha = 5$, the highest possible level of insulin influence. After the first month, the curve for LH shows not one monthly spike in LH levels, but two points each month where LH increases rapidly. Given the importance of a single LH spike in the process of ovulation, this is highly problematic [17]. Additionally, P_4 levels become extremely low compared to the normal profile, given in black; this is also problematic due to the importance of maintaining higher P_4 levels after ovulation to having a healthy menstrual cycle [17]. It is clear from the model that a person with extremely high resting insulin levels is likely to have anovulation, highly irregular periods, and elevated androgen levels. In other words, this person would have a type of PCOS. Resting insulin levels, also known as fasting insulin levels, commonly increase as a result of insulin resistance, providing a connection between insulin resistance and PCOS [21].

Rather than have α be given by discrete integer values, we can instead define it as a continuous linear piecewise function by using the fact that 10 mU/L is considered the normal fasting insulin concentration and any fasting concentration greater than 18 mU/L is considered extremely high

[2, 21]:

$$\alpha(I) = \begin{cases} 0 & \text{if } 9 \le I < 10 \\ 0.625I - 6.25 & \text{if } 10 \le I \le 18 \\ 5 & \text{if } 18 < I \end{cases} \cdot \tag{54}$$

I represents the fasting insulin level in mU/L. We assume that α increases linearly as fasting insulin levels in increase, starting at $\alpha = 0$ when $I = 10$ and ending at $\alpha = 5$ when I crosses the threshold for extremely high fasting insulin levels [21]. It is important to note that the Graham-Selgrade model does not account for potential effects of hypoinsulinemia, or extremely low fasting insulin concentration, on ovulatory regulation. We can allow for slight fluctuations in an otherwise normal fasting insulin concentration by setting the lower bound of I to be 9 mU/L; however, we can't make any assumptions beyond this.

By incorporating the effects of insulin on testosterone production in the ovulatory cycle, the Graham-Selgrade model gives valuable mathematical insight into the link between insulin, testosterone and PCOS. This can provide insight into why diabetes medications such as semaglutide can be effective in allievating PCOS symptoms. We can now begin construction of a combined model that incorporates the effects of Ozempic.

4.4   Addition of Ozempic to Each Model

The Siewe-Friedman model, published in March of 2024, simulates both the stimulatory effects of Ozempic on GLP-1 concentration and its inhibition of long term glucose accumulation [36]. The original model provides differential equations measuring both the change in GLP-1 concentration as amplified by Ozempic and the change in glucose concentration as diminished by Ozempic [36]. By modifying our three models according to the assumptions made by Siewe and Friedman, we can create a comprehensive combined model that incorporates the impact of Ozempic both at the cellular level through the expanded Takeda et al. model and at the macroscopic level through the Brubaker et al. and Graham-Selgrade models.

To start, we assume that once Ozempic is injected into the body, the rate of change in its concentration can be modeled as a single-compartment pharmacokinetic model. In other words, we do not consider differences in how Ozempic interacts with the various tissues in the body; rather, we assume the body acts as one unit that metabolizes Ozempic at a rate proportional to the present concentration of of the drug [9]. This is primarily done for the purpose of model simplification, but it is also due to the current dearth of information about the pharmacokinetics of Ozempic, as the drug only came to market in 2019 [20]. Based on this assumption, the equation for the rate of change of Ozempic concentration after the initial dosing is

$$\frac{d[D]}{dt} = -\mu_D[D], \tag{55}$$

where $[D]$ is the concentration of Ozempic and μ_D is its degradation rate [36].

Then, we incorporate a term to represent the support Ozempic provides to GLP-1 circulating throughout the body into our differential equations representing the change in free GLP-1 concentration [36]. We start with the GLP-1 equation in the complete Takeda et al. model:

$$\frac{d[GLP1]}{dt} = \gamma_L \left(1 + \frac{[D]}{K_D + [D]} \right) - \mu_{LR}[GLP1][R]. \tag{56}$$

$\frac{[D]}{K_D + [D]}$ is a Michaelis-Menten equation describing the reaction rate of Ozempic, where K_D is the concentration of Ozempic required to reach a half maximal reaction rate [36]. Therefore, in addition to a constant rate of secretion after a meal, the concentration of GLP-1 also increases at a rate proportional to the reaction rate of Ozempic.

Since Ozempic is a GLP-1 receptor agonist, it also binds to free GLP-1 receptors. To add Ozempic to other equations in the GLP-1 receptor activation model, we first assume that GLP-1 and Ozempic are not in competition to bind to free receptors; instead, they act alongside each other. Therefore, we are assuming the receptor binding affinity values for GLP-1 and Ozempic are essentially the same. However, they do not combine to form a new compound, so the law of mass action does not apply here; instead, these two compounds simply coexist. Therefore, rather than incorporate the product of the concentrations of GLP-1 and Ozempic into the receptor activation model, we use the sum of their concentrations to reflect the impact of their combined concentration on the $\beta-$ cell. Figure 18 provides an updated version of the reaction scheme used to initially derive the completed Takeda et al. model that incorporates Ozempic into the system.
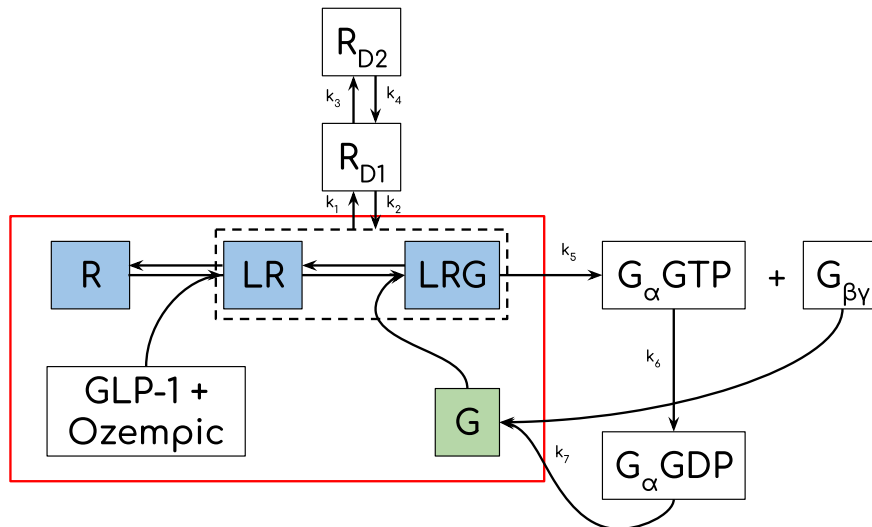

Figure 18: Reaction diagram showing GLP-1 receptor activation with the addition of Ozempic to the system. The reactions in the red rectangle are still assumed to be at instantaneous equilibrium.

The instantaneous equilibrium assumption still applies to the updated system, due to the speed

at which GLP-1 receptor agonists activate the G_s protein binding compared to the speed of other $\beta-$cell processes [38]. Therefore, the equation for $\frac{d[LR]}{dt}$ becomes

$$\frac{d[LR]}{dt} = \frac{1}{K_{d_1}} \left[([D] + [GLP1])\frac{d[R]}{dt} + [R] \left(\frac{d[D]}{dt} + \frac{d[GLP1]}{dt} \right) \right]. \tag{57}$$

By repeating the derivation process used to obtain the complete GLP-1 receptor activation model, we also obtain the new equation for $\frac{d[R]}{dt}$:

$$\frac{d[R]}{dt} = \frac{k_2[R_{D1}] - k_1([R_t] - [R] - [R_{D1}] - [R_{D2}]) - \left(\frac{d[D]}{dt} + \frac{d[GLP1]}{dt} \right) \left(\frac{[R]}{K_{d_1}} + \frac{[G][R]}{K_{d_1}(K_{d_2}+[LR])} \right)}{1 + \frac{[D]+[GLP1]}{K_{d_1}} + \frac{[G]([D]+[GLP1])}{K_{d_1}(K_{d_2}+[LR])}}$$

$$- \frac{(k_5([G_t] - [G] - [G_{\beta\gamma}]) - k_7[G_\alpha GDP][G_{\beta\gamma}]) \left[\frac{[LR]}{K_{d_2}+[LR]} \right]}{1 + \frac{[D]+[GLP1]}{K_{d_1}} + \frac{[G]([D]+[GLP1])}{K_{d_1}(K_{d_2}+[LR])}}. \tag{58}$$

The product $\left[\left(\frac{d[D]}{dt} + \frac{d[GLP1]}{dt} \right) \left(\frac{[R]}{K_{d_1}} + \frac{[G][R]}{K_{d_1}(K_{d_2}+[LR])} \right) \right]$ in the numerator represents both the binding of GLP-1 and the GLP-1 receptor agonist to the GLP-1 receptor and the interactions between the compounds activating the receptor and the G protein complex to create the LRG complex [38]. The terms $\frac{[D]+[GLP1]}{K_{d_1}}$ and $\frac{[G]([D]+[GLP1])}{K_{d_1}(K_{d_2}+[LR])}$ in the denominator result from the combined concentrations of GLP-1 and Ozempic and their interactions with G_s proteins during the receptor binding process inhibiting the accumulation of free GLP-1 receptors. The equation for $\frac{d[G]}{dt}$ remains the same again, as all of the model changes are incorporated in the $\frac{d[LR]}{dt}$ term in Equation (23).

Now that we have modeled the effects of Ozempic at the microscopic level, we can incorporate the Siewe-Friedman model into the incretin effect model from Brubaker et al. [2, 36]. Since the incretin effect model provides equations for both change in glucose and change in incretins, including GLP-1, we modify both Equations (39) and (41) according to the guidelines set by Siewe and Friedman:

$$\frac{dInc}{dt} = \frac{Ra_{Inc}}{V} \left(1 + \frac{[D]}{K_D + [D]} \right) + k_5 Duod_G - k_6 Inc, \tag{59}$$

$$\frac{dGluc}{dt} = \frac{Ra_{GutG}}{V} \left(\frac{1}{1 + \frac{[D]}{\hat{K}_D}} \right) + \frac{Hepbal_G}{V} - k_1 Gluc^{1.3} - k_2 I + \gamma \frac{dI}{dt}. \tag{60}$$

$\hat{K}_D$ is the saturation of Ozempic that inhibits the accumulation of glucose; in this model, $K_D = \hat{K}_D$, and they both equal the initial dose of Ozempic [36]. The original Siewe-Friedman model multiplies the terms $1 + \frac{[D]}{K_D+[D]}$ and $\frac{1}{1+\frac{[D]}{\hat{K}_D}}$ by the appearance rates of of GLP-1 and glucose, respectively, after a meal [36]. Because both GLP-1 and GIP are represented in $\frac{dInc}{dt}$, we will assume that Ozempic effects them both equally for the purposes of this model. Therefore, when modifying the incretin effect model, we multiply $1 + \frac{[D]}{K_D+[D]}$ and $\frac{1}{1+\frac{[D]}{\hat{K}_D}}$ by $\frac{Ra_{Inc}}{V}$ and $\frac{Ra_{GutG}}{V}$ respectively [2, 36]. Although no new terms are added to $\frac{dI}{dt}$, it is more than reasonable to assume insulin levels will also change with the addition of Ozempic due to the feedback loops between glucose, incretins, and insulin.

We can use Equation (40), the equation for $\frac{dI}{dt}$, both in the original system and with the modified equations to obtain the fasting insulin levels with Ozempic and without it. The fasting insulin levels we get through performing these simulations then become inputs for Equation (54) to provide a concrete way to measure the impact of Ozempic on insulin-mediated testosterone production and, by extension, PCOS. With the creation of this combined model, we have forged a mathematical link between semaglutide and PCOS. By providing an overview of the overall results of our simulations, we gain new insights into this mathematical link.

5   Results

After expanding the Takeda et al. model to include $\frac{d[R]}{dt}$, $\frac{d[G]}{dt}$, and $\frac{d[LR]}{dt}$, we use MATLAB to solve for $[R]$, $[LR]$, $[LRG]$, $[RD1]$ (the concentration of receptors in the first stage of desensitization), $[RD2]$, (the concentration of receptors in the second stage of desensitization), $[G]$ (concentration of full G_s protein trimer), $[G_\alpha GTP]$, $[G_\alpha GDP]$, $[G_{\beta\gamma}]$, $[GLP1]$, and $[cAMP]$. In the case of constant GLP-1 concentration, we can also plot Equations (18) and (19) to visualize GLP-1 and LRG concentration. Additionally we can also plot Equations (20), (34), and (35) to find the solution curves in the case of non-constant GLP-1 concentration without Ozempic. To see the model solutions with the addition of Ozempic, we plot the solution the system with Equations (56)-(58) as well. Figure 19 depicts the solution curves showing the concentration of each receptor type under those 3 conditions.
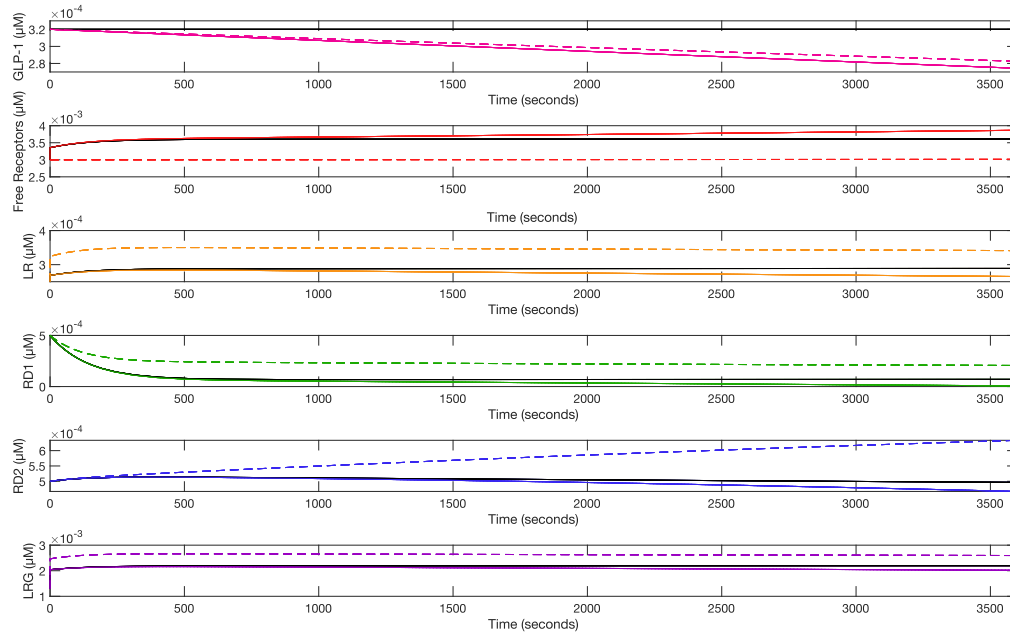
Figure 19: Concentrations of GLP-1 receptors in various stages under three conditions: constant GLP-1 concentration (black line), non-constant GLP-1 concentration without Ozempic (solid line), and non-constant GLP-1 concentration with Ozempic (dashed line). The initial conditions are $[R](0) = 0.003$, $[LR](0) = 0.00024$, $[R_{D1}](0) = [R_{D2}](0) = 0.0005$, and $[GLP1](0) = 0.00032$.

Under constant GLP-1 concentration, the concentrations of each receptor type approach a steady state due to the continuous activation of free receptors. If GLP-1 concentration decreases without the support of Ozempic, the concentration of free receptors increases while the concentration of every other receptor type decreases over time. This is due to the overall decrease in GLP-1 concentration over time and the movement of receptors from the desensitized receptor populations into the free receptors population after a certain time. However, when Ozempic is added to the system, the concentrations of GLP-1 bound receptors LR and LRG both increase, reflecting the nature of GLP-1 receptor agonists, and free receptors are at their lowest concentrations across all three conditions due to increased receptor activation. The concentration of GLP-1 also decreases at a slower rate with the support of Ozempic.

Figure 20 shows the concentrations of each G_s protein type under the three conditions of GLP-1 concentration. It is important to note that in each case, the overall concentration of G proteins rapidly approaches the constant equilibrium of 2.83 μM, which is the total concentration of G_s proteins in the $\beta-$cell given by Takeda et al. [38]. This supports the model assumption that the total concentration of G proteins remains constant.
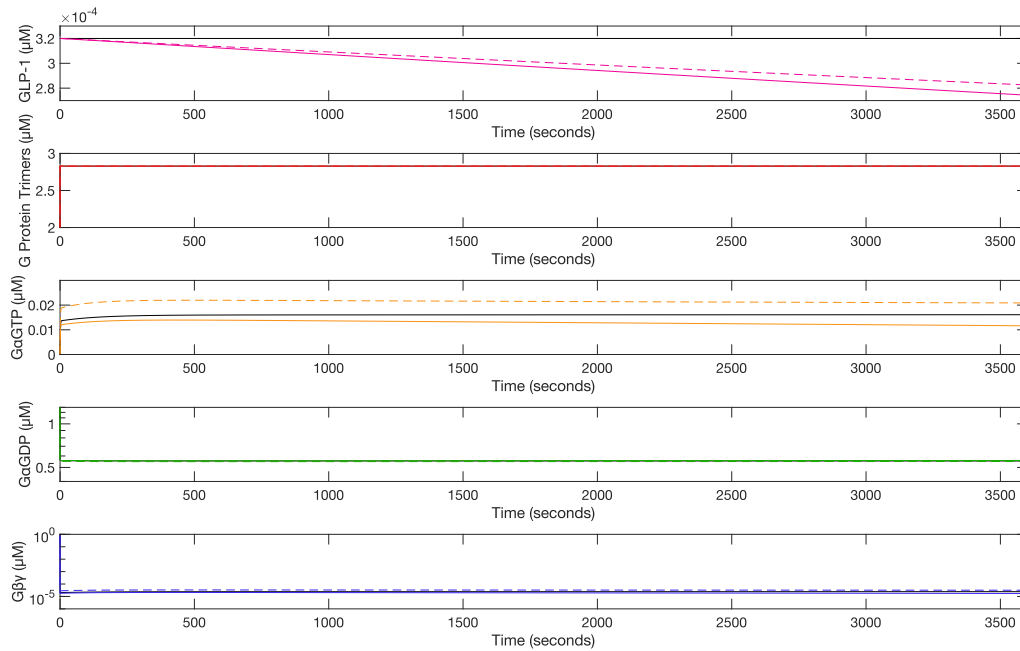
Figure 20: Concentrations of G proteins for the initial conditions $[G](0) = 2.0$, $[G_\alpha GTP](0) = 0.0002$, $[G_\alpha GDP](0) = 1.4$ and $[G_{\beta\gamma}](0) = 0.83$ under the same three conditions as in Figure 19: constant GLP-1 concentration (black line), non-constant GLP-1 concentration without Ozempic (solid line), and non-constant GLP-1 concentration with Ozempic (dashed line).

Additionally, based on Figure 20, the concentrations of each type of G protein approach a steady state due to the constant G protein concentration. However, when Ozempic is added to the system, $G_\alpha GTP$ concentration is greater. Because $G_\alpha GTP$ activates the AC system in the $\beta-$cell, this would indicate that more cAMP is accumulated with the use of GLP-1 receptor agonists. Figure 21 shows that this is indeed the case.
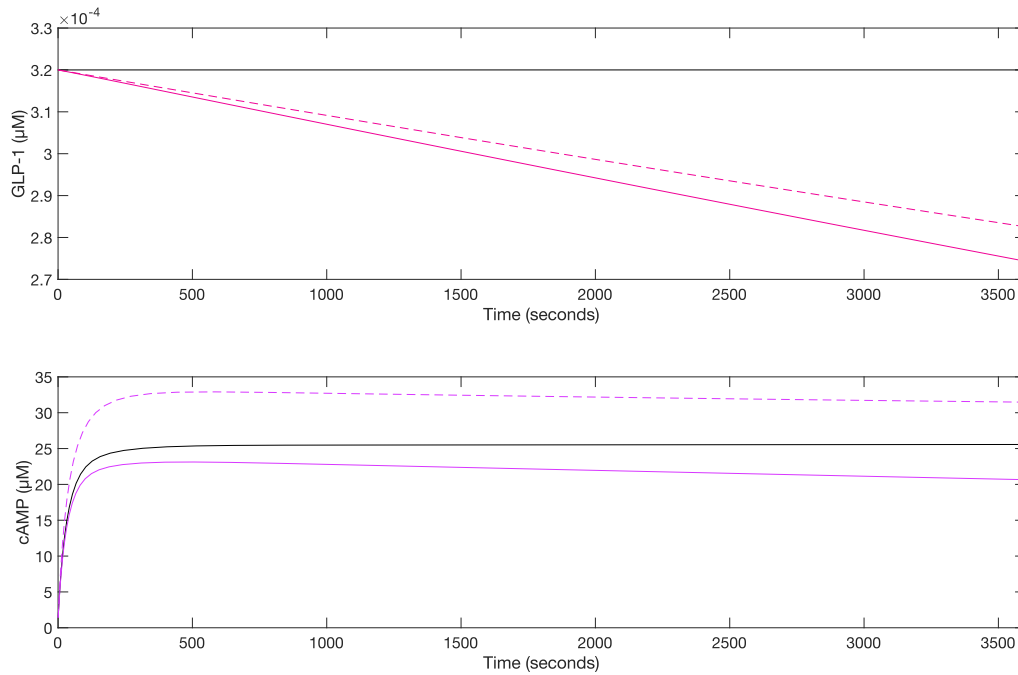
Figure 21: Concentrations of cAMP under constant GLP-1 concentration (black line), non-constant GLP-1 concentration without Ozempic (solid line), and non-constant GLP-1 concentration with Ozempic (dashed line). The initial condition is $[cAMP](0) = 1.4$.

cAMP accumulation is significantly higher in the β−cell of a person using Ozempic, and it remains higher for the duration of the hour-long period that we are simulating to reflect the appearance of GLP-1 during the hour after eating a meal. It approaches a steady state under constant GLP-1 concentration due to the continuous activation of GLP-1 receptors and the AC system. However, when GLP-1 concentration is decreasing, in both cases, the cAMP accumulation also decreases after reaching a maximum concentration. It is important to note, though, that cAMP concentration decreases at a slower rate with the use of Ozempic compared to the decrease in cAMP concentration without Ozempic. This implies that insulin levels increase while using Ozempic.

By plotting the solution curves to the modified incretin effect model alongside the original model that does not incorporate the effects of Ozempic, as in Figure 22, it is clear that insulin levels do in fact increase slightly when a person uses Ozempic as simulated by the modified model. Additionally, glucose levels decrease, reflecting the inhibition of glucose accumulation by Ozempic.
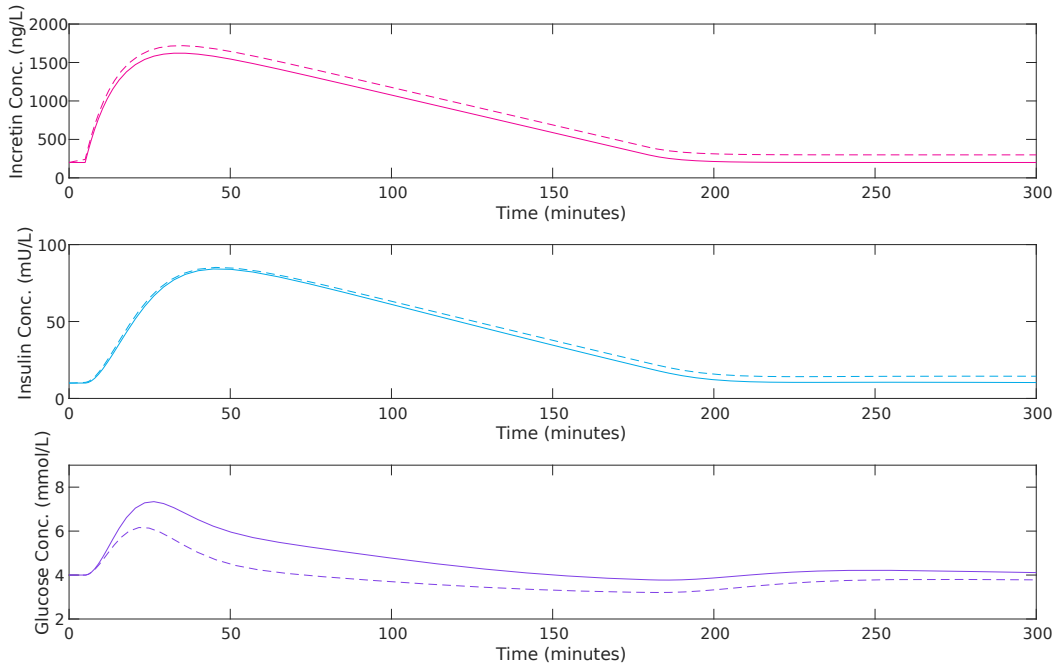
Figure 22: Plasma concentration of incretin hormones, insulin and glucose under normal conditions ($k_2 = 0.00204$) without Ozempic (solid line) and with Ozempic (dashed line).

Recall that in the Brubaker et al. model, k_2 represents insulin-mediated glucose uptake (IMGU) [2]. From Figure 22, it is clear that with a normal k_2 value fasting insulin levels are higher with Ozempic than without it under our current model constraints. A lower k_2 indicates that insulin is having a reduced impact on the clearance of glucose from the bloodstream, which is required to maintain healthy blood glucose levels. Therefore, k_2 provides us which a concrete way to simulate insulin resistance and measure the potential impact of Ozempic on a PCOS hormone profile. By decreasing k_2 to simulate insulin resistance, we can measure fasting insulin levels after an oral glucose tolerance test (OGTT) under insulin resistance, both with and without the influence of Ozempic. Then, we can use these fasting insulin levels as inputs into $\alpha(I)$ to measure the potential effects of Ozempic on PCOS.

5.1 Experimentation

To start, the original Brubaker et al. paper provides a way to simulate an OGTT with a 50 gram glucose load and a 100 gram glucose load [2]. To account for the worst case scenario, we assume that each test is conducted with a 100 gram glucose load. We then gradually lower k_2 and measure insulin and glucose levels 1 hour, 2 hours, and one day after the OGTT, both in the original incretin model and in the incretin model that incorporates the influence of Ozempic. The insulin levels after one day are then assumed to be the fasting insulin levels. By taking these measurements, we can

track not only fasting insulin levels, but also glucose regulation and overall insulin sensitivity both with and without Ozempic, allowing us to form hypotheses about the impact of Ozempic on both the incretin system and the menstrual cycle.

First, it is important to visualize how changes in IMGU impact insulin levels in an otherwise normal incretin-insulin-glucose feedback loop without Ozempic. Based on Figure 23, which simulates insulin levels for 13 hours after an OGTT under the assumption that there is no more glucose introduced into the system, a decrease in k_2 is associated with a rise in fasting insulin levels, indicating impaired IMGU and insulin resistance.
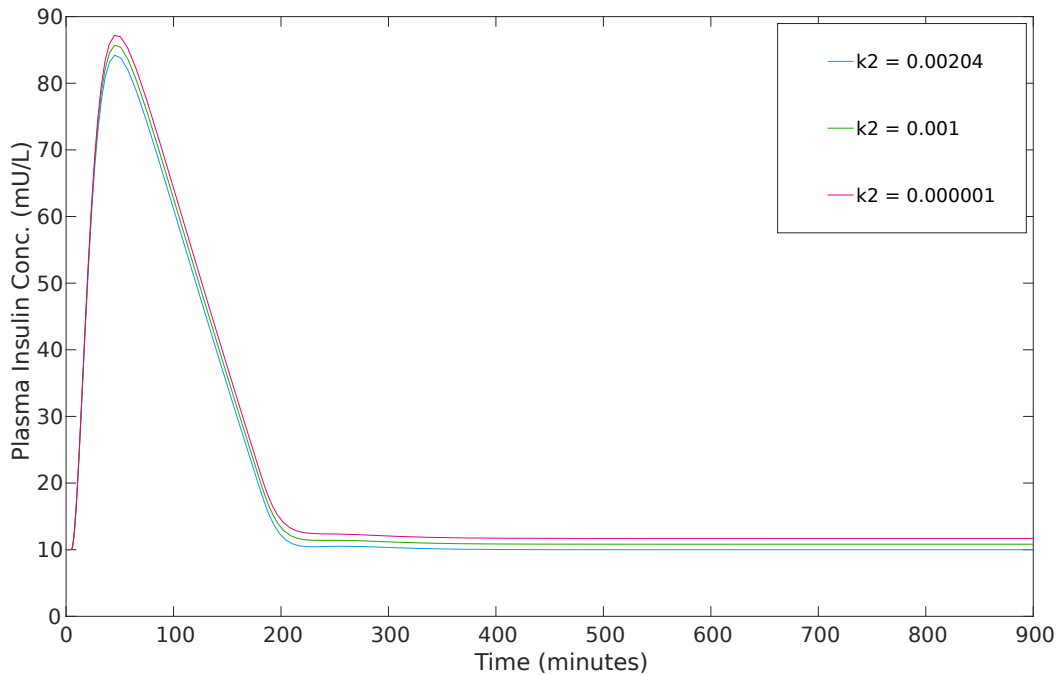
Figure 23: Insulin at basal, or fasting, levels without Ozempic for differing values of k_2, which measures the insulin-mediated glucose uptake (IMGU) in the Brubaker et al. model [2]. Note that a decrease in IMGU results in a rise in fasting insulin levels, indicating that a person with low IMGU has greater insulin resistance.

In order to better understand how Ozempic impacts insulin levels across various IMGU values, we simulate both the original incretin effect model and the modified model over a 60 minute period for 10 k_2 values and find the insulin concentration at time $t = 60$ minutes. Figure 24 plots insulin as a function of k_2 concentration 1 hour after an OGTT, both with and without Ozempic.

Insulin and insulin-mediated glucose uptake (IMGU) 1 hour after OGTT
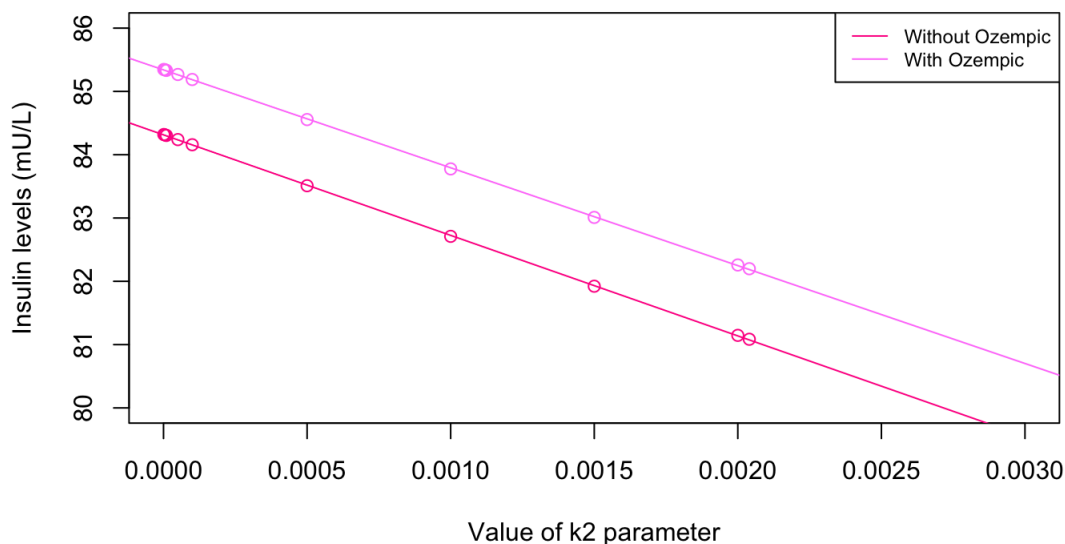
Figure 24: A graph showing the relationship between IMGU and insulin levels one hour taking an oral glucose tolerance test.

The relationship between IMGU and insulin appears to be linear, and finding the linear regression using R yields the equation $I = 84.32 - 1588.62k_2$ for the linear model relating I to k_2 without Ozempic and the equation $I = 85.34 - 1546.61k_2$ for the model with Ozempic. While the implications of this are currently unclear, one interpretation of these linear models is that they reflect a overall change insulin sensitivity between the system with Ozempic and the system without Ozempic. The shallower slope that occurs with Ozempic could indicate that initially after an oral glucose tolerance test, insulin levels do not vary across different IMGU values as widely as they do without Ozempic.

After finding the insulin concentration after 1 hour, it is also important to measure insulin concentration after 2 hours to determine how the body reacts to the sudden influx of highly concentrated glucose over a longer time frame. Figure 25 plots IMGU as a function of insulin concentration 2 hours after the OGTT is administered. Although insulin levels are still more elevated at this time when using Ozempic compared to a system without Ozempic, the linear regression models represented by each line also indicate a change in insulin sensitivity possibly mediated by Ozempic. Now, the equation for the line without Ozempic is $I = 53.45 - 1483.37k_2$, and the equation for the line with Ozempic is $I = 55.97 - 1472.62k_2$. It is again possible that the equations indicate that insulin concentrations do not change as much across k_2 values with Ozempic compared to the changes in insulin concentration across k_2 without Ozempic, even if the difference is small.

Insulin levels and IMGU 2 hours after OGTT
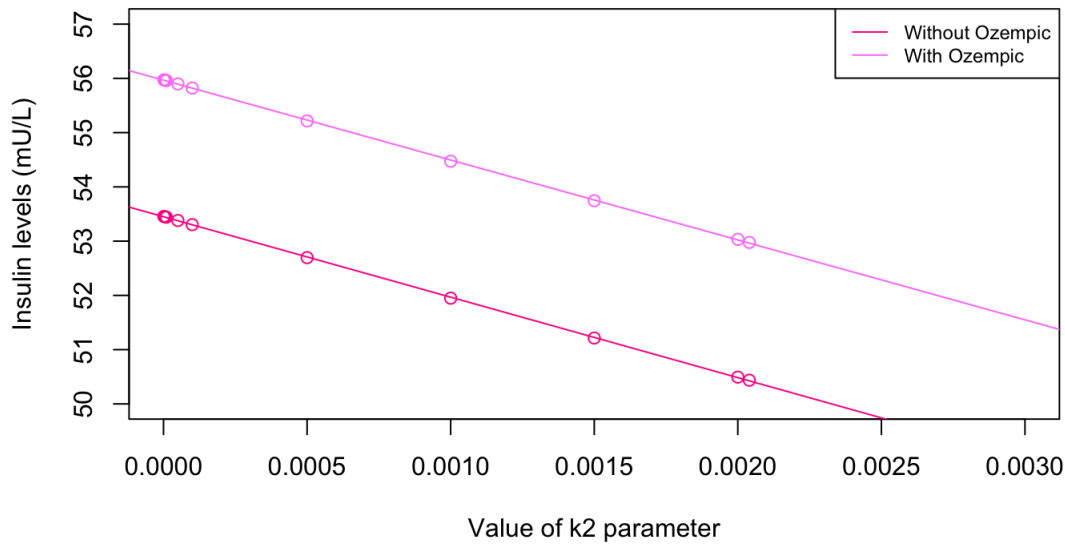
Figure 25: IMGU and insulin levels 2 hours after an OGTT.

Figure 26 plots k_2 as a function of insulin concentration measured one day after the administration of the OGTT, assuming there was no other form of glucose delivered to the system. This is unrealistic, but unfortunately the Brubaker et al. model does not allow for meal simulations, only one-time OGTT administration. Therefore, this was the best way to approximate fasting insulin levels within the confines of our current model.

Figure 26 indicates that fasting insulin levels are much higher under the influence of Ozempic. Additionally, the relationship between I and k_2 is still linear at this point, given by $I = 11.69 - 837.46k_2$ without Ozempic and $I = 16.15 - 994.14k_2$ with Ozempic. Now, the slope when I is under influence of Ozempic is steeper than the slope of I without Ozempic. This could indicate an greater increase in overall insulin sensitivity in the system that incorporates Ozempic, as even a slight change in IMGU indicates a greater change in fasting insulin levels with Ozempic compared to the change in fasting insulin across IMGU values without Ozempic. If this were the case, this could explain why Ozempic can be a successful way to treat insulin resistant PCOS. Even if there is a short term increase in fasting insulin after starting treatment with Ozempic, a long term increase in insulin sensitivity indicates a long term decrease in insulin resistance, as the body no longer needs to produce elevated levels of insulin to impact glucose regulation and other insulin mediated processes. This is ultimately beneficial to those with insulin resistant PCOS, so even though initial elevated fasting insulin may seem counter-intuitive, considering this within the context of potential long term benefits clarifies some confusion.

Insulin levels and IMGU after one day
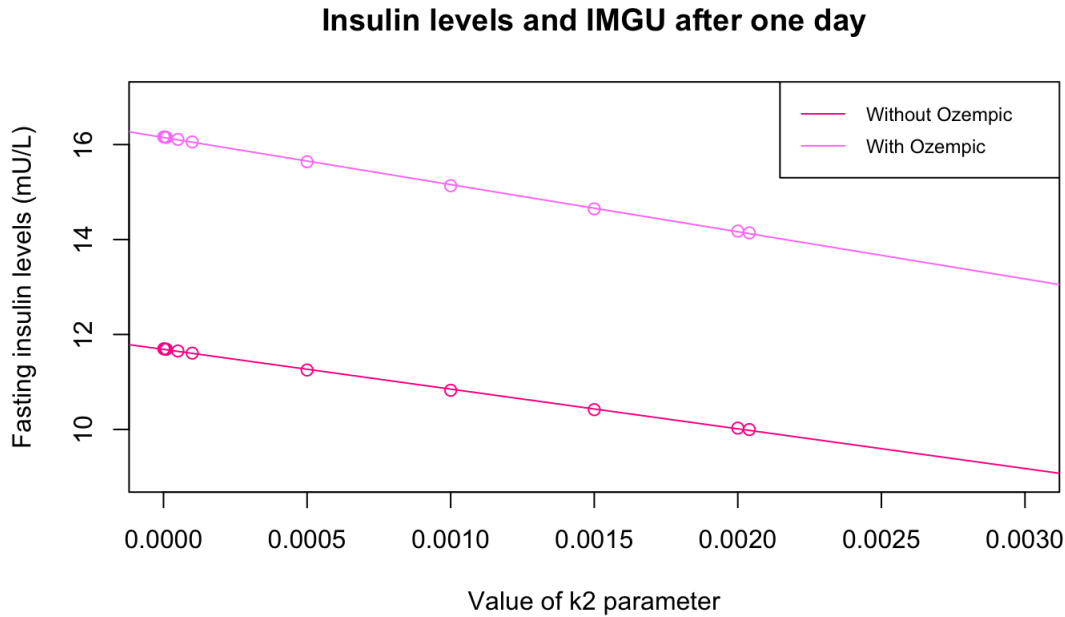
Figure 26: IMGU and insulin levels after 1 day of simulated meals. These are considered the fasting insulin levels for other parts of the simulation.

5.1.1 Simulating PCOS treatment

To measure potential effects of Ozempic on PCOS under our current model, we can first assume that this person has insulin resistant PCOS, as that is the primary population of PCOS patients taking Ozempic to control their symptoms [37]. We then compare the fasting insulin levels both with and without insulin for someone with the highest insulin resistance measured so far. This would be the lowest k_2 value, so we are looking that the fasting insulin concentrations when $k_2 = 0.000001$. These concentrations then become our inputs for Equation (54), or $\alpha(I)$, which is currently the primarily way to measure the impact of fasting insulin on testosterone production and, by extension, the menstrual cycle. We can then compare the hormone profile under the influence of fasting insulin without Ozempic to the hormone profile under the influence of fasting insulin with Ozempic, as shown in Figure 27. The simulated menstrual cycle become more dysfunctional as α increases, and α increases as fasting insulin increases. Since fasting insulin has a much higher concentration with Ozempic than without it under our current model, as shown in Figure 26, it would seem that taking Ozempic would actually increase ovulatory dysfunction. Figure 27 appear to affirm this suspicion.
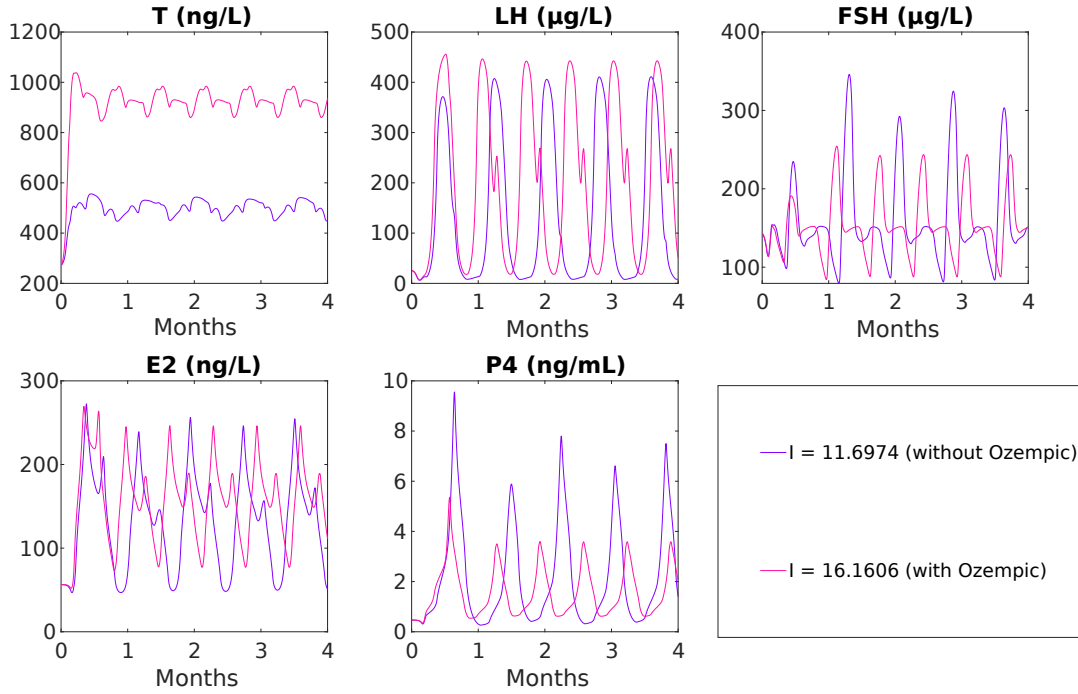
Figure 27: A menstrual cycle simulated for 4 months in a person whose IMGU is represented by $k_2 = 0.000001$. This person would be insulin resistant and have PCOS tendencies based on the Graham-Selgrade model. The purple profile represents their hormone profile without using Ozempic, and the pink profile represents their hormone profile while taking Ozmepic under the current model constraints. The pink profile contains abnormal LH and P_4 levels, indicating ovulatory dysfunction.

Why, then, would a person with insulin resistance and already elevated insulin levels with a condition made worse by high insulin concentration take a drug that appears to elevate insulin and perpetuate abnormalities in the menstrual cycle? These results initially appear very contradictory. However, we are making key assumptions based on the incretin effect models that impact the measurement of fasting insulin concentration and, by extension, the corresponding α value. Because the incretin model only allows us to measure insulin with respect to one OGTT, we can only find one fasting insulin value for a given k_2 value. We then assume fasting insulin remains the same for the 4 months the menstrual cycle is simulated. However, there are many other factors that impact fasting insulin levels, such as additional meals, that are not necessarily taken into account in the incretin effect model and may impact how fasting insulin changes over several months. For the modified incretin model that incorporates Ozempic, fasting insulin is measured with respect to one OGTT and the first dosage of Ozempic a person takes. However, Ozempic alters the incretin system and repairs insulin resistance over a long term treatment regimen in ways that are not initially obvious from simply looking at fasting insulin.

The primary potential impact of Ozempic on insulin resistance appears to be the long term

increase of insulin sensitivity, which decreases insulin resistance. Analyzing the linear relationship between k_2 and insulin as measured with the incretin effect model provides potential evidence of this hypothesis. Since OGTT is designed to measure a body's glucose tolerance, it is also important to measure glucose concentration from these simulations along with the insulin concentration. Figure 28 shows the glucose levels for various k_2 values 1 hour after a simulated OGTT.
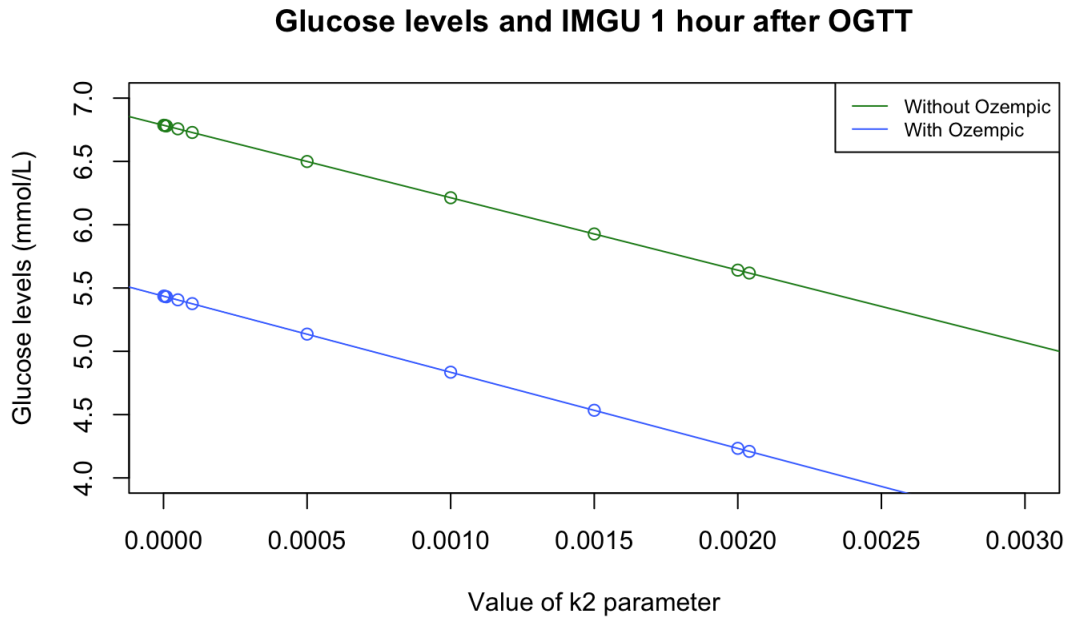
Figure 28: A graph showing the relationship between glucose levels and IMGU 1 hour after eating.

We can develop linear models for the relationship between glucose and k_2 similar to the linear models developed to measure the impact of k_2 on insulin. Without Ozempic, $G = 6.786 - 572.425k_2$, where G is the glucose concentration. With Ozempic, $G = 5.437 - 601.684k_2$. Based on the linear models, glucose levels appear to be more sensitive to changes in IMGU with the usage of Ozempic, which could indicate increased insulin sensitivity with the usage of Ozempic.

To continue the measurement of the potential impact of Ozempic on glucose regulation, we next find glucose levels two hours after the simulated OGTT. The linear relationship between k_2 and glucose concentration after 2 hours is depicted in Figure 29. It is clear from both Figures 28 and 29 that Ozempic lowers glucose levels, which could also lower insulin levels over time. By analyzing the linear models as well, we can continue to see the impact of Ozempic on insulin sensitivity.
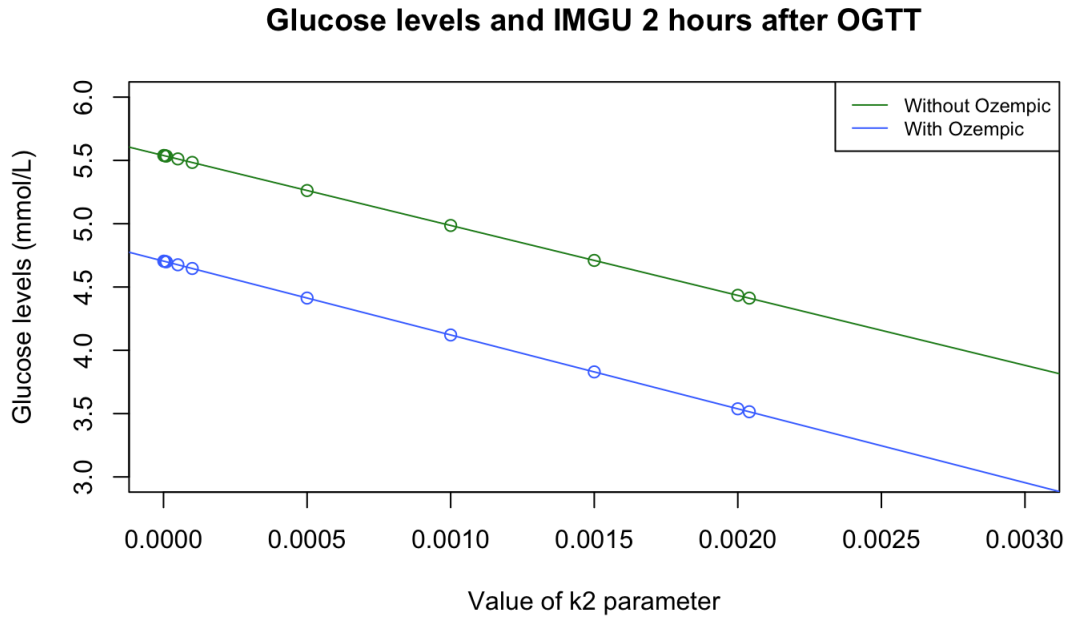
Figure 29: IMGU and glucose levels 2 hours after eating.

The equation for the green line without Ozempic is $G = 5.539 - 552.62k_2$, and the equation for the blue line with Ozempic is $G = 4.705 - 583.444k_2$. The continued sensitivity of glucose levels to IMGU under the influence of Ozempic forms a possible link between Ozempic and increased insulin sensitivity, which would benefit people with insulin resistant PCOS. It is also important to note the link between decreased glucose levels and IMGU according to Figure 29: after two hours, a person with a k_2 value of 0.000001 taking Ozempic would have the same blood glucose concentration 2 hours after an OGTT as a person with a k_2 value of 0.0015 who is not taking Ozempic. This indicates a higher rate of insulin-mediated glucose clearance while taking Ozempic, demonstrating an increased sensitivity to insulin.

One day after the OGTT, glucose concentration in an Ozempic user remains lower than glucose concentration in a person not taking Ozempic, as shown in Figure 30. Glucose levels also remain more sensitive to changes in insulin-mediated glucose clearance in Ozempic users. The equation for the linear relationship without Ozempic is $G = 4.671 - 331.586k_2$, and the linear model with Ozempic is $G = 4.555 - 398.722k_2$, once again indicating a potential link between Ozempic and increased insulin sensitivity.

Glucose levels and IMGU after one day
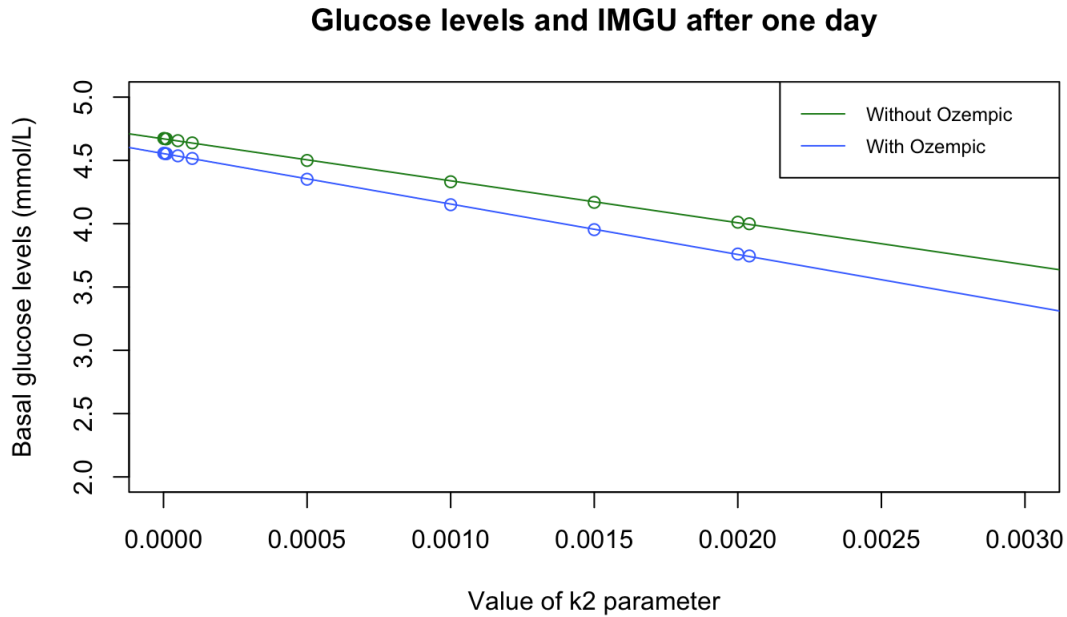
Figure 30: IMGU and glucose levels after one day of simulated meals. These are the basal glucose levels used in other parts of the simulation.

Another way to measure the possible effects of Ozempic on the incretin system is by plotting I as a function of G. As shown in Figure 31, this function is linear both with and without Ozempic, given by $I = 2.5258G - 0.1089$ without Ozempic and $I = 2.493G + 4.796$ with Ozempic. This means that relative to the fasting insulin levels, it requires more insulin to regulate glucose after one day with Ozempic than after one day without it, according to the model results. This is an interesting result, as this corresponds with a decrease in insulin sensitivity and a potential increase in insulin resistance, which would contradict other results obtained from these model simulations. Therefore, the relationship between glucose levels and insulin levels after one day both with and without Ozempic should be closely studied in future research.

Glucose levels and insulin levels after one day
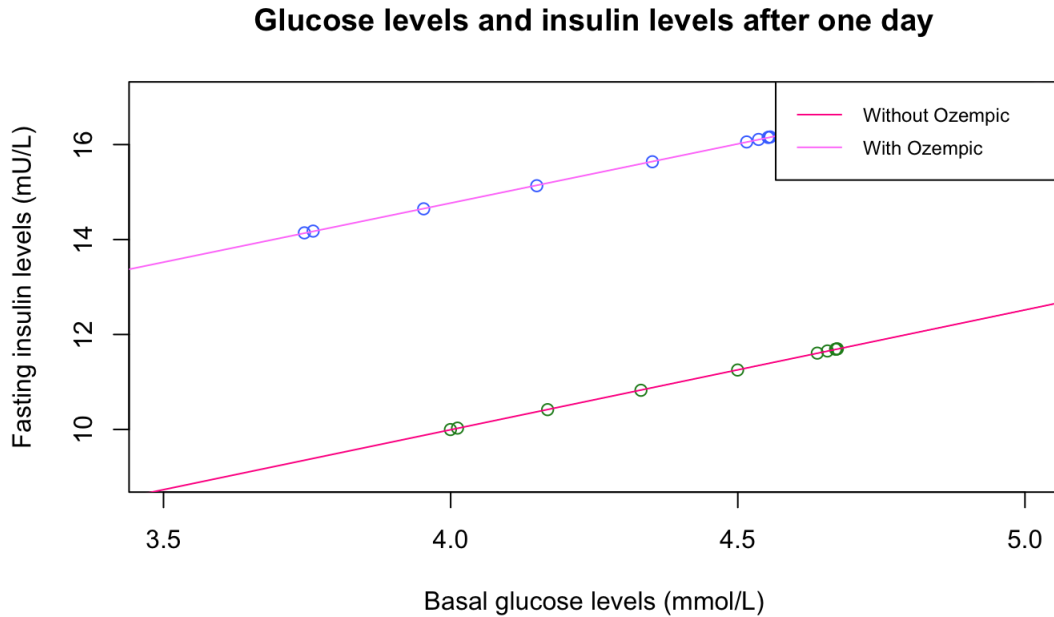
Figure 31: A graph showing the relationship between basal glucose levels and fasting insulin levels, which are the glucose and insulin levels measured after one day.

We can also examine the impact of glucose concentration on α by plotting α as a function of G, depicted in Figure 32. Through linear regression modeling, the equation $\alpha = 1.579G - 6.318$ fits the data without Ozempic, and $\alpha = 1.558G - 3.253$ fits the data with Ozempic. This indicates that under our current models, glucose has less of an impact on the change in α relative to the initial α value. This would imply that with Ozempic even higher levels of glucose would cause a smaller change in α relative to the initial α, which could mean that even elevated glucose levels become less disruptive of testosterone production over time. This would benefit people with PCOS, who are theorized to have impaired IMGU and elevated glucose levels as a result.
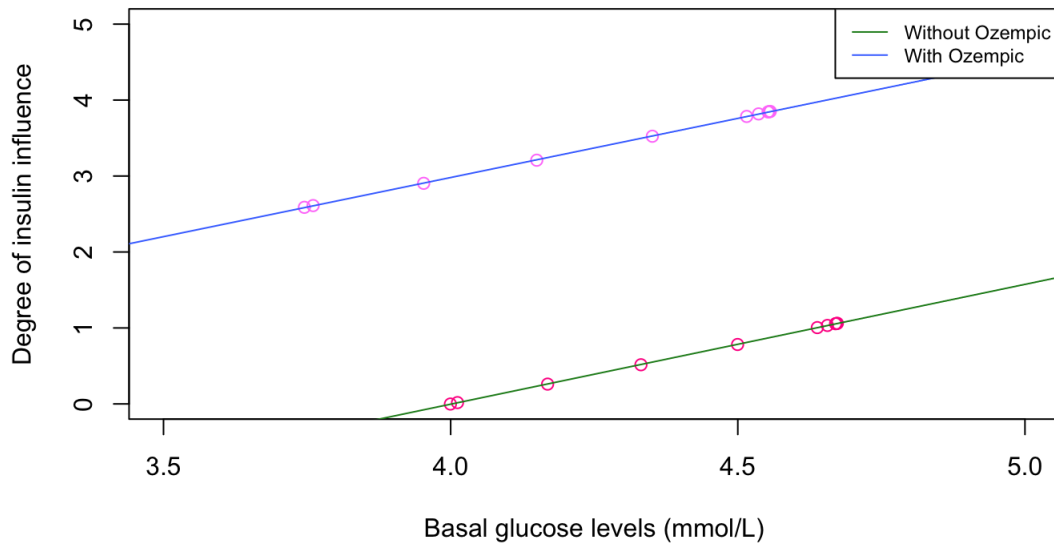
Figure 32: A graph showing the relationship between basal glucose levels and the degree of insulin influence on the ovulatory cycle, given by $\alpha(I)$.

The relationship between k_2 and α is the final clue into the link between Ozempic and PCOS that we will examine in this paper. If we plot α as a function of k_2, as shown in Figure 33, we see that α is greater overall with Ozempic, but that sensitivity to changes in IMGU is also greater. Without Ozempic, $\alpha = 1.056 - 523.413k_2$ but with Ozempic, $\alpha = 3.846 - 621.339k_2$. This means that α is more sensitive to changes in k_2 with Ozempic compared to without it, as a change in k_2 results in a larger change in α with Ozempic compared to a change in α without Ozempic over the same k_2 interval. Therefore, as insulin resistance decreases, which is given by an increase in k_2, the degree of insulin influence on testosterone production decreases more rapidly wth Ozempic. This implies that the system with Ozempic is more sensitive to changes in insulin-mediated processes, which could be interpreted as an increase in insulin sensitivity.
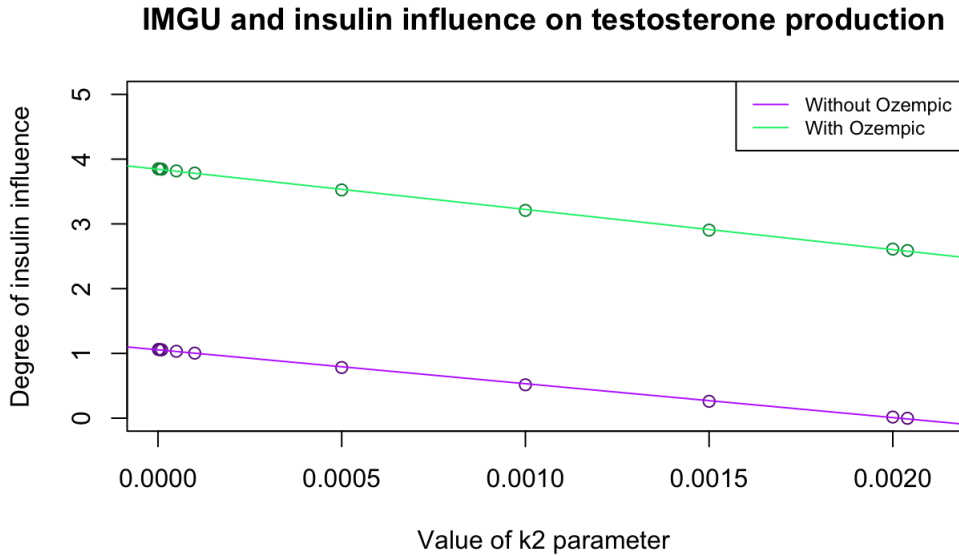
Figure 33: A graph showing the relationship between k_2 and the degree of insulin influence on the ovulatory cycle, given by $\alpha(I)$.

Overall, our combined model produces results that are both expected and surprising. The increase in cAMP production when Ozempic is incorporated into the GLP-1 receptor model shown in Figure 21 was a predictable outcome given the increased receptor activation and the subsequent increase in AC system activation. The link between the resultant increase in insulin and its impact on a dysfunctional hormone profile is less clear. At first, the results shown in Figure 27 appear to indicate that using Ozempic *increases* hormone imbalances characteristic of PCOS, contradicting anecdotal evidence of the treatment's effectiveness. However, a closer examination of crucial model parameters k_2 and α, as well as some reflection on the current shortcomings of our model, allows us to form a tenuous hypothesis about the link between Ozempic and PCOS: Ozempic potentially increases insulin sensitivity in the long term, so despite an initial increase in fasting insulin under the incretin model, it is possible that there will be a long term decrease in fasting insulin concentration as insulin resistance decreases. This would reverse any ovulatory disruption caused by long term elevated insulin levels, resulting in a reduction of PCOS symptoms. Further simulation would be required to clarify other potential links, and further model adjustments would first have to be made.

6   Discussion

Although the model used in this paper provides a solid foundation to build on, it is highly simplified, and there are changes that must be made in order to research the results presented here further. First and foremost, there needs to be a way to simulate the long term effects of Ozempic on glucose and insulin levels beyond a single oral glucose tolerance test. The simplest way to achieve this would

be to provide a way to simulate multiple meals in the incretin effect model. This may require a reworking of the entire incretin model by adding terms to incorporate food into Equations (39)-(41). Until there is a way to simulate the impact of Ozempic over longer periods of time, no conclusions can be drawn about its effectiveness as a PCOS treatment.

One other major improvement that needs to be made is the disentanglement of GLP-1 and GIP in the equation for $\frac{dInc}{dt}$. The effects of both incretins are combined in that equation, and while our model assumption that Ozempic supports both equally has not produced any wildly unrealistic results, that assumption might not be true. It would be beneficial to tease out the two incretins into two separate differential equations and then add the Ozempic support to the equation representing GLP-1 at the macroscopic level.

Additionally, while the fasting insulin levels and basal glucose levels in Figures 26 and 30 vary across different k_2 values, the insulin and glucose concentrations measured for the lowest k_2 value without Ozempic are not considered highly "abnormal" and do not accurately reflect the insulin and glucose levels one would expect to find in a system with such a low IMGU. In future research, there should be a more realistic simulation of severe hyperinsulinemia and insulin resistance that would likely be present in a person with hyperandrogenic PCOS. Brubaker, et al. mention that hyperinsulinemia found in type 2 diabetes can be simulated by adjusting k_1 in Equation (41), which represents non-insulin mediated glucose uptake (NIMGU), in addition to k_2 [2]. There should also be a way to track the potential decrease of insulin resistance over long term usage of Ozempic, as k_2 is currently a constant term.

There are also several possible improvements to the GLP-1 receptor model. In the original Takeda et al. paper, no initial conditions were given for the differential equations except for $\frac{d[cAMP]}{dt}$. Reasonable assumptions were made based on other model parameters; future research efforts should attempt to derive the actual initial conditions used, if such a derivation is possible. Concentrations of ATP and Ca^{2+} were also assumed to be constant in the original paper for the purposes of model simplification. In reality, concentrations of ATP and Ca^{2+} in the $\beta-$cell oscillate in response to other stimuli, such as glucose ingestion into the cell and changes in cell membrane voltage [12, 31]. A 2003 model of Ca^{2+} flux in the $\beta-$cells by Fridlyand et al. accounts for these oscilliations and provides differential equations describing the rate of change of ATP and Ca^{2+} that can be incorporated into the GLP-1 receptor model [12]. Additionally, clarifying mathematically how an increase in cAMP results in an increase in insulin would provide a concrete way to link the incretin model to the GLP-1 receptor model. This could be done either by adding a term to Equation 40 reflecting how cAMP amplifies insulin release at the macroscopic level or by modeling the release of insulin at the $\beta-$cell level and incorporating this into the incretin model.

Any further research into the relationship between Ozempic and PCOS using this model would require further analysis of k_2 and α. It would also be worthwhile to determine what other parameters in the combined model contribute most to changes in model behavior, as this could provide other links between PCOS and Ozempic. This could be achieved through a bifurcation analysis and a

sensitivity analysis. Additionally, since there is now a method to map both k_2 and G to α, it would also be possible to examine the impacts of both IMGU and glucose on insulin-mediated testosterone production through this mathematical model.

Ultimately, the factors that entwine PCOS, insulin resistance and Ozempic weave a complex story with many unknown players at work. It is imperative that research into PCOS, namely into the biological processes underlying it, is prioritized alongside refinement of any mathematical models simulating the condition. It is only through empathy and a desire to understand the experiences of PCOS patients that meaningful progress is made towards finding the best ways to improvement the quality of life of PCOS patients. Through this convergence of mathematics and humanity, mathematics takes on its true form as a way for people to better understand the world we inhabit.

A Model Parameters

A.1 Model of GLP-1 Receptor Activation

Name	Initial Condition	Units	Source
$[R]$	0.003	μM	est. based on $[R_t]$
$[LR]$	0.00024	μM	est. based on $[R_t]$
$[G]$	2	μM	est. based on $[G_t]$
$[R_{D1}]$	0.0005	μM	est. based on $[R_t]$
$[R_{D2}]$	0.0005	μM	est. based on $[R_t]$
$[G_\alpha GTP]$	0.0002	μM	est.
$[G_\alpha GDP]$	1.4	μM	est.
$[G_{\beta\gamma}]$	0.8299	μM	est. based on $[G_t]$
$[cAMP]$	1.4	μM	[38]
$[CaCaM]$	0	μM	est. based on [11]
$[GLP1]$	0.32	nM	est. based on $[R]$ and $[LR]$
$[D]$	335	μM	[28]

Table 1: Initial conditions for state variables.

Name	Value	Units	Source
$[R_t]$	0.00434	μM	[38]
K_{d_1}	0.004	μM	[38]
K_{d_2}	0.004	μM	[38]
$[G_t]$	2.83	μM	[38]
k_1	0.0025	s^{-1}	[38]
k_2	0.005833	s^{-1}	[38]
k_3	0.0002833	s^{-1}	[38]
k_4	0.00005	s^{-1}	[38]
k_5	16	s^{-1}	[38]
k_6	1	s^{-1}	[38]
k_7	1200	$\mu M^{-1} s^{-1}$	[32]
γ_L	5.729×10^{-19}	μM s^{-1}	[24, 36]
μ_{LR}	0.0115278	μM s^{-1}	[24, 36]
μ_D	1.11×10^{-6}	s^{-1}	[5]
K_D	335	μM	[28]
$\hat{K}_D$	335	μM	[28]

Table 2: Parameters for the G protein-coupled receptor subsystem (Equations (6)-(10) and (22)-(24)), the GLP-1 concentration model (Equation (34)), and the Ozempic model (Equation (55)).

Name	Value	Units	Source
$V_{max_{AC}}$	0.6173	μM s^{-1}	[38]
$[ATP]$	3000	μM	[38]
$V_{max_{AC_G}}$	17.38	μM s^{-1}	[38]
$f_{Cd_{AC}}$	0.6	#	[38]
$[Ca^{2+}]$	0.5	μM	[38]
$V_{max_{PDE}}$	15	μM s^{-1}	[38]
f	0.012	#	[38]
K_{mL}	0.4148	μM	[38]
K_{mH}	53.98	μM	[38]
$f_{Cd_{PDE}}$	0.2	μM	[38]
k_{1f}	2300	μM$^{-1}s^{-1}$	[11]
k_{1b}	2400	s^{-1}	[11]
k_{2f}	2300	μM$^{-1}s^{-1}$	[11]
k_{2b}	2400	s^{-1}	[11]
k_{3f}	160000	μM$^{-1}s^{-1}$	[11]
k_{3b}	405000	s^{-1}	[11]
k_{4f}	160000	μM$^{-1}s^{-1}$	[11]
k_{4b}	405000	s^{-1}	[11]
$[CaM]$	11.25	μM	[11]

Table 3: Parameters for AC system submodel (Equations (25)-(33)) .

A.2 Model of the Incretin Effect

Name	Initial Condition	Units	Source
$Gluc$	4	mmol L^{-1}	[2]
Inc	200	ng L^{-1}	[2]
I	10	mU L^{-1}	[2]
$Hepbal_{GB}$	0.8549	mmol L^{-1}	[2]
$Duod_G$	0	mmol L^{-1}	[2]
Ra_{GutG}	0	mmol L^{-1}	[2]
t	0	min	[2]
$[D]$	0.335	mM	[28]

Table 4: Initial conditions for state variables and time-dependent parameters.

Name	Value	Units	Source
k_1	0.00671	$L^{0.3}mmol^{-0.3}min^{-1}$	[2]
k_2	0.00204	$mmol\ min^{-1}mU^{-1}$	[2]
k_3	0.0718	$L\ min^{-1}$	[2]
k_4	0.717	$mmol\ min^{-1}$	[2]
k_5	27.64	$ng\ L^{-1}mmol^{-1}$	[2]
k_6	0.1	min^{-1}	[2]
k_7	0.125	$mU\ min^{-1}mmol^{-1.3}L^{-0.3}$	[2]
k_8	0.005	$mU\ min^{-1}ng^{-1}$	[2]
k_9	0.1	min^{-1}	[2]
M	0.02, 0.03 if $G < 3$	$L^2mU^{-1}min^{-1}$	[2]
Ra_{Inc}	280	$ng\ min^{-1}$	[2]
V	14	L	[2]
α	1.0	$mmol^2mU\ L^{-2}min^{-1}$	[2]
β	-0.758	$mU\ L^{-1}min^{-1}$	[2]
γ	0.06 if $Ra_{GutG} > 0$	$mmol\ mU^{-1}$	[2]
μ_D	6.66×10^{-5}	min^{-1}	[5]
K_D	0.335	mM	[28]
$\hat{K}_D$	0.335	mM	[28]

Table 5: Parameter values.

A.3 Model of Ovulatory Regulation

Name	Value	Units	Source
FSH_ρ	116.82	μg	[14]
FSH	142.5	μg L^{-1}	[14]
LH_ρ	250.35	μg	[14]
LH	25.34	μg L^{-1}	[14]
Φ	0.50185	μg	[14]
Ω	9.7509	μg	[14]
Λ	4.102	μg	[14]
S	0.050498	#	[14]
T	273.67	ng L^{-1}	[14]
T_γ	0.003999	ng L$^{-1}\mu$g^{-1}	[14]
E_2	56.387	ng L^{-1}	[14]
P_4	0.468	ng mL^{-1}	[14]

Table 6: Initial conditions for state variables.

Name	Value	Units	Source
$c_{F,E}$	0.0022729	L ng^{-1}	[14]
$c_{F,I}$	1.9488	#	[14]
$c_{F,P}$	60.428	L μg^{-1}	[14]
$c_{L,E}$	0.0010404	L ng^{-1}	[14]
$c_{L,P}$	0.0099415	L μg^{-1}	[14]
$c_{L,T}$	0.0095942	L ng^{-1}	[14]
δ_F	8.21	day^{-1}	[14]
δ_L	14	day^{-1}	[14]
k_F	2.5412	day^{-1}	[14]
$K_{F,I}$	107.01	μg	[14]
$K_{iL,P}$	0.34952	μg L^{-1}	[14]
$K_{L,T}$	420	ng L^{-1}	[14]
K_{mL}	183.56	μg L^{-1}	[14]
k_L	0.74567	day^{-1}	[14]
n	8	#	[14]
V	2.5	L	[14]
v_{0L}	1051.7	μg day^{-1}	[14]
v_{1L}	34838	μg day^{-1}	[14]
v_F	3236.6	μg day^{-1}	[14]

Table 7: Parameters used in pituitary subsystem.

Name	Value	Units	Source
$c_{\Phi,F}$	0.01127	L μg^{-1}	[14]
δ_S	0.74702	day^{-1}	[14]
f_0	0.0025112	μg day^{-1}	[14]
f_1	4.3764	day^{-1}	[14]
f_2	27.812	day^{-1}	[14]
h_1	590.32	μg L^{-1}	[14]
h_2	1815.2	μg L^{-1}	[14]
h_P	20.764	μg L^{-1}	[14]
h_S	12.329	μg L^{-1}	[14]
l	0.49017	day^{-1}	[14]
m	4	#	[14]
$\hat{s}$	2.378	day^{-1}	[14]
w	0.23173	day^{-1}	[14]

Table 8: Parameters used in follicular dynamics subsystem.

Name	Value	Units	Source
c_{T,F_2}	123.8136	μg L^{-1}	[14]
δ_E	1.1	day^{-1}	[14]
δ_P	0.5	day^{-1}	[14]
δ_T	5.5	day^{-1}	[14]
e_0	44.512	ng L^{-1}day^{-1}	[14]
η	1.1087	#	[14]
h_3	17.796	μg L^{-1}	[14]
κ_1	1.09	#	[14]
κ_2	22.28645	μg L^{-1}	[14]
κ_3	113.9188	μg^{2}L^{-2}	[14]
p	0.3734	L^{-1}day^{-1}	[14]
t_0	741.68	ng L^{-1}	[14]
t_1	0.57088	ng L$^{-1}\mu$g^{-1}day^{-1}	[14]
t_2	1.3481	ng L$^{-1}\mu$g^{-1}day^{-1}	[14]
τ_1	5.3989	#	[14]
τ_2	0	#	[14]
τ_3	430.91	μg	[14]
t_{g1}	6.6548	ng L$^{-1}\mu$g^{-1}day^{-1}	[14]
t_{g2}	186.27	day^{-1}	[14]
Ψ	2004.3	μg	[14]

Table 9: Parameters used in ovarian hormone synthesis subsystem [14].

B   Results of Incretin Model Simulations

	Without Ozempic		With Ozempic	
k_2	Glucose (mmol/L)	Insulin (mU/L)	Glucose (mmol/L)	Insulin (mU/L)
0.00204	5.61833	81.0846	4.20944	82.1989
0.002	5.64117	81.1462	4.23352	82.2582
0.0015	5.92692	81.9225	4.53418	83.0094
0.001	6.21296	82.7105	4.83494	83.7757
0.0005	6.49932	83.51	5.13581	84.5553
0.0001	6.72868	84.1574	5.37668	85.1882
0.00005	6.75734	84.239	5.40674	85.2676
0.00001	6.78031	84.3045	5.43082	85.3323
0.000005	6.78321	84.3125	5.43383	85.3403
0.000001	6.78548	84.3192	5.43623	85.3467

Table 10: Glucose and insulin concentrations, with and without Ozempic, at various k_2 values one hour after an OGTT is administered.

	Without Ozempic		With Ozempic	
k_2	Glucose (mmol/L)	Insulin (mU/L)	Glucose (mmol/L)	Insulin (mU/L)
0.00204	4.41239	50.4366	3.5146	52.9768
0.002	4.43441	50.4936	3.53792	53.033
0.0015	4.71001	51.2144	3.82944	53.7445
0.001	4.98599	51.9488	4.121	54.4722
0.0005	5.26208	52.6962	4.41277	55.2157
0.0001	5.48408	53.304	4.64636	55.8215
0.00005	5.51187	53.3805	4.67557	55.8979
0.00001	5.53404	53.4418	4.69894	55.9591
0.000005	5.5368	53.4495	4.70187	55.9667
0.000001	5.53904	53.4557	4.7042	55.9729

Table 11: Glucose and insulin concentrations, with and without Ozempic, at various k_2 values 2 hours after an OGTT is administered.

k_2	Without Ozempic		With Ozempic	
	Glucose (mmol/L)	Insulin (mU/L)	Glucose (mmol/L)	Insulin (mU/L)
0.00204	3.99955	9.99747	3.74527	14.1408
0.002	4.01186	10.0278	3.76048	14.1776
0.0015	4.16878	10.4169	3.95302	14.6467
0.001	4.33133	10.8246	4.14992	15.1335
0.0005	4.49961	11.2516	4.35121	15.6384
0.0001	4.63841	11.6073	4.5154	16.0555
0.00005	4.65602	11.6527	4.53612	16.1085
0.00001	4.67015	11.6891	4.55273	16.151
0.000005	4.67192	11.6937	4.55481	16.1563
0.000001	4.67333	11.6974	4.55648	16.1606

Table 12: Glucose and insulin concentrations, with and without Ozempic, at various k_2 values 1 day after an OGTT is administered.

C MATLAB Source Code

C.1 Model of GLP-1 Receptor Activation

C.1.1 Defining Parameters

ozempicpara.m

```
%Concentrations are in micromoles (mcM), and time is in seconds!
Rt = 0.00434; %mcM
KD1 = 0.004; %mcM
Gt = 2.83; %mcM
k5 = 16; %seconds^-1
k6 = 1; %s^-1
k7 = 1200;% 1/mcM*s, originally k7 = 1200000 1/mM*s
k1 = 0.0025; %s^-1
k2 = 0.005833; %s^-1
k3 = 0.0002833; %s^-1
k4 = 0.00005; %s^-1
VmaxAC = 0.6173; %mcM/s, originally VmaxAC = 0.0006173 mM/s
VmaxACG = 17.38; % mcM/s, originally 0.01738 mM/s
fCdAC = 0.6;
VmaxPDE = 15; %mcM/s originally 0.015 mM/s
fCdPDE = 0.2;
Kml = 0.4148; %mcM, 0.0004148 mM;
KmH = 53.98; %mcM; 0.05398 mM;
frac = 0.012;
KD2 = 0.372; %mM; 0.000372 mcM
ATP = 3000; %mcM, 3 mM
Ca2 = 0.5 ; %mcM, 500 nM
CaM = 11.25; %mcM
k1f = 2300; %1/mcM*s, 2.3 1/mcM*ms;
k2f = 2300; %1/mcM*s, 2.3 1/mcM*ms;
k3f = 160000; %1/mcM*s, 160 1/mcM*ms;
k4f = 160000; %1/mcM*s, 160 1/mcM*ms;
k1b = 2400; %1/s, 2.4 1/ms
k2b = 2400; %1/s, 2.4 1/ms
k3b = 405000; %1/s, 405 1/ms
k4b = 405000; %1/s, 405 1/ms
Kozempic = 335; %mcM
yL = 5.729e-19; %mcM/s
```

```
uD = 1.11e-6; %1/s
uLB = 0.0115278; %mcM/s
```

C.1.2 Defining Differential Equations

```
beta.m
function ddt = beta(~,y)
run ozempicpara.m
ddt = zeros(10,1);
R = y(1);
LR = y(2);
G = y(3);
RD1 = y(4);
RD2=y(5);
GaGTP=y(6);
GaGDP = y(7);
Gbg = y(8);
cAMP = y(9);
CaCaM = y(10);
L = (KD1.*LR)./(R);
%%%%
Ca2CaM = (k2f./k2b).*Ca2.*CaCaM;
Ca3CaM = (k3f./k3b).*Ca2.*Ca2CaM;
Ca4CaM = (k4f./k4b).*Ca2.*Ca3CaM;
%%%%
a = (Ca3CaM+Ca4CaM)./(Ca3CaM+Ca4CaM+0.348);
x = (1-fCdAC)+(fCdAC.*a.*(75./(75+Ca2)));
V_AC = VmaxAC.*(0.4./(0.4+GaGTP)).*(ATP./(ATP+1030));
V_AC_G = VmaxACG.*(GaGTP./(0.4+GaGTP)).*(ATP./(ATP+315)).*x;
VAC_t = V_AC+V_AC_G;
b = (frac.*cAMP)./(cAMP+Kml);
c = ((1-frac).*cAMP)./(cAMP+KmH);
d = 1+(L./KD1)+((G.*L)./(KD1.*(KD2+LR)));
h = LR./(KD2+LR);
V_PDE = (VmaxPDE.*(b+c)).*((1-fCdPDE)+fCdPDE.*a);
%%%%
%R'
ddt(1)= (k2.*RD1-k1.*(Rt-R-RD1-RD2)-((k5.*(Gt-G-Gbg)-k7.*GaGDP.*Gbg).*h))./d;
%LR'
```

```
ddt(2)= (L./KD1).*ddt(1);
%G'
ddt(3)=(k7.*GaGDP.*Gbg-k5.*(Gt-G-Gbg)-((G./KD2).*ddt(2)))./(1+LR./KD2);
%RD1'
ddt(4) = k1.*(Rt-R-RD1-RD2)-k2.*RD1-k3.*RD1+k4.*RD2;
%RD2'
ddt(5) = k3.*RD1 - k4.*RD2;
%GaGTP'
ddt(6) = k5.*(Gt-G-Gbg) - k6.*GaGTP;
%GaGDP'
ddt(7) = k6.*GaGTP - k7.*GaGDP.*Gbg;
%Gbg'
ddt(8) = k5.*(Gt-G-Gbg) - k7.*GaGDP.*Gbg;
%cAMP'
ddt(9) = VAC_t - 0.2.*V_PDE;
%CaCaM'
ddt(10)= (k1f.*Ca2.*CaM)-(k1b.*CaCaM);
end


ozempic.m
function ddt = ozempic(~,y)
run ozempicpara.m
ddt = zeros(11,1);
GLP1 = y(1);
R = y(2);
LR = y(3);
G = y(4);
RD1 = y(5);
RD2=y(6);
GaGTP=y(7);
GaGDP = y(8);
Gbg = y(9);
cAMP = y(10);
CaCaM = y(11);
%%%%
Ca2CaM = (k2f./k2b).*Ca2.*CaCaM;
Ca3CaM = (k3f./k3b).*Ca2.*Ca2CaM;
Ca4CaM = (k4f./k4b).*Ca2.*Ca3CaM;
```

```
%%%
a = (Ca3CaM+Ca4CaM)./(Ca3CaM+Ca4CaM+0.348);
x = (1-fCdAC)+(fCdAC.*a.*(75./(75+Ca2)));
V_AC = VmaxAC.*(0.4./(0.4+GaGTP)).*(ATP./(ATP+1030));
V_AC_G = VmaxACG.*(GaGTP./(0.4+GaGTP)).*(ATP./(ATP+315)).*x;
VAC_t = V_AC+V_AC_G;
b = (frac.*cAMP)./(cAMP+Kml);
c = ((1-frac).*cAMP)./(cAMP+KmH);
d = 1+(GLP1./KD1)+((G.*GLP1)./(KD1.*(KD2+LR)));
h = LR./(KD2+LR);
V_PDE = (VmaxPDE.*(b+c)).*((1-fCdPDE)+fCdPDE.*a);
k = ((G.*R)./(KD1.*(KD2+LR)));
%%%
%GLP1'
ddt(1) = yL - uLB.*GLP1.*R;
%R'
ddt(2)= (k2.*RD1-k1.*(Rt-R-RD1-RD2)-((k5.*(Gt-G-Gbg)-k7.*GaGDP.*Gbg).*h)...
    -(k.*ddt(1)))./d;
%LR'
ddt(3)= ((GLP1./KD1).*ddt(2)) + ((R./KD1).*ddt(1));
%G'
ddt(4)=(k7.*GaGDP.*Gbg-k5.*(Gt-G-Gbg)-((G./KD2).*ddt(3)))./(1+LR./KD2);
%RD1'
ddt(5) = k1.*(Rt-R-RD1-RD2)-k2.*RD1-k3.*RD1+k4.*RD2;
%RD2'
ddt(6) = k3.*RD1 - k4.*RD2;
%GaGTP'
ddt(7) = k5.*(Gt-G-Gbg) - k6.*GaGTP;
%GaGDP'
ddt(8) = k6.*GaGTP - k7.*GaGDP.*Gbg;
%Gbg'
ddt(9) = k5.*(Gt-G-Gbg) - k7.*GaGDP.*Gbg;
%cAMP'
ddt(10) = VAC_t - 0.2.*V_PDE;
%CaCaM'
ddt(11)= (k1f.*Ca2.*CaM)-(k1b.*CaCaM);
end
```

```matlab
ozempic2.m
function ddt = ozempic2(~,y)
run ozempicpara.m
ddt = zeros(12,1);
D = y(1); %D is the diff. eq. for Ozempic
GLP1 = y(2);
R = y(3);
LR = y(4);
G = y(5);
RD1 = y(6);
RD2=y(7);
GaGTP=y(8);
GaGDP = y(9);
Gbg = y(10);
cAMP = y(11);
CaCaM = y(12);
%%%%
Ca2CaM = (k2f./k2b).*Ca2.*CaCaM;
Ca3CaM = (k3f./k3b).*Ca2.*Ca2CaM;
Ca4CaM = (k4f./k4b).*Ca2.*Ca3CaM;
%%%%
a = (Ca3CaM+Ca4CaM)./(Ca3CaM+Ca4CaM+0.348);
x = (1-fCdAC)+(fCdAC.*a.*(75./(75+Ca2)));
V_AC = VmaxAC.*(0.4./(0.4+GaGTP)).*(ATP./(ATP+1030));
V_AC_G = VmaxACG.*(GaGTP./(0.4+GaGTP)).*(ATP./(ATP+315)).*x;
VAC_t = V_AC+V_AC_G;
b = (frac.*cAMP)./(cAMP+Kml);
c = ((1-frac).*cAMP)./(cAMP+KmH);
d = 1+((D+GLP1)./KD1)+((G.*(GLP1+D))./(KD1.*(KD2+LR)));
h = LR./(KD2+LR);
V_PDE = (VmaxPDE.*(b+c)).*((1-fCdPDE)+fCdPDE.*a);
k = (R./KD1)+((G.*R)./(KD1.*(KD2+LR)));
%%%%
%D'
ddt(1)= -uD.*D;
%GLP1'
ddt(2) = yL.*(1+(D./(Kozempic + D))) - uLB.*GLP1.*R;
%R'
```

```
ddt(3)= (k2.*RD1-k1.*(Rt-R-RD1-RD2)-((k5.*(Gt-G-Gbg)-k7.*GaGDP.*Gbg).*h)...
    -(k.*(ddt(2)+ddt(1)))./d;
%LR'
ddt(4)= (1/KD1).*(((GLP1+D).*ddt(3)) + (R.*(ddt(2)+ddt(1))));
%G'
ddt(5)=(k7.*GaGDP.*Gbg-k5.*(Gt-G-Gbg)-((G./KD2).*ddt(4)))./(1+LR./KD2);
%RD1'
ddt(6) = k1.*(Rt-R-RD1-RD2)-k2.*RD1-k3.*RD1+k4.*RD2;
%RD2'
ddt(7) = k3.*RD1 - k4.*RD2;
%GaGTP'
ddt(8) = k5.*(Gt-G-Gbg) - k6.*GaGTP;
%GaGDP'
ddt(9) = k6.*GaGTP - k7.*GaGDP.*Gbg;
%Gbg'
ddt(10) = k5.*(Gt-G-Gbg) - k7.*GaGDP.*Gbg;
%cAMP'
ddt(11) = VAC_t - 0.2.*V_PDE;
%CaCaM'
ddt(12)= (k1f.*Ca2.*CaM)-(k1b.*CaCaM);
end
```

C.1.3   Plotting Figures 19-21

```
run ozempicpara.m


sol3 = ode23s(@beta, [0 3600], [0.003 0.00024 2.0 0.0005 0.0005 0.0002 1.4...
    0.8299 1.4 0]); %constant GLP-1 concentration
%Initial conditions to get a GLP-1 concentration of 0.32 nM


C = sol3.y;


for n=1:9
    min(C(n,:))
end %to make sure none of the differential equations have negative outputs


GLP_1 = (KD1.*C(2,:))./(C(1,:));
LRG_1 = (C(2,:).*C(3,:))./KD2; %LRG = (LR*G)/Kd2
%~~~~
```

```matlab
solution2 = ode23s(@ozempic, [0 3600],...
    [3.2e-4 0.003 0.00024 2.0 0.0005 0.0005 0.0002 1.4 0.83 1.4 0]);
%non-constant GLP-1 concentration, no Ozempic
X = solution2.y;

for n=1:11
    min(X(n,:))
end
LRG_2 = (X(3,:).*X(4,:))./KD2;
%~~~~
solution = ode23s(@ozempic2, [0 3600],...
    [335 3.2e-4 0.003 0.00024 2.0 0.0005 0.0005 0.0002 1.4 0.83 1.4 0]);
%Non-constant GLP-1 concentration with Ozempic
%Ozempic dosage is always 335 mcM (1.34 mg/mL)
W = solution.y;

for n=1:12
    min(W(n,:))
end
LRG_3 = (W(4,:).*W(5,:))./KD2;
%%%
figure(1); %GLP-1 receptor solution curves for all 3 conditions
subplot(6,1,1)
plot(sol3.x,GLP_1,Color = '#000000')
hold on
plot(solution2.x,X(1,:),Color = '#F00396')
hold on
plot(solution.x,W(2,:),Color = '#F00396',LineStyle='--')
xlabel('Time (seconds)')
ylabel('GLP-1 (M)')
xlim([0 3600])
ylim([2.7e-4 3.3e-4])

subplot(6,1,2)
plot(sol3.x,C(1,:),Color='#000000')
hold on
plot(solution2.x,X(2,:),Color='#FD1A1A')
hold on
```

```
plot(solution.x,W(3,:),Color='#FD1A1A',LineStyle='--')
xlabel('Time (seconds)')
ylabel('Free Receptors (M)')
xlim([0 3600])
ylim([2.5e-3 4e-3])


subplot(6,1,3)
plot(sol3.x,C(2,:),Color='#000000')
hold on
plot(solution2.x,X(3,:),Color='#F99215')
hold on
plot(solution.x,W(4,:),Color='#F99215',LineStyle='--')
xlabel('Time (seconds)')
ylabel('LR (M)')
xlim([0 3600])
ylim([2.5e-4 4e-4])


subplot(6,1,4)
plot(sol3.x,C(4,:),Color='#000000')
hold on
plot(solution2.x,X(5,:),Color='#1AAA01')
hold on
plot(solution.x,W(6,:),Color='#1AAA01',LineStyle='--')
xlabel('Time (seconds)')
ylabel('RD1 (M)')
xlim([0 3600])


subplot(6,1,5);
plot(sol3.x,C(5,:),Color='#000000')
hold on
plot(solution2.x,X(6,:),Color='#3725F0')
hold on
plot(solution.x,W(7,:),Color='#3725F0',LineStyle='--')
xlabel('Time (seconds)')
ylabel('RD2 (M)')
xlim([0 3600])


subplot(6,1,6)
```

```
plot(sol3.x,LRG_1,Color='#000000')
hold on
plot(solution2.x,LRG_2,Color='#9A00C2')
hold on
plot(solution.x,LRG_3,Color='#9A00C2',LineStyle='--')
xlabel('Time (seconds)')
ylabel('LRG (M)')
xlim([0 3600])
%%%
figure(2); %G protein solution curves for all 3 conditions
subplot(5,1,1)
plot(sol3.x,GLP_1,Color = '#000000')
hold on
plot(solution2.x,X(1,:),Color = '#F00396')
hold on
plot(solution.x,W(2,:),Color = '#F00396',LineStyle='--')
xlabel('Time (seconds)')
ylabel('GLP-1 (M)')
xlim([0 3600])
ylim([2.7e-4 3.3e-4])

subplot(5,1,2)
plot(sol3.x,C(3,:),Color='#000000')
hold on
plot(solution2.x,X(4,:),Color='#FD1A1A')
hold on
plot(solution.x,W(5,:),Color='#FD1A1A',LineStyle='--')
xlabel('Time (seconds)')
ylabel('Gs Protein Trimers (M)')
xlim([0 3600])

subplot(5,1,3)
plot(sol3.x,C(6,:),Color='#000000')
hold on
plot(solution2.x,X(7,:),Color='#F99215')
hold on
plot(solution.x,W(8,:),Color='#F99215',LineStyle='--')
xlabel('Time (seconds)')
```

```
ylabel('GGTP (M)')
xlim([0 3600])
ylim([0 0.03])


subplot(5,1,4)
semilogy(sol3.x,C(7,:),Color='#000000')
hold on
semilogy(solution2.x,X(8,:),Color='#1AAA01')
hold on
semilogy(solution.x,W(9,:),Color='#1AAA01',LineStyle='--')
xlabel('Time (seconds)')
ylabel('GGDP (M)')
xlim([0 3600])
ylim([0.4 1.3])


subplot(5,1,5)
semilogy(sol3.x,C(8,:),Color='#000000')
hold on
semilogy(solution2.x,X(9,:),Color='#3725F0')
hold on
semilogy(solution.x,W(10,:),Color='#3725F0',LineStyle = '--')
xlabel('Time (seconds)')
ylabel('G (M)')
xlim([0 3600])
ylim([1e-6 1])
%%%
figure(3); %cAMP in all three conditions
figure(3)
subplot(2,1,1)
plot(sol3.x,GLP_1,Color = '#000000')
hold on
plot(solution2.x,X(1,:),Color = '#F00396')
hold on
plot(solution.x,W(2,:),Color = '#F00396',LineStyle='--')
xlabel('Time (seconds)')
ylabel('GLP-1 (M)')
xlim([0 3600])
ylim([2.7e-4 3.3e-4])
```

```
subplot(2,1,2)
plot(sol3.x,C(9,:),Color='#000000')
hold on
plot(solution2.x,X(10,:),Color='#D837FF')
hold on
plot(solution.x,W(11,:),Color='#D837FF',LineStyle='--')
xlabel('Time (seconds)')
ylabel('cAMP (M)')
xlim([0 3600])
```

C.2   Model of the Incretin Effect

C.2.1   Defining Parameters

```
k1 = 0.00671;
k3 = 0.0718;
k4 = 0.717;
k5 = 27.64;
k6 = 0.1;
k7 = 0.125;
k8 = 0.005;
k9 = 0.1;
RaInc = 280;
V = 14;
a = 1;
B = -0.758;
Kozempic = 0.335; %mM, for model with addition of Ozempic
uD = 6.66e-5;%min^-1
```

C.2.2   Defining Differential Equations

```
incretin.m
function ddt = incretin(t,y)
run incretinpara.m
ddt=zeros(3,1);
Inc = y(1);
I=y(2);
G=y(3);
```

```
k2 = 0.00204;
if G<3
    M=0.03;
else
    M=0.02;
end
Hepbalg = 0.8549 + (M.*(4-G).*I);
Duodg = (6.349-0.0353.*t).*(t>=5 & t<=179.9);
RaGutg = (0.36.*(t-5).^1.05.*exp(-0.029.*(t-5))).*(t>=5);
if t>=5
    g = 0.06;
else
    g = 0;
end
%Inc'(t)
ddt(1) = RaInc./V + k5.*Duodg - k6.*Inc;
%I'(t)
ddt(2) = k7.*(G.^(1.3)) + k8.*Inc-k9.*I+B;
%G'(t)
ddt(3) = (RaGutg./V)+(Hepbalg./V) - k1.*(G.^(1.3))-k2.*I+g.*ddt(2);
end


glp1ra.m
function ddt = glp1ra(t,y)
run incretinpara.m
ddt=zeros(4,1);
D = y(1);
Inc = y(2);
I=y(3);
G=y(4);
k2 = 0.00204;
if G<3
    M = 0.03;
else
    M = 0.02;
end
Hepbalg = 0.8549 + (M.*(4-G).*I);%+((1./(G.*I))-(1./(40)));
Duodg = (6.349-0.0353.*t).*(t>=5 & t<=179.9);
```

```
RaGutg = (0.36.*(t-5).^1.05.*exp(-0.029.*(t-5))).*(t>=5);
if t>=5
    g = 0.06;
else
    g = 0;
end
%D'(t)
ddt(1) = -uD.*D;
%Inc'(t)
ddt(2) = ((RaInc./V).*(1+(D./(Kozempic + D)))) + k5.*Duodg - k6.*Inc;
%I'(t)
ddt(3) = k7.*(G.^(1.3)) + k8.*Inc-k9.*I+B;
%G'(t)
ddt(4) = (Hepbalg./V)+((RaGutg./V).*(1./(1+(D./Kozempic)))) - k1.*(G.^(1.3))...
    -k2.*I+g.*ddt(3);
end
```

C.2.3 Plotting Figures 12 and 13

```
run incretinpara.m
sol2 = ode23s(@incretin,[0 300],[200 10 4]);
Z = sol2.y;
%plot of Inc(t)
figure(1);
subplot(3,1,1)
plot(sol2.x,Z(1,:),Color="#F00396")
xlabel('Time (minutes)')
ylabel('Incretin Conc. (ng/L)')
ylim([0 1700])
%Plot of I(t)
subplot(3,1,2)
plot(sol2.x,Z(2,:),Color='#00AAE8')
xlabel('Time (minutes)')
ylabel('Insulin Conc. (mU/L)')
%Plot of G(t)
subplot(3,1,3)
plot(sol2.x,Z(3,:),Color='#8040E6')
xlabel('Time (minutes)')
ylabel('Glucose Conc. (mmol/L)')
```

To plot Figure 13, I set `Duodg = 0` in the function `incretin.m`.

C.2.4   Plotting Figure 22

```
run incretinpara.m
sol6 = ode23s(@incretin,[0 300],[200 10 4]);
Z = sol6.y; %without Ozempic
sol7 = ode23s(@glp1ra,[0 300],[0.335 200 10 4]);
A = sol7.y; %with Ozempic

%plot of Inc(t)
figure(1);
subplot(3,1,1)
plot(sol6.x,Z(1,:),Color="#F00396")
hold on
plot(sol7.x,A(2,:),Color="#F00396",LineStyle='--')
xlabel('Time (minutes)')
ylabel('Incretin Conc. (ng/L)')
ylim([0 2000])

%Plot of I(t)
subplot(3,1,2)
plot(sol6.x,Z(2,:),Color='#00AAE8')
hold on
plot(sol7.x,A(3,:),Color='#00AAE8',LineStyle='--')
xlabel('Time (minutes)')
ylabel('Insulin Conc. (mU/L)')

%Plot of G(t)
subplot(3,1,3)
plot(sol6.x,Z(3,:),Color='#8040E6')
hold on
plot(sol7.x,A(4,:),Color='#8040E6',LineStyle='--')
xlabel('Time (minutes)')
ylabel('Glucose Conc. (mmol/L)')
ylim([2 9])
```

C.2.5   Plotting Figure 23

```
run incretinpara.m
```

```
so1 = ode23s(@incretin,[0 900],[200 10 4]);
F = so1.y;
so2 = ode23s(@incretink20001,[0 900],[200 10 4]);
G = so2.y;
so4 = ode23s(@incretink20000001,[0 900],[200 10 4]);
J = so4.y;
%Plot of I(t)
figure(1);
plot(so1.x,F(2,:),Color='#1797DB')
hold on
plot(so2.x,G(2,:),Color='#29A600')
hold on
plot(so4.x,J(2,:),Color='#E80083')
xlabel('Time (minutes)')
ylabel('Plasma Insulin Conc. (mU/L)')
```

To get `@incretink20001` and `@incretink20000001`, I set `k2 = 0.001` and `k2 = 0.000001` respectively in `incretin.m`.

C.3   Model of Ovulatory Regulation

C.3.1   Defining Parameters

```
testopara.m
cFE = 0.0022729;
cFI = 1.9488;
cFP = 60.428;
cLE = 0.0010404;
cLP = 0.0099415;
cLT = 0.0095942;
dF = 8.21;
dL = 14;
kF = 2.5412;
KFI = 107.01;
KiLP = 0.34952;
KLT = 420;
KmL = 183.56;
kL = 0.74567;
n = 8;
V = 2.5;
```

```
v0L = 1051.7;
v1L = 34838;
vF = 3236.6;
cPF = 0.01127;
dS = 0.74702;
f0 = 0.0025112;
f1 = 4.3764;
f2 = 27.812;
h1 = 590.32;
h2 = 1815.3;
hP = 20.764;
hs = 12.329;
l = 0.49017;
m = 4;
s = 2.378;
w = 0.23173;
cTF2 = 123.8136;
dE = 1.1;
dP = 0.5;
dT = 5.5;
e0 = 44.512;
N = 1.1087;
h3 = 17.796;
K1 = 1.09;
K2 = 22.28645;
K3 = 113.9188;
p = 0.3734;
T0 = 273.67;
t0 = 741.68;
t1 = 0.57088;
t2 = 1.3481;
T1 = 5.3989;
%T2 = 0;
T3 = 430.91;
tg1 = 6.6548;
tg2 = 186.27;
Psi = 2004.3;
cPT = 0.19878;
```

C.3.2 Defining Differential Equations

```
function ddt = testo(~,y)
run testopara.m
ddt = zeros(12,1);
FSHp = y(1);
FSH = y(2);
LHp = y(3);
LH = y(4);
Phi = y(5);
Omega = y(6);
Lambda = y(7);
S = y(8);
T = y(9);
Tgamma = y(10);
E2 = y(11);
P4 = y(12);
a = 0;
G1 = 1+a;
q = ((S.*Lambda)./(KFI+S.*Lambda));
b = (((1+(cFP.*P4))./(1+(cFE.*E2.^2))));
c = (T./(KLT+T));
d = ((E2.^8)./((KmL.^8)+(E2.^8)));
e = (P4./(KiLP.*(1+(cLT.*T))));
f = (((1+(cLP.*P4))./(1+(cLE.*E2))));
g = (h1./(1+((cPT.*T)./T0)));
h = (h2./(1+(cPF.*FSH)));
j = ((Phi+Omega+Lambda)./Psi);
k = (Phi+(T1.*Omega)+(T3.*(1-j)));
F1 = (LH.^2./(K1.*LH.^2+K2.*LH+K3));
F2 = (LH./(K1.*LH.^2+K2.*LH+K3));
pp = ((t1.*G1.*(F1+(cTF2.*F2)))+(t2.*G1.*F1));
r = (((tg2.*FSH)./(h3+FSH)).*Tgamma);
u = ((p.*LH)./(LH+hP));
%FSHp'
ddt(1) = (vF./(1+cFI.*q))-(kF.*b.*FSHp);
%FSH'
ddt(2) = ((1/V).*kF.*b.*FSHp)-(dF.*FSH);
%LHp'
```

```
ddt(3) = (((v0L.*c)+(v1L.*d)).*(1./(1+e)))-(kL.*f.*LHp);
%LH'
ddt(4) = ((1/V).*kL.*f.*LHp)-(dL.*LH);
%Phi'
ddt(5) = ((f0.*T)./T0)+(Phi.*(((f1.*FSH.^2)./(g.^2+FSH.^2))-...
    ((f2.*LH.^2)./(h.^2+LH.^2))));
%Omega'
ddt(6) = (((f2.*LH.^2)./(h.^2+LH.^2)).*Phi)-(w.*S.*Omega);
%Lambda'
ddt(7) = (w.*S.*Omega) - (l.*(1-S).*Lambda);
%S'
ddt(8) = (((s.*LH.^4)./(hs.^4+LH.^4)).*(1-S))-(dS.*S);
%T'
ddt(9) = t0 - (dT.*T) + (pp.*k);
%Tgamma'
ddt(10) = (tg1.*G1.*F1) - r;
%E2'
ddt(11) = e0-(dE.*E2)+(r.*(Phi+(N.*Lambda.*S)));
%P4'
ddt(12) = -(dP.*P4) + (Lambda.*S.*u);
end
```

C.3.3   Plotting Figures 14-16

```
run testopara.m
sol = ode23s(@testo, [0 400], [116.82 142.5 250.35 25.34 0.50185 9.7509 ...
    4.102 0.050498 273.67 0.003999 56.387 0.468]);
Z=sol.y;
figure(1);
%FSHp
subplot(4,1,1)
plot(sol.x,Z(1,:),Color='#FFC73D')
xlabel('Time (days)')
ylabel('Reserve FSH (g/L)')
%FSH
subplot(4,1,2)
plot(sol.x,Z(2,:),Color='#979797')
xlabel('Time (days)')
ylabel('FSH (g/L)')
```

```
%LHp
subplot(4,1,3)
plot(sol.x,Z(3,:),Color='#8102CC')
xlabel('Time (days)')
ylabel('Reserve LH (g/L)')
%LH
subplot(4,1,4)
plot(sol.x,Z(4,:),Color='#000000')
xlabel('Time (days)')
ylabel('LH (g/L)')
%~
figure(2);
%Phi
subplot(2,1,1)
plot(sol.x,Z(5,:),Color='#FFC73D')
%Omega
hold on
plot(sol.x,Z(6,:),Color='#979797')
%Lambda
hold on
plot(sol.x,Z(7,:),Color='#8102CC')
xlabel('Time (days)')
ylabel('Ovarian Mass (g)')
%S
subplot(2,1,2)
plot(sol.x,Z(8,:),Color='#000000')
xlabel('Time (days)')
ylabel('LH Support')
%~
figure(3);
%T
subplot(4,1,1)
plot(sol.x,Z(9,:),Color='#FFC73D')
xlabel('Time (days)')
ylabel('T (ng/L)')
%Tgamma
subplot(4,1,2)
plot(sol.x,Z(10,:),Color='#979797')
```

```
xlabel('Time (days)')
ylabel('T (ng/L)')
%E2
subplot(4,1,3)
plot(sol.x,Z(11,:),Color='#8102CC')
xlabel('Time (days)')
ylabel('E_2 (ng/L)')
%P4
subplot(4,1,4)
plot(sol.x,Z(12,:),Color='#000000')
xlabel('Time (days)')
ylabel('P_4 (ng/L)')
```

C.3.4 Plotting Figure 17

```
sol0 = ode23s(@testo, [0 365], [116.82 142.5 250.35 25.34 0.50185 9.7509 ...
    4.102 0.050498 273.67 0.003999 56.387 0.468]);
Z0 = sol0.y;


sol1 = ode23s(@testo1, [0 365], [116.82 142.5 250.35 25.34 0.50185 9.7509 ...
    4.102 0.050498 273.67 0.003999 56.387 0.468]);
Z1 = sol1.y;


sol2 = ode23s(@testo2, [0 365], [116.82 142.5 250.35 25.34 0.50185 9.7509 ...
    4.102 0.050498 273.67 0.003999 56.387 0.468]);
Z2 = sol2.y;


sol3 = ode23s(@testo3, [0 365], [116.82 142.5 250.35 25.34 0.50185 9.7509 ...
    4.102 0.050498 273.67 0.003999 56.387 0.468]);
Z3 = sol3.y;


sol4 = ode23s(@testo4, [0 365], [116.82 142.5 250.35 25.34 0.50185 9.7509 ...
    4.102 0.050498 273.67 0.003999 56.387 0.468]);
Z4 = sol4.y;


sol5 = ode23s(@testo5, [0 365], [116.82 142.5 250.35 25.34 0.50185 9.7509 ...
    4.102 0.050498 273.67 0.003999 56.387 0.468]);
Z5 = sol5.y;
```

```
TMat = [Z0(9,1:500); Z1(9,1:500); Z2(9,1:500); Z3(9,1:500); Z4(9,1:500);...
    Z5(9,1:500)];


LHMat = [Z0(4,1:500); Z1(4,1:500); Z2(4,1:500); Z3(4,1:500);...
    Z4(4,1:500); Z5(4,1:500)];


FSHMat = [Z0(2,1:500); Z1(2,1:500); Z2(2,1:500); Z3(2,1:500);...
    Z4(2,1:500); Z5(2,1:500)];


E2Mat = [Z0(11,1:500); Z1(11,1:500); Z2(11,1:500); Z3(11,1:500);...
    Z4(11,1:500); Z5(11,1:500)];


P4Mat = [Z0(12,1:500); Z1(12,1:500); Z2(12,1:500); Z3(12,1:500);...
    Z4(12,1:500); Z5(12,1:500)];
figure(1)
subplot(2,3,1)
plot(1:500,TMat)
title('T (ng/L)')
subplot(2,3,2)
plot(1:500,LHMat)
title('LH (g/L)')
subplot(2,3,3)
plot(1:500,FSHMat)
title('FSH (g/L)')
subplot(2,3,4)
plot(1:500,E2Mat)
title('E2 (ng/L)')
subplot(2,3,5)
plot(1:500,P4Mat)
title('P4 (ng/mL)')
```

To obtain the functions `testo1.m`, `testo2.m`, `testo3.m`, `testo4.m`, and `testo5.m`, I set `a` equal to `1, 2, 3, 4` and `5` respectively in `testo.m`.

C.3.5 Plotting Figure 27

```
testoi116974.m
function ddt = testoi116974(~,y)
```

```
run testopara.m
ddt = zeros(12,1);
FSHp = y(1);
FSH = y(2);
LHp = y(3);
LH = y(4);
Phi = y(5);
Omega = y(6);
Lambda = y(7);
S = y(8);
T = y(9);
Tgamma = y(10);
E2 = y(11);
P4 = y(12);
I = 11.6974;
a = 0.625.*I-6.25;
G1 = 1+a;
q = ((S.*Lambda)./(KFI+S.*Lambda));
b = (((1+(cFP.*P4))./(1+(cFE.*E2.^2))));
c = (T./(KLT+T));
d = ((E2.^8)./((KmL.^8)+(E2.^8)));
e = (P4./(KiLP.*(1+(cLT.*T))));
f = (((1+(cLP.*P4))./(1+(cLE.*E2))));
g = (h1./(1+((cPT.*T)./T0)));
h = (h2./(1+(cPF.*FSH)));
j = ((Phi+Omega+Lambda)./Psi);
k = (Phi+(T1.*Omega)+(T3.*(1-j)));
F1 = (LH.^2./(K1.*LH.^2+K2.*LH+K3));
F2 = (LH./(K1.*LH.^2+K2.*LH+K3));
pp = ((t1.*G1.*(F1+(cTF2.*F2)))+(t2.*G1.*F1));
r = (((tg2.*FSH)./(h3+FSH)).*Tgamma);
u = ((p.*LH)./(LH+hP));
%FSHp'
ddt(1) = (vF./(1+cFI.*q))-(kF.*b.*FSHp);
%FSH'
ddt(2) = ((1/V).*kF.*b.*FSHp)-(dF.*FSH);
%LHp'
ddt(3) = (((v0L.*c)+(v1L.*d)).*(1./(1+e)))-(kL.*f.*LHp);
```

```matlab
%LH'
ddt(4) = ((1/V).*kL.*f.*LHp)-(dL.*LH);
%Phi'
ddt(5) = ((f0.*T)./T0)+(Phi.*(((f1.*FSH.^2)./(g.^2+FSH.^2))-...
    ((f2.*LH.^2)./(h.^2+LH.^2))));
%Omega'
ddt(6) = (((f2.*LH.^2)./(h.^2+LH.^2)).*Phi)-(w.*S.*Omega);
%Lambda'
ddt(7) = (w.*S.*Omega) - (l.*(1-S).*Lambda);
%S'
ddt(8) = (((s.*LH.^4)./(hs.^4+LH.^4)).*(1-S))-(dS.*S);
%T'
ddt(9) = t0 - (dT.*T) + (pp.*k);
%Tgamma'
ddt(10) = (tg1.*G1.*F1) - r;
%E2'
ddt(11) = e0-(dE.*E2)+(r.*(Phi+(N.*Lambda.*S)));
%P4'
ddt(12) = -(dP.*P4) + (Lambda.*S.*u);
end


testoi161606.m
function ddt = testoi161606(~,y)
run testopara.m
ddt = zeros(12,1);
FSHp = y(1);
FSH = y(2);
LHp = y(3);
LH = y(4);
Phi = y(5);
Omega = y(6);
Lambda = y(7);
S = y(8);
T = y(9);
Tgamma = y(10);
E2 = y(11);
P4 = y(12);
I = 16.1606;
```

```
a = 0.625.*I-6.25;
G1 = 1+a;
q = ((S.*Lambda)./(KFI+S.*Lambda));
b = (((1+(cFP.*P4))./(1+(cFE.*E2.^2))));
c = (T./(KLT+T));
d = ((E2.^8)./((KmL.^8)+(E2.^8)));
e = (P4./(KiLP.*(1+(cLT.*T))));
f = (((1+(cLP.*P4))./(1+(cLE.*E2))));
g = (h1./(1+((cPT.*T)./T0)));
h = (h2./(1+(cPF.*FSH)));
j = ((Phi+Omega+Lambda)./Psi);
k = (Phi+(T1.*Omega)+(T3.*(1-j)));
F1 = (LH.^2./(K1.*LH.^2+K2.*LH+K3));
F2 = (LH./(K1.*LH.^2+K2.*LH+K3));
pp = ((t1.*G1.*(F1+(cTF2.*F2)))+(t2.*G1.*F1));
r = (((tg2.*FSH)./(h3+FSH)).*Tgamma);
u = ((p.*LH)./(LH+hP));
%FSHp'
ddt(1) = (vF./(1+cFI.*q))-(kF.*b.*FSHp);
%FSH'
ddt(2) = ((1/V).*kF.*b.*FSHp)-(dF.*FSH);
%LHp'
ddt(3) = (((v0L.*c)+(v1L.*d)).*(1./(1+e)))-(kL.*f.*LHp);
%LH'
ddt(4) = ((1/V).*kL.*f.*LHp)-(dL.*LH);
%Phi'
ddt(5) = ((f0.*T)./T0)+(Phi.*(((f1.*FSH.^2)./(g.^2+FSH.^2))-...
    ((f2.*LH.^2)./(h.^2+LH.^2))));
%Omega'
ddt(6) = (((f2.*LH.^2)./(h.^2+LH.^2)).*Phi)-(w.*S.*Omega);
%Lambda'
ddt(7) = (w.*S.*Omega) - (l.*(1-S).*Lambda);
%S'
ddt(8) = (((s.*LH.^4)./(hs.^4+LH.^4)).*(1-S))-(dS.*S);
%T'
ddt(9) = t0 - (dT.*T) + (pp.*k);
%Tgamma'
ddt(10) = (tg1.*G1.*F1) - r;
```

```
%E2'
ddt(11) = e0-(dE.*E2)+(r.*(Phi+(N.*Lambda.*S)));
%P4'
ddt(12) = -(dP.*P4) + (Lambda.*S.*u);
end


s1 = ode23s(@testoi116974, [0 365], [116.82 142.5 250.35 25.34 0.50185 9.7509 ...
    4.102 0.050498 273.67 0.003999 56.387 0.468]);
X1 = s1.y;


s2 = ode23s(@testoi161606, [0 365], [116.82 142.5 250.35 25.34 0.50185 9.7509 ...
    4.102 0.050498 273.67 0.003999 56.387 0.468]);
X2 = s2.y;


TMatI = [X1(9,1:1000); X2(9,1:1000)];


LHMatI = [X1(4,1:1000); X2(4,1:1000)];


FSHMatI = [X1(2,1:1000); X2(2,1:1000)];


E2MatI = [X1(11,1:1000); X2(11,1:1000)];


P4MatI = [X1(12,1:1000); X2(12,1:1000)];


figure(1)
subplot(2,3,1)
plot(1:1000,TMatI)
title('T (ng/L)')
subplot(2,3,2)
plot(1:1000,LHMatI)
title('LH (g/L)')
subplot(2,3,3)
plot(1:1000,FSHMatI)
title('FSH (g/L)')
subplot(2,3,4)
plot(1:1000,E2MatI)
title('E2 (ng/L)')
subplot(2,3,5)
```

```
plot(1:1000,P4MatI)
title('P4 (ng/mL)')
```

D R Source Code

D.1 Plotting Figures 24-26

```r
k2 = c(0.00204,0.002,0.0015,0.001,0.0005,0.0001,0.00005,0.00001,0.000005,0.000001)
binsulin_no_ozempic_1hour = c(81.0846,81.1462,81.9225,82.7105,
83.51,84.1574,84.239,84.3045,84.3125,84.3192)
binsulin_ozempic_1hour = c(82.1989,82.2582,83.0094,83.7757,
84.5553,85.1882,85.2676,85.3323,85.3403,85.3467)
lm5 = lm(binsulin_no_ozempic_1hour~k2)
lm6 = lm(binsulin_ozempic_1hour~k2)
plot(k2, binsulin_no_ozempic_1hour, col = "deeppink1", xlim = c(0,0.003),
ylim = c(80, 86), main = 'Insulin and insulin-mediated glucose uptake (IMGU)
1 hour after OGTT', xlab = "Value of k2 parameter", ylab = "Insulin levels (mU/L)")
abline(lm5,col = "deeppink1")
points(k2, binsulin_ozempic_1hour, col = "orchid1")
abline(lm6,col = "orchid1")
legend("topright", legend = c("Without Ozempic", "With Ozempic"), col =
c("deeppink1", "orchid1"), lty = c(1,1), cex = 0.75)


k2 = c(0.00204,0.002,0.0015,0.001,0.0005,0.0001,0.00005,0.00001,0.000005,0.000001)
binsulin_no_ozempic_2hour = c(50.4366,50.4936,51.2144,51.9488,52.6962,
53.304,53.3805,53.4418,53.4495,53.4557)
binsulin_ozempic_2hour = c(52.9768,53.033,53.7445,54.4722,55.2157,55.8215,
55.8979,55.9591,55.9667,55.9729)
lm7 = lm(binsulin_no_ozempic_2hour~k2)
lm8 = lm(binsulin_ozempic_2hour~k2)
plot(k2, binsulin_no_ozempic_2hour, col = "deeppink1", xlim = c(0,0.003),
ylim = c(50,57), main = 'Insulin levels and IMGU 2 hours after OGTT',
xlab = "Value of k2 parameter", ylab = "Insulin levels (mU/L)")
abline(lm7,col = "deeppink1")
points(k2, binsulin_ozempic_2hour, col = "orchid1")
abline(lm8,col = "orchid1")
legend("topright", legend = c("Without Ozempic", "With Ozempic"),
col = c("deeppink1", "orchid1"), lty = c(1,1), cex = 0.75)


k2 = c(0.00204,0.002,0.0015,0.001,0.0005,0.0001,0.00005,0.00001,0.000005,0.000001)
binsulin_no_ozempic_1day = c(9.99747,10.0278,10.4169,
10.8246,11.2516,11.6073,11.6527,11.6891,11.6937,11.6974)
```

```
binsulin_ozempic_1day = c(14.1408,14.1776,14.6467,15.1335,15.6384,
16.0555,16.1085,16.151,16.1563,16.1606)
lm1 = lm(binsulin_no_ozempic_1day~k2)
lm2 = lm(binsulin_ozempic_1day~k2)
plot(k2, binsulin_no_ozempic_1day, col = "deeppink1", xlim = c(0,0.003),
ylim = c(9, 17), main = 'Insulin levels and IMGU after one day',
xlab = "Value of k2 parameter", ylab = "Fasting insulin levels (mU/L)")
abline(lm1,col = "deeppink1")
points(k2, binsulin_ozempic_1day, col = "orchid1")
abline(lm2,col = "orchid1")
legend("topright", legend = c("Without Ozempic", "With Ozempic"),
col = c("deeppink1", "orchid1"), lty = c(1,1), cex = 0.75)
```

D.1.1   Plotting Figures 28-30

```
k2 = c(0.00204,0.002,0.0015,0.001,0.0005,0.0001,0.00005,0.00001,0.000005,0.000001)
bglucose_no_ozempic_1hour = c(5.61833,5.64117,5.92692,6.21296,
6.49932,6.72868,6.75734,6.78031,6.78321,6.78548)
bglucose_ozempic_1hour = c(4.20944,4.23352,4.53418,4.83494,
5.13581,5.37668,5.40674,5.43082,5.43383,5.43623)
lm9 = lm(bglucose_no_ozempic_1hour~k2)
lm10 = lm(bglucose_ozempic_1hour~k2)
plot(k2, bglucose_no_ozempic_1hour, col = "forestgreen", xlim = c(0,0.003),
ylim = c(4,7), main = 'Glucose levels and IMGU 1 hour after OGTT',
xlab = "Value of k2 parameter", ylab = "Glucose levels (mmol/L)",)
abline(lm9,col = "forestgreen")
points(k2, bglucose_ozempic_1hour, col = "royalblue1")
abline(lm10,col = "royalblue1")
legend("topright", legend = c("Without Ozempic", "With Ozempic"),
col = c("forestgreen", "royalblue1"), lty = c(1,1), cex = 0.75)


k2 = c(0.00204,0.002,0.0015,0.001,0.0005,0.0001,0.00005,0.00001,0.000005,0.000001)
bglucose_no_ozempic_2hour = c(4.41239,4.43441,4.71001,4.98599,
5.26208,5.48408,5.51187,5.53404,5.5368,5.53904)
bglucose_ozempic_2hour = c(3.5146,3.53792,3.82944,4.121,
4.41277,4.64636,4.67557,4.69894,4.70187,4.7042)
lm11 = lm(bglucose_no_ozempic_2hour~k2)
lm12 = lm(bglucose_ozempic_2hour~k2)
plot(k2, bglucose_no_ozempic_2hour, col = "forestgreen", xlim = c(0,0.003),
```

```
ylim = c(3,6), main = 'Glucose levels and IMGU 2 hours after OGTT',
xlab = "Value of k2 parameter", ylab = "Glucose levels (mmol/L)",)
abline(lm11,col = "forestgreen")
points(k2, bglucose_ozempic_2hour, col = "royalblue1")
abline(lm12,col = "royalblue1")
legend("topright", legend = c("Without Ozempic", "With Ozempic"),
col = c("forestgreen", "royalblue1"), lty = c(1,1), cex = 0.75)


k2 = c(0.00204,0.002,0.0015,0.001,0.0005,0.0001,0.00005,0.00001,0.000005,0.000001)
bglucose_no_ozempic_oneday = c(3.99955,4.01186,4.16878,4.33133,
4.49961,4.63841,4.65602,4.67015,4.67192,4.67333)
bglucose_ozempic_oneday = c(3.74527,3.76048,3.95302,4.14992,
4.35121,4.5154,4.53612,4.55273,4.55481,4.55648)
lm3 = lm(bglucose_no_ozempic_oneday~k2)
lm4 = lm(bglucose_ozempic_oneday~k2)
plot(k2, bglucose_no_ozempic_oneday, col = "forestgreen", xlim = c(0,0.003),
ylim = c(2,5), main = 'Glucose levels and IMGU after one day',
xlab = "Value of k2 parameter", ylab = "Basal glucose levels (mmol/L)")
abline(lm3,col = "forestgreen")
points(k2, bglucose_ozempic_oneday, col = "royalblue1")
abline(lm4,col = "royalblue1")
legend("topright", legend = c("Without Ozempic", "With Ozempic"),
col = c("forestgreen", "royalblue1"), lty = c(1,1), cex = 0.75)
```

D.1.2   Plotting Figure 31

```
lm13=lm(binsulin_no_ozempic_1day~bglucose_no_ozempic_oneday)
lm14=lm(binsulin_ozempic_1day~bglucose_ozempic_oneday)
plot(bglucose_no_ozempic_oneday,binsulin_no_ozempic_1day,col='forestgreen',
xlim=c(3.5,5),ylim = c(9,17),
main = 'Glucose levels and insulin levels after one day',
xlab = "Basal glucose levels (mmol/L)", ylab = "Fasting insulin levels (mU/L)")
abline(lm13,col='deeppink1')
points(bglucose_ozempic_oneday,binsulin_ozempic_1day,col='royalblue1')
abline(lm14,col='orchid1')
legend("topright", legend = c("Without Ozempic", "With Ozempic"),
col = c("deeppink1", "orchid1"), lty = c(1,1), cex = 0.75)
```

D.1.3 Plotting Figures 32 and 33

```
alpha= function(I) 0.625*I-6.25
plot(bglucose_ozempic_oneday,alpha(binsulin_ozempic_1day),col='orchid1',
xlim=c(3.5,5), ylim=c(0,5), main = 'Glucose levels and insulin influence on
testosterone production', xlab = "Basal glucose levels (mmol/L)",
ylab = "Degree of insulin influence")
points(bglucose_no_ozempic_oneday,alpha(binsulin_no_ozempic_1day),col='deeppink1')
lm15=lm(alpha(binsulin_no_ozempic_1day)~bglucose_no_ozempic_oneday)
lm16=lm(alpha(binsulin_ozempic_1day)~bglucose_ozempic_oneday)
abline(lm15,col='forestgreen')
abline(lm16,col='royalblue1')
legend("topright", legend = c("Without Ozempic", "With Ozempic"),
col = c("forestgreen", "royalblue1"), lty = c(1,1), cex = 0.75)


lm20 = lm(alpha(binsulin_no_ozempic_1day)~k2)
lm21 = lm(alpha(binsulin_ozempic_1day)~k2)
plot(k2,alpha(binsulin_no_ozempic_1day), xlim=c(0,0.0021),
ylim=c(0,5),col='darkorchid4',
main='IMGU and insulin influence on testosterone production',
xlab = "Value of k2 parameter", ylab = "Degree of insulin influence")
points(k2,alpha(binsulin_ozempic_1day),col='springgreen4')
abline(lm20,col='darkorchid1')
abline(lm21,col='springgreen2')
legend("topright", legend = c("Without Ozempic", "With Ozempic"),
col = c("darkorchid1", "springgreen2"), lty = c(1,1), cex = 0.75)
```

References

[1] Boswell-Smith, V., Spina, D., & Page, C.P. (2006). Phosphodiesterase inhibitors. *British Journal of Pharmacology*, 147, 252–257.

[2] Brubaker, P. L., Ohayon, E.L., D'Alessandro, L.M., & Norwich, K.H. (2007). A mathematical model of the oral glucose tolerance test illustrating the effects of incretins. *Annals of Biomedical Engineering*, 35, 1286–1300.

[3] Bruce, N.J., Gaurav, K.G., Kokh, D.B., Sadiq, S.K., & Wade, R.C. (2018). New approaches for computing ligand-receptor binding kinetics. *Current Opinion in Structural Biology*, 49, 1–10.

[4] Buteau, J. (2008). GLP-1 receptor signalling: Effects on pancreatic $\beta-$cell proliferation and survival. *Diabetes & Metabolism*, 34, 73–77.

[5] Carlsson Petri, K.C., Ingwersen, S.H., Flint, A., Zacho, J., & Overgaard, R.V. (2018). Semaglutide s.c. once-weekly in type 2 diabetes: A population pharmacokinetic analysis. *Diabetes Therapy*, 9, 1533–1547.

[6] Dahan, M.H. & Reaven, G. (2019). Relationship among obesity, insulin resistance, and hyperinsulinemia in the polycystic ovary syndrome. *Endocrine*, 64, 685–689.

[7] Dewailly, D. (2016). Diagnostic criteria for PCOS: Is there a need for a rethink?. *Best Practice & Research Clinical Obstetrics & Gynaecology*, 37, 5–11.

[8] Dumitrescu, R., Mehedintu, C., Briceag, I., Purcărea, V.L., & Hudita, D. (2015). Metformin - Clinical pharmacology in PCOS. *Jounral of Medicine and Life*, 8, 187–192.

[9] Edelstein-Keshet, L. (2005). *Mathematical models in biology*. Society for Industrial and Applied Mathematics.

[10] Eunice Kennedy Shriver National Institute of Child Health and Human Development. (n.d.). "Polycystic Ovary Syndrome (PCOS)". *National Institute of Health*. https://www.nichd.nih.gov/health/topics/factsheets/pcos.

[11] Fridlyand, L.E., Harbeck, M.C., Roe, M.W., & Philipson, L.H. (2007). Regulation of cAMP dynamics by Ca^{2+} and G protein-coupled receptors in the pancreatic $\beta-$cell: A computational approach. *American Journal of Physiology: Cell Physiology*, 293, 1924–1933.

[12] Fridlyand, L.E., Tamarina, N., & Philipson, L.H. (2003). Modeling of Ca^{2+} flux in pancreatic $\beta-$cells: role of the plasma membrane and intracellular stores. *American Journal of Physiology: Endocrinology and Metabolism*, 285, 138–154.

[13] Graham, E.J., Elhadad, N., & Albers, D. (2023). Reduced model for female endocrine dynamics: Validation and functional variations. *Mathematical Biosciences*, 358, 1-16.

[14] Graham, E. J., & Selgrade, J.F. (2017). A model of ovulatory regulation examining the effects of insulin-mediated testosterone production on ovulatory function. *Journal of Theoretical Biology*, 416, 1286–1300.

[15] Hansen, K.R., Knowlton, N.S., Thyer, A.C., Charleston, J.S., Soules, M.R., & Klein, N.A. (2008). A new model of reproductive aging: the decline in ovarian non-growing follicle number from birth to menopause. *Human Reproduction*, 23, 699–708.

[16] Harris, L. A., Schlosser, P.M., & Selgrade, J. F. (2003). Multiple stable periodic solutions in a model for hormonal control of the menstrual cycle. *Bulletin of Mathematical Biology*, 65, 157–173.

[17] Harris, L. A. & Selgrade, J. F. (2014). Modeling endocrine regulation of the menstrual cycle using delay differential equations. *Mathematical Biosciences*, 257, 11–22.

[18] Hawkins, S.M., & Matzuk, M.M. (2008). The menstrual cycle - Basic biology. *Annals of the New York Academy of Sciences*, 1135, 10–18.

[19] Hopkins, C. (2023). "Researchers keep discovering new uses for Ozempic. Proving it works isn't easy." *NBC News*, `https://www.nbcnews.com/health/health-news/ozempic-other-health-conditions-pcos-alzheimers-rcna90457`.

[20] Knudsen, L.B., & Lau, J. (2019). The discovery and development of liraglutide and semaglutide. *Frontiers in Endocrinology*, 10, 1–32.

[21] Laakso, M. (1993). How good a marker is insulin level for insulin resistance?. *American Journal of Epidemiology*, 137(9), 959–965.

[22] Lauffenburger, D.A., & Linderman, J. (1993). *Receptors: Models for binding, trafficking, and signaling*. New York: Oxford University Press.

[23] Levitzki, A. (1986). Regulation of adenylate cyclase by hormones and G-proteins. *FEBS Letters*, 211(2), 113–118.

[24] Marchetti, P., Lupi, R., Bugliani, M., Kirkpatrick, C.L., Sebastiani, G., Grieco, F.A., Del Guerra, S., D'Aleo, V., Piro, S., Marselli, L., Boggi, U., Filipponi, F., Tinti, L., Salvini, L., Wollheim, C.B., Purrello, F., & Dotta, F. (2012). A local glucagon-like peptide 1 (GLP-1) system in human pancreatic islets. *Diabetologia*, 55, 3262–3272.

[25] Mathi, S.K, Chan, Y., Xinfang, L., & Wheeler, M.B. (1997). Scanning of the glucagon-like peptide-1 receptor localizes G protein-activating determinants primarily to the N terminus of the third intracellular loop. *Molecular Endocrinology*, 11(4), 424–432.

[26] "Menstrual Cycle Diagram." `https://veritasfertility.com/wp-content/uploads/2020/11/menstrual-cycle-diagram.jpg`

[27] Müller, T.D., Finan, B., Bloom, S.R., D'Alessio, D., Drucker, D.J., Flatt, P.R., Fritsche, A., Gribble, F., Grill, H.J., Habener, J.F., Holst, J.J., Langhans, W., Meier, J.J., Nauck, M.A., Perez-Tilve, D., Pocal, A., Reimann, F., Sandoval, D.A., Schwartz, T.W., Seeley, R.J., ...Tschöp, M.H. (2019). Glucagon-like peptide 1 (GLP-1). *Molecular Metabolism*, 30, 72–130.

[28] Novo Nordisk Canada Inc. (2018). Ozempic (semaglutide injection). [Product monograph].

[29] Ozturk, S.S., Dressman, J.B., & Palsson, B.O. (1990). On the use of the quasi-equilibrium assumption for drug dissolution. *Pharmaceutical Research*, 7(4), 425–429.

[30] Pacini, G., Ahrén, B., Göbl, C., & Tura, A. (2022). Assessing the effect of incretin hormones and other insulin secretagogues on pancreatic beta-cell function: Review on mathematical modelling approaches. *Biomedicines*, 10, 1–17.

[31] Rorsman, P., & Renström, E. (2003). Insulin granule dynamics in pancreatic beta cells. *Diabetologica*, 46, 1029–1045.

[32] Saucerman, J.J., Brunton, L.L., Michailova, A.P., & McCulloch, A.D. (2003). Modeling β-adrenergic control of cardiac myocyte contractility *in silico*. *Mechanisms of Signal Transduction*, 278(48), 47997–48003.

[33] Selgrade, J.F., & Schlosser, P.M. (1999). A model for the production of ovarian hormones during the menstrual cycle. *Fields Institute Communications*, 21, 429–446.

[34] Shafee, T. (2015). [Diagram of a general Michaelis-Menten curve]. *Wikimedia Commons*, `https://en.m.wikipedia.org/wiki/File:MichaelisMentencurve2.svg`

[35] Sharma, D., Verma, S., Vaidya, S., Kalia, K., & Tiwari, V. (2018). Recent updates on GLP-1 agonists: Current advancements & challenges. *Biomedicine & Pharmacotherapy*, 108, 952–962.

[36] Siewe, N., & Friedman, A. (2024). A mathematical model of obesity-induced type 2 diabetes and efficacy of anti-diabetic weight reducing drug. *Journal of Theoretical Biology*, 581, 1–13.

[37] Szczesnowicz, A., Szeliga, A., Niwczyk, O., Bala, G., & Meczekalski, B. (2023). Do GLP-1 analogs have a place in the treatment of PCOS? New insights and promising therapies. *Journal of Clinical Medicine*, 12, 1–13.

[38] Takeda, Y., Amano, A., Noma, A., Nakamura, Y., Fujimoto, S., & Inagaki, N. (2011). Systems analysis of GLP-1 receptor signaling in pancreatic $\beta-$cells. *American Journal of Physiology-Cell Physiology*, 301, 792–803.

[39] Wettschureck, N., & Offermanns, S. (2005). Mammalian G proteins and their cell type specific functions. *Physiology Review*, 85, 1159–1204.

[40] Wilcox, G. (2005). Insulin and insulin resistance. *Clinical Biochemistry Review*, 26, 19–39.

[41] van der Velden, W.J.C., Heitman, L.H., & Rosenkilde, M.M. (2020). Perspective: Implications of ligand-receptor binding kinetics for therapeutic targeting of G protein-coupled receptors. *ACS Pharmacology and Translational Science*, 3, 179–189.

[42] Vrbikova, J. & Cibula, D. (2005). Combined oral contraceptives in the treatment of polycystic ovary syndrome. *Human Reproduction Update*, 11, 277–291.

[43] Yu, X., Byrne, J.H., & Baxter, D.A. (2004). Modeling interactions between electrical activity and second-messenger cascades in *Aplysia* neuron R15. *Journal of Neurophysiology*, 91, 2297–2311.